Stephan Sagmeister

Excitonic Effects in Solids: Time-Dependent Density Functional Theory versus the Bethe-Salpeter Equation

DISSERTATION

zur Erlangung des akademischen Grades
Doktor rerum naturalium (Dr. rer. nat.)
eingereicht an der

Naturwissenschaftlichen Fakultät der
Karl-Franzens-Universität Graz

Betreuerin:
Univ.-Prof. Dr. Dr. h.c. Claudia Ambrosch-Draxl

August 2009

to Lisa

"The laws of nature are constructed in such a way
as to make the universe as interesting as possible."
Freeman Dyson

Contents

Chapter 1

Introduction

The precise description of the optical properties of a solid is a very complicated task. One has to consider a system of many interacting electrons including various non-trivial quantum effects, such as the formation of electron-hole pairs caused by an incident light wave. The study of such an optically driven excitation in a semiconducting polymer is, *e.g.*, important for technological applications to light-emitting diodes. In any case, optical properties of solids give a broad field of investigating the role of the interaction of electrons and holes and related phenomena.

Generally, there are three ways of treating a many-particle system. The first one is to use the concept of Green's functions, and quasi-particles providing a systematic scheme of studying interacting particles. A Second approach is directly wave function based and very limited to few particle systems. The third approach is based upon the idea of describing the system's observables by means of the density alone. Such an approach is verified in the so-called density functional theory[1] (DFT) which is not as demanding as the latter Green's function based approach but unfortunately does not provide us with excited state energies caused by the interaction with a light wave. It is the development of time-dependent density functional theory which combines the simplicity of density functional theory with the possibility to study time-dependent perturbations. Within this theory the relevant quantum effects of the many-particle system are cast into a functional of the density, the so-called exchange-correlation kernel, which is formally known to exist, but has to be approximated. The afore mentioned Green's function based approach

[1] Walter Kohn was awarded the Nobel Price in Chemistry 1998 for the development of density functional theory.

on the other hand is more involved in the formalism as well as the actual approximations to the interactions among the quasi-particles. However, the construction of approximated quantities therein seems to be mainly guided by means of physically interacting particles, in contrast to DFT where a functional of the density has to be designed, most importantly, for the total energy. It shall be the goal of this work to apply both, the Green's function based approach as well as time-dependent density functional theory to prototypical semiconductors and insulators, as well as to study low-dimensional systems such as polymers by means of the latter theories.

This thesis is organized as follows. In Chapter 2 the general concepts and implications of the quantum theory of a many-particle system is reviewed. It is targeted towards the description of one and two-particle excitations. The concept of Green's functions is introduced, which allows for the evaluation of the relevant observables in the system under study. First the Dyson equation is presented as equation of motion for the one-particle Green's function. In this context the self-energy is introduced bearing all exchange and correlation effects of the interacting system. After presenting the so-called *GW* approximation (Hedin 1965) for the self-energy we proceed to derive the equation of motion for the two-particle correlation function, which is called the Bethe-Salpeter equation (BSE). The latter is capable of describing excitations involving two particles, an electron and a hole, triggered by an electromagnetic wave as perturbation.

Chapter 3 presents the basic formalism of density functional theory (DFT) being an effective theory for describing the ground state properties of an interacting many-electron system. The fundamental theorems (Hohenberg & Kohn 1964, Kohn & Sham 1965) are reviewed and approximations to the functionals of the density, *i.e.,* to the exchange and correlation effects are discussed. An extension of DFT for the description of the time-evolution of a many-particle system, called *time-dependent* DFT (Runge & Gross 1984) is introduced in Chapter 4. Within the linear response framework a Dyson equation is formulated bearing all the information of the much more complicated Bethe-Salpeter equation concerning charge neutral excitations. As in the case of DFT the TDDFT formalism also contains an unknown functional of the density, the so-called *exchange-correlation kernel* which is discussed in the context of relevant approximations to it.

In Chapter 5 we try to unify the formalism of DFT and many body perturbation theory (MBPT). A relation between the density functional for the potential in DFT and the electron self-energy is shown. This idea is pro-

moted to the time-dependent case, where the exchange-correlation kernel is linked to the effective two-particle interaction entering the BSE (Reining et al. 2002, Adragna et al. 2003, Sottile et al. 2003, Marini et al. 2003, Bruneval et al. 2005).

The optical properties of periodic solids are the subject of Chapt. 6. We present the macroscopic dielectric function (MDF) from the self-consistent field method (Adler 1962, Wiser 1963) within the random phase approximation. Moreover, the MDF is formulated within the framework of the BSE as well as TDDFT linear response.

In Chapter 7 we briefly review the LAPW method, whereas in Chapter 8 the actual implementation of BSE and TDDFT within the LAPW framework is presented. All the expressions are derived which are necessary to calculate the macroscopic dielectric function.

Finally, in Chapter 9 the dielectric function of two inorganic semiconductors, namely GaAs and Si, is discussed in both the BSE and the TDDFT formalism. Furthermore LiF is studied as an example for strongly bound excitons. At the end of this thesis two polymers, namely poly-acetylene and poly(phenylene-vinylene) serve as examples for low-dimensional systems to study electron-hole correlations.

The appendices in this work provide supplementary in-depth information being too specialized to be included in the main text. They cover aspects of the second quantization, details on MBPT as well as conventions of the Fourier transform. A list of publications which have been composed during the development of this work are given at the end of this document.

Chapter 2

Many Body Quantum Physics

2.1 Introduction

Although the final aim of this work is to describe the properties of a system consisting of many interacting particles by means of an effective one-particle model, we shall start here to review the basic concepts and conclusions of quantum mechanics of a many body system. We are doing this because we belief that the concept of quasi-particles and effective interactions is closer to our physical picture and understanding as non-interacting effective particles, to be described in Chapt. 3.

Studying an interacting many-electron system, especially for the case of a larger number of electrons, as present in larger molecules or in the unit cell of a solid, is a complicated task. The calculation of the exact many-body wave function $\Psi(\mathbf{r}_1, \ldots, \mathbf{r}_N)$ is truly out of reach for the systems mentioned above. An early approximation to the wave function in terms of a product of single-particle wave functions $\psi_j(\mathbf{r}_j)$ has been proposed by HARTREE. In this case a local potential, the so-called *Hartree* potential accounts for the interaction of one electron with the electron density distribution of the remaining electrons. However, a product of single-particle wave functions violates the fermionic nature of the electrons. One way to overcome this problem is to extend the approximation of the many-body wave function to a Slater determinant of single-particle wave functions. In this case, we also obtain a set of single-particle Schrödinger equations, but with a *non-local* potential, the so-called *Hartree-Fock* potential, containing the Hartree potential.

Going back to the original problem of an interacting many-electron system

there is no way of calculating relevant properties out of the wave function in practice. However, one has found a way to reduce the fully interacting system to an interaction of a small number of particles with the remaining system which we know as Green's function theory. Therein, we extract information from the system by the concept of quasi-particles. Such a quasi-particle, also called a *dressed* or *screened* particle, contains the information about the interaction with other particles at least within the vicinity of the test particle under consideration. This has lead to a framework in terms of one- and two-particles propagators (Green's functions) from which the expectation values of all one- and two-particle operators can be calculated. The one-particle propagator is, for instance, used to describe excitations in a system due to the addition or removal of a particle, whereas the two-particle propagator is able to describe optical excitations, as they include two particles, an electron and a hole in the excitation process. It is important to note that the many-body effects are mainly contained in the so-called *self-energy*, which is the most important quantity within this framework, as well as in all effective interactions, like for instance the effective two-particle interaction appearing in the Bethe-Salpeter equation. Many-body perturbation theory provides therefore a systematic way of approximating the self-energy and the effective interactions with the help of Feynman diagrams, which depict physically meaningful interaction processes of the particles with themselves or with other particles. As a motivating example we look at the above mentioned Hartree and Hartree-Fock approximation from the point of view of MBPT. In Fig. 2.1 the two terms of the irreducible self-energy are shown, where the first one is the Hartree term and the second one the Fock term. The solid lines in this figure indicate the one-particle Green's function, whereas the wiggly line denotes the bare Coulomb interaction.

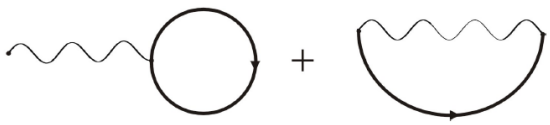

Figure 2.1: Diagrammatic expansion of the self-energy within the Hartree-Fock approximation. Figure taken from Reference (Schöne 2001).

This chapter is based upon the concept of second quantization which

is the prerequisite of the field-theoretical approach of many-body theory. A short collection of some important aspects therein can be found in Appendix A. Using the second quantization allows us, therefore, to study a system with a not a priori specified number of particles. The main part of this chapter is to introduce the equation of motion for the one- and two-particle Green's function (the Dyson equation and Bethe-Salpeter equation) finally by functional-derivative techniques. In general, we follow FETTER and WALECKA (Fetter & Walecka 1971) and to some extent ZAGOSKIN (Zagoskin 1998) and ECONOMOU and (Economou 2006).

2.2 Green's Functions

2.2.1 One particle Green's Function

We continue our discussion on the properties of a many-particle system with the definition of the one-particle Green's function. For the details of the derivations we refer to (Fetter & Walecka 1971, Schöne 2001, Economou 2006, Zagoskin 1998, Mattuck 1992). As our aim is to study electronic systems we will restrict ourselves in the following to the fermionic case. Additionally, the case of zero temperature is considered. The *one particle Green's function* $G(\mathbf{r}, t; \mathbf{r}', t')$ is defined as

$$-iG(\mathbf{r}, t; \mathbf{r}', t') = \left\langle \hat{T}\left[\hat{\psi}(\mathbf{r}, t)\hat{\psi}^{\dagger}(\mathbf{r}', t')\right]\right\rangle_{|\psi_0\rangle}. \tag{2.1}$$

Here, $\hat{T}$ is the time-ordering operator that orders a product of operators in a way that operators at later times stand left of all operators at earlier times. For each transposition of field operators starting from the original ordering a factor of -1 is multiplied to the product - a fact that reflects the fermionic nature of the particles. The average is taken at the Heisenberg ground state, as well as the field operators are in the Heisenberg picture. Eq. (2.1) is now rewritten with the help of the time-ordering operator as

$$\begin{aligned} iG(\mathbf{r}, t; \mathbf{r}', t') = &\left\langle \hat{\psi}(\mathbf{r}, t)\hat{\psi}^{\dagger}(\mathbf{r}', t')\right\rangle_{|\Psi_0\rangle} \theta(t - t') \\ &- \left\langle \hat{\psi}^{\dagger}(\mathbf{r}', t')\hat{\psi}(\mathbf{r}, t)\right\rangle_{|\Psi_0\rangle} \theta(t' - t). \end{aligned} \tag{2.2}$$

Let us now shed some light on the very abstract and general definition of the Green's function - at least from the point of view of the levels of the many-particle system. The insertion of a complete set of eigenstates between the

field operators of Eq. (2.2) and working out the time-dependence of the field operators yields (Fetter & Walecka 1971)

$$\begin{aligned} iG(\mathbf{r},t;\mathbf{r}',t') = & \\ \sum_n \big[& \theta(t-t')e^{-i[E-E_n(N+1)](t-t')}\langle\Psi_0|\hat{\psi}(\mathbf{r})|\Psi_n^{N+1}\rangle\langle\Psi_n^{N+1}|\hat{\psi}^\dagger(\mathbf{r}')|\Psi_0\rangle \\ & -\theta(t'-t)e^{i[E-E_n(N-1)](t-t')}\langle\Psi_0|\hat{\psi}^\dagger(\mathbf{r}')|\Psi_n^{N-1}\rangle\langle\Psi_n^{N-1}|\hat{\psi}(\mathbf{r})|\Psi_0\rangle\big]. \end{aligned} \tag{2.3}$$

Finally, a Fourier transform with respect to $t-t'$ leads to the expression

$$\begin{aligned} G(\mathbf{r},\mathbf{r}';\omega) = \sum_n \Bigg[& \frac{\langle\Psi_0|\hat{\psi}(\mathbf{r})|\Psi_n^{N+1}\rangle\langle\Psi_n^{N+1}|\hat{\psi}^\dagger(\mathbf{r}')|\Psi_0\rangle}{\omega-[E_n(N+1)-E]+i\delta} \\ & + \frac{\langle\Psi_0|\hat{\psi}^\dagger(\mathbf{r}')|\Psi_n^{N-1}\rangle\langle\Psi_n^{N-1}|\hat{\psi}(\mathbf{r})|\Psi_0\rangle}{\omega+[E_n(N-1)-E]-i\delta}\Bigg], \end{aligned} \tag{2.4}$$

where the limit $\delta \to 0, \delta > 0$ is assumed. This result is called the Lehmann representation of the Green's function and is remarkable, since all the energy-dependence is found in the denominators of both terms in the above expression for the Green's function. We will now try to identify the energy differences there as the excitation energies of the system. Let us assume that the Heisenberg ground state $|\Psi_0\rangle$ corresponds to a system with N particles. As a consequence, the states $|\Psi_n^{N\pm1}\rangle$ must correspond to systems with $N+1$ and $N-1$ particles, respectively. The denominator of the first term can be rewritten as

$$\begin{aligned} \omega-[E_n-E] &= \omega-[E_n(N+1)-E(N)] \\ &= \omega-[E_n(N+1)-E(N+1)]-[E(N+1)-E(N)] \end{aligned} \tag{2.5}$$

since the energy E_n is related to the $N+1$ particle system. If we introduce the chemical potential

$$\mu(N) = E(N+1)-E(N) \tag{2.6}$$

and the n-th excitation energy

$$\Omega_n(N) = E_n(N)-E(N) \tag{2.7}$$

we can rewrite the Green's function in the Lehmann representation as

$$G(\mathbf{r},\mathbf{r}';\omega) = \sum_n \left[\frac{\langle\Psi_0|\hat{\psi}(\mathbf{r})|\Psi_n^{N+1}\rangle\langle\Psi_n^{N+1}|\hat{\psi}^\dagger(\mathbf{r}')|\Psi_0\rangle}{\omega-\mu-\Omega_n(N+1)+i\delta} + \frac{\langle\Psi_0|\hat{\psi}^\dagger(\mathbf{r}')|\Psi_n^{N-1}\rangle\langle\Psi_n^{N-1}|\hat{\psi}(\mathbf{r})|\Psi_0\rangle}{\omega-\mu+\Omega_n(N-1)-i\delta} \right] \tag{2.8}$$

where we have assumed the chemical potential μ to be independent of the number of particles of the system if this number is very large (e.g. in a solid $N \sim 10^{23}$), *i.e.* $\mu(N) = \mu(N-1) = \mu$.

The Green's function is neither analytic in the upper nor in the lower half plane of the complex numbers with respect to the energy argument ω. In some cases it is helpful to work with the so-called retarded Green's function (Fetter & Walecka 1971) $G^R(\mathbf{r},t;\mathbf{r}',t')$, defined as

$$iG^R(\mathbf{r},t;\mathbf{r}',t') = \left\langle \{\hat{\psi}(\mathbf{r},t),\hat{\psi}^\dagger(\mathbf{r}',t')\} \right\rangle_{|\Psi_0\rangle} \theta(t-t'). \tag{2.9}$$

with a corresponding Lehmann representation

$$G^R(\mathbf{r},\mathbf{r}';\omega) = \sum_n \left[\frac{\langle\Psi_0|\hat{\psi}(\mathbf{r})|\Psi_n^{N+1}\rangle\langle\Psi_n^{N+1}|\hat{\psi}^\dagger(\mathbf{r}')|\Psi_0\rangle}{\omega-\mu-\Omega_n(N+1)+i\delta} + \frac{\langle\Psi_0|\hat{\psi}^\dagger(\mathbf{r}')|\Psi_n^{N-1}\rangle\langle\Psi_n^{N-1}|\hat{\psi}(\mathbf{r})|\Psi_0\rangle}{\omega-\mu+\Omega_n(N-1)+i\delta} \right]. \tag{2.10}$$

It differs merely in the sign of the infinitesimal δ in the second term from the original (time-ordered) definition of the Green's function. All poles lie in the lower half plane rendering G^R analytic in the upper half plane. From the structure of the denominators we also see that the poles correspond to the excitation energies of the N-particle system due to a change of the particle number by ± 1.

These findings show that spectroscopic experiments in which a change in the particle number by ± 1 appears like photoemisson and inverse photoemisson are described by the one particle Green's function. However, excitations generated by the interaction of radiation with the system causing, *e.g.*, interacting particle-hole pairs are not captured by the concept of the one-particle Green's function. It would be tempting to look at absorption as a combination of photoemission and inverse photoemission, but finally, the electron

does never leave the interacting system and therefore the processes cannot be decoupled (Onida et al. 2002). It will be the two-particle Green's function that will be in charge of describing absorption processes.

2.2.2 Relation to Observables

Before we finish this section, let us annotate the relation of the Green's function to the observables of our system. Let $\hat{A}$ be a one particle operator which is given in the second quantization as

$$\hat{A} = \int \mathrm{d}^3 r \, \hat{\psi}^\dagger(\mathbf{r}) A(\mathbf{r}) \hat{\psi}(\mathbf{r}). \tag{2.11}$$

It is now possible to express the expectation value of this operator with respect to the ground state $|\Psi_0\rangle$ with the help of the Green's function

$$\langle \hat{A} \rangle = -i \int \mathrm{d}^3 r \lim_{\mathbf{r}' \to \mathbf{r}} A(\mathbf{r}) G(\mathbf{r}, t; \mathbf{r}', t'). \tag{2.12}$$

The application of this rule for the expectation value of an operator together with the commutation relations, Eq. (A.36), allows us to give an expression for the density $n(\mathbf{r})$

$$n(\mathbf{r}) = \langle \hat{\psi}^\dagger(\mathbf{r}) \hat{\psi}(\mathbf{r}) \rangle = -iG(\mathbf{r}, t; \mathbf{r}, t^+) \tag{2.13}$$

where we have introduced the quantity t^+ meaning that a limiting procedure $\lim_{t' \to t, t' > t}$ is thought to be present for the expression in which t^+ appears. Therefore, the particle density is just given by the diagonal of the Green's function. Another important quantity, the current density $\mathbf{j}(\mathbf{r})$, is obtained from the general formula (2.12). Starting form the operator of the current density $\hat{\mathbf{j}}(\mathbf{r})$ (Fetter & Walecka 1971), given by

$$\hat{\mathbf{j}}(\mathbf{r}) = \frac{1}{2i} \left([\nabla \hat{\psi}^\dagger(\mathbf{r})] \hat{\psi}(\mathbf{r}) - \hat{\psi}^\dagger(\mathbf{r}) [\nabla \hat{\psi}(\mathbf{r})] \right), \tag{2.14}$$

we apply a so-called hair-splitting trick (Zagoskin 1998) in order to place the gradients in front of the Green's function

$$\mathbf{j}(\mathbf{r}) = -\frac{1}{2} \lim_{t \to 0^-} \lim_{\mathbf{r} \to \mathbf{r}'} [\nabla_{\mathbf{r}'} - \nabla_{\mathbf{r}}] G(\mathbf{r}', t; \mathbf{r}, 0). \tag{2.15}$$

The total energy of an interacting many-particle system is also accessible through the Green's function and we just denote the result (which follows from a lengthy but straightforward algebra)

$$E = \langle H \rangle = -\frac{i}{2} \int \mathrm{d}^3 r \lim_{t' \to t^+} \lim_{\mathbf{r}' \to \mathbf{r}} \left[i \frac{\partial}{\partial t} + h(\mathbf{r}) \right] G(\mathbf{r}, t; \mathbf{r}', t') \tag{2.16}$$

with the single particle Hamiltonian from Eq. (A.1), see Appendix.

2.2.3 Physical Interpretation

The Green's function $G(\mathbf{r}, t; \mathbf{r}', t')$ in the form of Eq. (2.2) can also be understood in terms of adding and removing particles to the system. Let us consider the first term $\hat{\psi}(\mathbf{r}, t)\hat{\psi}^\dagger(\mathbf{r}', t')$. The second field operator $\hat{\psi}^\dagger(\mathbf{r}', t')$ acts as the creation of a particle at position $\mathbf{r}'$ and time t' whereas the first field operator $\hat{\psi}(\mathbf{r}, t)$ removes the particle at position $\mathbf{r}$ and time t. In between the two processes the particle propagates through time from t' to t. Analogously, the second term of Eq. (2.2) can be interpreted as a hole traveling back in time from t to t' (Feynman 1949*b*, Feynman 1949*a*). This interpretation supports the understanding of the Lehmann representation where the excitation energies correspond to a system with one particle added and subtracted, respectively.

2.2.4 Two Particle Green's Function

We have noted at the end of Section 2.2.1 that the one-particle Green's function is not capable of describing charge-neutral excitations, e.g. the interaction of a particle-hole pair with the many-body system. The concept of the one-particle Green's function (2.1) can be extended to any finite number of particles, say n. The n-particle Green's function is defined as (Zagoskin 1998)

$$\begin{aligned} & i^n G_{(n)}(\mathbf{r}_1, t_1, \ldots, \mathbf{r}_n, t_n; \mathbf{r}'_1, t'_1, \ldots, \mathbf{r}'_n, t'_n) \\ & \quad = \left\langle \hat{T} \left[\hat{\psi}(\mathbf{r}_1, t_1) \ldots \hat{\psi}(\mathbf{r}_n, t_n) \hat{\psi}^\dagger(\mathbf{r}'_n, t'_n) \ldots \hat{\psi}^\dagger(\mathbf{r}'_1, t'_1) \right] \right\rangle \end{aligned} \tag{2.17}$$

where creation and annihilation processes of n particles appear. Most widely used in many body theory is – apart from the one-particle Green's function

– the two-particle Green's function G_2, given by

$$i^2 G_2(\mathbf{r}_1, t_1, \mathbf{r}_2, t_2; \mathbf{r}_1', t_1', \mathbf{r}_2', t_2') = \left\langle \hat{T}\left[\hat{\psi}(\mathbf{r}_1, t_1)\hat{\psi}(\mathbf{r}_2, t_2)\hat{\psi}^\dagger(\mathbf{r}_2', t_2')\hat{\psi}^\dagger(\mathbf{r}_1', t_1')\right]\right\rangle . \tag{2.18}$$

We will see in the remaining part of this chapter that the two-particle Green's function is part of the particle-hole correlation function which is the key-ingredient for studying two-particle excitation processes like absorption.

2.3 Equation of Motion for the One Particle Green's Function

Now, we will study a system being subject to an external time-dependent (non-local) perturbation $u(\mathbf{r}, \mathbf{r}', t)$ and our aim is to learn how the Green's function is changing with respect to a variation of this perturbation, *i.e.* how the system will change from its ground state to an excited state. This method is also called the *functional-derivative method*. In this section we shall follow the ideas of Baym and Kadanoff (Baym & Kadanoff 1961, Baym 1962) as well as Schwinger and Martin (Schwinger 1951, Martin & Schwinger 1959). A more detailed review of the subject is found in Strinati (Strinati 1988).

The Hamiltonian of our system is now given by

$$\hat{H}_{\text{tot}} = \hat{H} + \hat{H}', \tag{2.19}$$

where $\hat{H}$ is the Hamiltonian of Eq. (A.37) and H' contains the perturbation

$$\hat{H}' = \int \mathrm{d}^3 r \int \mathrm{d}^3 r' \, \hat{\psi}^\dagger(\mathbf{r}) u(\mathbf{r}, \mathbf{r}', t) \hat{\psi}(\mathbf{r}'). \tag{2.20}$$

As it is explained in Appendix A it is useful to include the time-dependence of the state vector $|\Psi\rangle$ entirely in the operators which lead us to the Heisenberg picture. For studying the dependence of a many-body system on a perturbation where the solution to the unperturbed system is (at least formally assumed to be) known, however, the so-called interaction picture is used to describe state vectors and operators. In our notation the field operators are defined for the Heisenberg picture Eq. (A.38) but now the Hamiltonian $\hat{H}$ is merely a part of the total Hamiltonian corresponding to the unperturbed

system. In this picture both, the operators and the state vectors, are time-dependent, if the perturbation is so.

We proceed to define the time-evolution operator[1] $\hat{S}(t_2, t_1)$

$$\hat{S}(t_2, t_1) = T\left[e^{-i\int_{t_1}^{t_2} \mathrm{d}t\, \hat{H}'_I(t)}\right], \tag{2.21}$$

and the S-operator

$$\hat{S} = \hat{S}(\infty, -\infty), \tag{2.22}$$

where $\hat{H}'_I$ is the Hamiltonian $\hat{H}'$ in the interaction picture

$$\hat{H}'_I = \int \mathrm{d}^3 r \int \mathrm{d}^3 r'\, \hat{\psi}^\dagger(\mathbf{r}, t^+) u(\mathbf{r}, \mathbf{r}', t) \hat{\psi}(\mathbf{r}', t). \tag{2.23}$$

Note that the creation operator acts at infinitesimally larger time t^+ as the annihilation operator, since the Hamiltonian $\hat{H}'_I$ will be used in a time-ordered product which is not defined for operators at equal times. We shall drop the explicit reference of the latter operator to the interaction picture for the rest of this chapter. In addition, it is more convenient to employ the following short-hand notation for the sake of a simpler and more compact writing

$$\begin{aligned} 1 &\to \{\mathbf{r}_1, t_1\} \\ 1^+ &\to \{\mathbf{r}_1, t_1^+\} \\ d(1) &\to \mathrm{d}^3 r_1 \mathrm{d}t_1 \\ \delta(1,2) &\to \delta(\mathbf{r}_1 - \mathbf{r}_2)\delta(t_1 - t_2). \end{aligned} \tag{2.24}$$

Moreover, the Coulomb potential that we are using here is instantaneous in time

$$v(1,2) = v(\mathbf{r}_1, \mathbf{r}_2)\delta(t_1 - t_2). \tag{2.25}$$

Now we are in the position to define the *generalized* single- and two-particle Green's functions (Strinati 1988) as

$$iG(1,2) = \frac{\langle N|T[\hat{S}\hat{\psi}(1)\hat{\psi}^\dagger(2)]|N\rangle}{\langle N|T[\hat{S}]|N\rangle} \tag{2.26}$$

[1]The time-ordered exponential is to be understood in the way that the time-ordering acts upon the corresponding series expansion of the exponential function. Therefore, this expression is purely formal.

and

$$i^2 G_2(1,2;1',2') = \frac{\langle N|T[\hat{S}\hat{\psi}(1)\hat{\psi}(2)\hat{\psi}^\dagger(2')\hat{\psi}^\dagger(1')]|N\rangle}{\langle N|T[\hat{S}]|N\rangle}, \tag{2.27}$$

respectively. Here, $|N\rangle$ denotes the ground state of the unperturbed N-electron system. If the perturbation u is allowed to vanish, we arrive at the expressions for the ordinary single- and two-particle Green's functions Eqs. (2.1) and (2.18). Differentiating Eq. (2.26) with respect to t_1 we obtain – after lengthy algebra – an equation of motion for the generalized Green's function

$$\begin{aligned}\left[i\frac{\partial}{\partial t_1} - \hat{h}(1)\right] G(1,2) = \delta(1,2) + \int \mathrm{d}(3)\, u(1,3)G(3,2) \\ - i\int \mathrm{d}(3)\, v(1,3)G_2(1,3^+;2,3^{++}),\end{aligned} \tag{2.28}$$

where we have used the notation

$$u(1,2) = u(\mathbf{r}_1,\mathbf{r}_2,t_1)\delta(t_1-t_2). \tag{2.29}$$

From Eq. (2.28) we see that the equation of motion (EOM) for the single-particle Green's function also contains the two-particle Green's function. The reason for that is found at the EOM for the field operators Eq. (A.39) which has to be used to express the time-derivative of the field operators in Eq. (2.28). The term containing the Coulomb potential in (A.39) generates two additional field operators. As a consequence, the EOM for the n particle Green's function involves the $n+1$ particle Green's function. In this way a whole hierarchy of equations, involving higher order Green's functions can be derived (Mattuck & Theumann 1971, Mattuck 1992) which we annotate for the sake of simplicity in the absence of perturbation

$$\begin{aligned}&\left[i\frac{\partial}{\partial t_j} - \hat{h}(j)\right] G_n(1,\ldots,n;1',\ldots,n') = \\ &\sum_{l'=1'}^{n'} \delta(j,l')(-1)^{j+l'} G_{n-1}(1,\ldots,\hat{j},\ldots,n;1',\ldots,\hat{l}',\ldots,n') \\ &- i\int \mathrm{d}(\bar{1})\, v(j,\bar{1})G_{n+1}(\bar{1},1,\ldots,n;\bar{1}^+,1',\ldots,n'),\end{aligned} \tag{2.30}$$

where $\hat{j}$ stands for omitting the variable j.

2.3.1 Dyson Equation

The EOM for the single-particle Green's function, Eq.(2.28) is not suitable for application to real problems since it is coupled to a higher order Green's function after all. Our aim is therefore to somehow get rid of this two-particle Green's function. To this end, let us consider the variation of $G(1,2)$ with respect to the perturbation u. Starting from the definition of the Green's function, Eq. (2.26), we evaluate the variation of the latter as

$$\begin{aligned}\delta G(1,2) &= (-i)\delta\frac{\langle N|T[S\hat{\psi}(1)\hat{\psi}^\dagger(2)]|N\rangle}{\langle N|T[S]|N\rangle} \\ &= (-i)\frac{\langle N|\delta T[S\hat{\psi}(1)\hat{\psi}^\dagger(2)]|N\rangle}{\langle N|T[S]|N\rangle} - G(1,2)\frac{\langle N|\delta T[S]|N\rangle}{\langle N|T[S]|N\rangle},\end{aligned} \tag{2.31}$$

since all the time-dependence is contained in the S-operator through the time-dependent potential u. A procedure sketched in Ref. (Strinati 1988) finally leads to the desired result

$$\frac{\delta G(1,2)}{\delta u(\mathbf{r},\mathbf{r}';t)} = -G_2(1,\mathbf{r}'t;2,\mathbf{r}t^+) + G(1,2)G(\mathbf{r}'t,\mathbf{r}t^+). \tag{2.32}$$

The two-particle Green's function comes into play through the variation of the S-operator providing an additional product of two field operators. For the case of the derivation of the Dyson equation we now assume u to be a local perturbation

$$u(1,2) = u(1)\delta(1,2). \tag{2.33}$$

Doing so and using Eq. (2.32) enables us to rewrite the EOM for the single-particle Green's function as

$$\begin{aligned}\left[i\frac{\partial}{\partial t_1} - \hat{h}(1) - u(1)\right]G(1,2) &= \delta(1,2) \\ - i\int \mathrm{d}(3)\, v(1,3)\left[G(1,2)G(3,3^+) - \frac{\delta G(1,2)}{\delta u(3)}\right].\end{aligned} \tag{2.34}$$

From the last equation we recognize the expression for the Hartree potential (the electrostatic potential an electron feels due to the presence of the other electrons) which we will now include into the total classical potential, V by

$$V(1) = u(1) - i\int \mathrm{d}(2)\, v(1,2)G(2,2^+). \tag{2.35}$$

By virtue of the latter, the EOM reads

$$\left[i\frac{\partial}{\partial t_1} - \hat{h}(1) - V(1)\right] G(1,2) = \delta(1,2) + i\int \mathrm{d}(3)\, v(1,3)\frac{\delta G(1,2)}{\delta u(3)}. \quad (2.36)$$

Right now, the form of the EOM is not suitable to take the limit $u \to 0$. But let us apply the functional derivative identity Eq.(B.6) to the variation of the Green's function, yielding

$$\begin{aligned}\left[i\frac{\partial}{\partial t_1} - \hat{h}(1) - V(1)\right] G(1,2) &= \delta(1,2) \\ - i\int \mathrm{d}(3,4,5)\, v(1,3)G(1,4)\frac{\delta G^{-1}(4,5)}{\delta u(3)}G(5,2).&\end{aligned} \quad (2.37)$$

It is now convenient to introduce the *self-energy operator*

$$\Sigma(1,2) = -i\int \mathrm{d}(3,4)\, v(1,3)G(1,4)\frac{\delta G^{-1}(4,2)}{\delta u(3)}. \quad (2.38)$$

Note that the self-energy arising from this definition is also called *mass operator* and does not contain the Hartree-part

$$\Sigma_H(1,2) = -i\delta(1,2)\int \mathrm{d}(3)\, v(1,3)G(3,3^+). \quad (2.39)$$

When it is necessary we will explicitly denote if we use the self-energy Σ or if we include the Hartree-part and use $\Sigma' = \Sigma + \Sigma_H$ in place. Note that other authors (Baym & Kadanoff 1961) start from a different definition of the self-energy (including the Hartree part)

$$\Sigma'(1,2) = -i\int \mathrm{d}(3,4)\, v(1,3)G_2(1,3;4,3^+)G^{-1}(4,2), \quad (2.40)$$

which is equivalent to our definition by virtue of Eq. (2.32). With the help of the self-energy, the EOM is finally cast in the following form

$$\left[i\frac{\partial}{\partial t_1} - \hat{h}(1) - V(1)\right] G(1,2) - \int \mathrm{d}(3)\, \Sigma(1,3)G(3,2) = \delta(1,2). \quad (2.41)$$

This equation expresses *Dyson's equation* for the Green's function in a differential form and reveals the self-energy as an energy-dependent effective, non-local single-particle potential.

To finish this section, we shall reformulate the Dyson equation in an integral form. In the absence of the interaction v among the electrons the zeroth-order Green's function on the Hartree level (in the presence of the Hartree- and the external potential) satisfies the equation (Fetter & Walecka 1971)

$$\left[i\frac{\partial}{\partial t_1} - \hat{h}(1) - V(1)\right] G_0(1,2) = \delta(1,2). \tag{2.42}$$

By virtue of Eq. (B.5) (see Appendix B) we identify the inverse of G_0 as

$$G_0^{-1}(1,2) = \left[i\frac{\partial}{\partial t_1} - \hat{h}(1) - V(1)\right] \delta(1,2). \tag{2.43}$$

With the help of the identity stated above the EOM is recast as

$$\int \mathrm{d}(3)\, G_0^{-1}(1,3)G(3,2) = \delta(1,2) + \int \mathrm{d}(3)\, \Sigma(1,3)G(3,2). \tag{2.44}$$

Multiplying the last equation with $G_0(4,1)$ ($G^{-1}(2,5)$)and integrating over 1 (2) leads to the well-known formulations of the Dyson equation in terms of the irreducible self-energy Σ

$$G(1,2) = G_0(1,2) + \int \mathrm{d}(3,4)\, G_0(1,3)\Sigma(3,4)G(4,2) \tag{2.45}$$

$$G_0^{-1}(1,2) = G^{-1}(1,2) + \Sigma(1,2). \tag{2.46}$$

The propagation of the electron G is now governed by the free propagation G_0 plus a term Σ including exchange- and correlation effects. In practice the exact expression for the self-energy is not known and has therefore to be approximated. We will investigate such an approximation in the following section.

The Dyson equation can also be obtained for the case of a non-local perturbation u as introduced in Eq. (2.29) and with the help of the Green's function G_0 at the independent-particle level

$$\left[i\frac{\partial}{\partial t_1} - \hat{h}(1)\right] G_0(1,2) = \delta(1,2). \tag{2.47}$$

The derivation for the Dyson equation differs only by the fact that the perturbing potential and the Hartree potential are not present for G_0 but the

perturbing potential appears explicitly in the expression for the Dyson equation and the contribution of the Hartree potential is included in the self-energy. We denote the result for the inverse Green's function

$$G_0^{-1}(1,2) = G^{-1}(1,2) + u(1,2) + \Sigma(1,2). \tag{2.48}$$

This relation will be used in the derivation of the Bethe-Salpeter equation.

Finally, for the sake of a practical application, Dyson's for the Green's function, Eq. (2.45), shall be reformulated in terms of the so-called *quasi-particle wave functions*. To this end, the Lehmann representation of the Green's function, Eq. (2.8), is slightly modified (Schöne 2001) by introducing the Lehmann amplitudes

$$\begin{aligned} \psi_m(\mathbf{r}) &= \langle \Psi_0 | \hat{\psi}(\mathbf{r}) | \Psi_m^{N+1} \rangle \\ \psi_m^*(\mathbf{r}) &= \langle \Psi_m^{N+1} | \hat{\psi}^\dagger(\mathbf{r}) | \Psi_0 \rangle \end{aligned} \tag{2.49}$$

for $\bar{\Omega}_m > \mu$ and

$$\begin{aligned} \psi_m(\mathbf{r}) &= \langle \Psi_m^{N-1} | \hat{\psi}(\mathbf{r}) | \Psi_0 \rangle \\ \psi_m^*(\mathbf{r}) &= \langle \Psi_0 | \hat{\psi}^\dagger(\mathbf{r}) | \Psi_m^{N-1} \rangle \end{aligned} \tag{2.50}$$

for $\bar{\Omega}_m \leq \mu$, where the modified excitation energies are introduced for the $N \pm 1$ particle systems as

$$\bar{\Omega}_m = \begin{cases} \mu + E_m(N+1) - E(N+1), & N+1 \text{ particles} \\ \mu - E_m(N-1) + E(N-1), & N-1 \text{ particles} \end{cases} \tag{2.51}$$

and

$$\Omega_m = \bar{\Omega}_m - \mu. \tag{2.52}$$

With the help of the Lehmann amplitudes $\psi_m(\mathbf{r})$ and the excitation energies $\bar{\Omega}_m$ we may readily express the Green's function as

$$G(\mathbf{r}, \mathbf{r}'; \omega) = \sum_m \psi_m(\mathbf{r}) \psi_m^*(\mathbf{r}') \left[\frac{\theta(\bar{\Omega}_m - \mu)}{\omega - \bar{\Omega}_m + i\delta} + \frac{\theta(\mu - \bar{\Omega}_m)}{\omega - \bar{\Omega}_m - i\delta} \right]. \tag{2.53}$$

Note that the structure of this equation for G is similar to the one of the Green's function for non-interacting particles (Fetter & Walecka 1971)

$$G^0(\mathbf{r}, \mathbf{r}'; \omega) = \sum_m \phi_m(\mathbf{r}) \phi_m^*(\mathbf{r}') \left[\frac{\theta(\epsilon_m - \epsilon_F)}{\omega - \epsilon_m + i\delta} + \frac{\theta(\epsilon_F - \epsilon_m)}{\omega - \epsilon_m - i\delta} \right], \tag{2.54}$$

where the ϕ_m and ϵ_m are the single-particle wave functions and energies stemming form the single-particle Hamiltonian, Eq. (A.1). For this reason the Lehmann amplitudes are called *quasi-particle wave functions*. They are orthonormal and form a complete set of basis functions. For the non-interacting Green's function, Eq. (2.54), the following equation is easily obtained

$$\left[\omega - \hat{h}(\mathbf{r})\right] G^0(\mathbf{r}, \mathbf{r}'; \omega) = \delta(\mathbf{r} - \mathbf{r}'). \tag{2.55}$$

A combination of the above equation and the Dyson equation for $\omega = \Omega_m$ finally leads to the Dyson equation for the quasi-particle wave function

$$\hat{h}(\mathbf{r})\psi_m(\mathbf{r}) + \int \mathrm{d}^3 r' \, \Sigma(\mathbf{r}, \mathbf{r}'; \Omega_m)\psi_m(\mathbf{r}') = \Omega_m \psi_m(\mathbf{r}). \tag{2.56}$$

The second term in this equation represents a non-local and energy-dependent operator acting on the wave function. Hence, this eigenvalue problem is quite complicated to solve, since the eigenvalues Ω_m also enter the expression for the self-energy.

2.3.2 Hedin's Equations

From the Dyson equation, Eq. (2.45), it is clear that from the knowledge of the self-energy Σ the full interacting Green's function can be calculated. It shall be the aim of this section to light the way towards a self-consistent scheme which allows for the determination of the self-energy (Hedin 1965, Hedin & Lundquist 1969, Strinati 1988). We start by introducing the scalar irreducible vertex function

$$\tilde{\Gamma}(1, 2; 3) = -\frac{\delta G^{-1}(1, 2)}{\delta V(3)} \tag{2.57}$$

$$= \delta(1, 3)\delta(2, 3) + \frac{\delta \Sigma(1, 2)}{\delta V(3)}, \tag{2.58}$$

where the second equation is found by expressing G^{-1} with the help of the Dyson equation, Eq. (2.46), and by using the definition of the total classical potential V, Eq. (2.35). By using the chain rule for functional differentiation, the identity, Eq. (B.6), we obtain an integral equation for $\tilde{\Gamma}$

$$\tilde{\Gamma}(1, 2; 3) = \delta(1, 3)\delta(2, 3) + \int \mathrm{d}(4, 5, 6, 7) \, \frac{\delta \Sigma(1, 2)}{\delta G(4, 5)} G(4, 6) G(7, 5) \tilde{\Gamma}(6, 7; 3), \tag{2.59}$$

where the limit $u \to 0$ can be taken explicitly. We proceed to define the *inverse (longitudinal) dielectric matrix* ϵ^{-1} as

$$\epsilon^{-1}(1,2) = \frac{\delta V(1)}{\delta u(2)}. \tag{2.60}$$

It accounts for the change in the total classical potential due to changes in the external potential. By using the definition of the potential V, the dielectric matrix is expressed as

$$\epsilon^{-1}(1,2) = \delta(1,2) + \int \mathrm{d}(3)\, v(1,3)\chi(3,2). \tag{2.61}$$

In Eq. (2.61) the *polarizability* χ of the system has been introduced as a variation of the average particle density n which is known from Eq. (2.13).

$$\chi(1,2) = \frac{\delta n(1)}{\delta u(2)}. \tag{2.62}$$

The variation of the density with respect to the external potential is a measure for the polarization of the system and hence the polarizability χ is connected to the density-density correlation function from linear response theory through the relation

$$\chi_{nn}(1,2) = -i\frac{\langle N|T[\hat{S}\hat{n}'(1)\hat{n}'(2)]|N\rangle}{\langle N|T[\hat{S}]|N\rangle}, \tag{2.63}$$

with the density deviation operator $\hat{n}'$ defined as

$$\hat{n}'(1) = \hat{n}(1) - \langle \hat{n}(1)\rangle\,. \tag{2.64}$$

This latter connection will be investigated in more detail in the next chapter. By virtue of the bosonic character of the density deviation operators, we conclude that the polarization $\hat{\chi}$ is symmetric with respect to their arguments

$$\chi(1,2) = \chi(2,1). \tag{2.65}$$

Now, we are in the position to single out the term of χ which is irreducible with respect to the bare Coulomb interaction, by using the definition of the

inverse dielectric matrix

$$\begin{aligned}\chi(1,2) &= \int \mathrm{d}(3)\, \frac{\delta n(1)}{\delta V(3)} \frac{\delta u(3)}{\delta V(2)} \\ &= \int \mathrm{d}(3)\, \frac{\delta n(1)}{\delta V(3)} \epsilon^{-1}(3,2) \\ &= \int \mathrm{d}(3)\, \frac{\delta n(1)}{\delta V(3)} \left[\delta(3,2) + \int \mathrm{d}(4)\, v(3,4) \frac{\delta n(4)}{\delta u(2)}\right].\end{aligned} \tag{2.66}$$

With the definition of the *irreducible polarizability*

$$\tilde{\chi}(1,2) = \frac{\delta n(1)}{\delta V(2)}, \tag{2.67}$$

we can further write for the last equation

$$\chi(1,2) = \tilde{\chi}(1,2) + \int \mathrm{d}(3,4)\, \tilde{\chi}(1,3) v(3,4) \chi(4,2). \tag{2.68}$$

Through utilizing the identity Eq. (B.6) the irreducible polarizability is connected to the irreducible vertex function as follows

$$\tilde{\chi}(1,2) = -i \int \mathrm{d}(3,4)\, G(1,3) G(4,1) \tilde{\Gamma}(3,4;2). \tag{2.69}$$

As in the case of the full polarizability also the irreducible one is symmetric with respect to its arguments

$$\tilde{\chi}(1,2) = \tilde{\chi}(2,1), \tag{2.70}$$

which we deduce from Eq. (2.68). The dielectric matrix is now connected to the irreducible polarizability

$$\epsilon(1,2) = \delta(1,2) - \int \mathrm{d}(3)\, v(1,3) \tilde{\chi}(3,2), \tag{2.71}$$

which follows from the definition of the total classical potential. It is further convenient to define the *dynamically screened Coulomb interaction* W as

$$W(1,2) = \int \mathrm{d}(3)\, \epsilon^{-1}(1,3) v(3,2). \tag{2.72}$$

The screened interaction is related to the polarizability of the system through Eq. (2.61)[2]

$$W(1,2) = v(1,2) + \int \mathrm{d}(3,4)\, v(1,3)\chi(3,4)v(4,2). \tag{2.73}$$

The above equation provides a formal solution for W and, in addition, shows that the screened interaction obeys the symmetry condition

$$W(1,2) = W(2,1). \tag{2.74}$$

Another relation for the screened interaction is found by connecting it to the irreducible polarization. This is achieved, if we multiply Eq. (2.72) with $\epsilon(4,1)$, integrate over 1 and use the relation between the dielectric matrix and the irreducible polarizability, Eq. (2.71)

$$\begin{aligned} \int \mathrm{d}(1)\, \epsilon(4,1)W(1,2) &= \int \mathrm{d}(1,3)\, \epsilon(4,1)\epsilon^{-1}(1,3)v(3,2) \\ \int \mathrm{d}(1)\, \left[\delta(4,1) - \int \mathrm{d}(5)\, v(4,5)\tilde{\chi}(5,1)\right] W(1,2) &= v(4,2). \end{aligned} \tag{2.75}$$

By rearranging the terms of the above equation, we obtain

$$W(1,2) = v(1,2) + \int \mathrm{d}(3,4)\, v(1,3)\tilde{\chi}(3,4)W(4,2). \tag{2.76}$$

This integral equation can be seen as an alternative definition of W. Finally, we relate the self-energy to the irreducible vertex function and the screened interaction by using the chain rule of the functional differentiation and the relation between the inverse dielectric matrix and the screened interaction

$$\begin{aligned} \Sigma(1,2) &= -i \int \mathrm{d}(3,4,5)\, v(1^+,3)G(1,4)\frac{\delta G^{-1}(4,2)}{\delta V(5)}\frac{\delta V(5)}{\delta u(3)} \\ &= i \int \mathrm{d}(3,4,5)\, v(1^+,3)G(1,4)\tilde{\Gamma}(4,2;5)\epsilon^{-1}(5,3). \end{aligned} \tag{2.77}$$

Combining the inverse dielectric matrix and the Coulomb potential we obtain

$$\Sigma(1,2) = \int \mathrm{d}(3,4)\, W(1^+,3)G(1,4)\tilde{\Gamma}(4,2;3). \tag{2.78}$$

[2]In fact, the screened interaction potential W was introduced exactly in that way by Hubbard (Hubbard 1957, Hedin 1965).

By putting together a selected set of equations derived so far (Eqs. (2.78), (2.76), (2.69), (2.58)) for the determination of the self-energy Σ, we end up with the so-called Hedin's equations, which we want to denote explicitly

$$\Sigma(1,2) = \int \mathrm{d}(3,4)\, W(1^+,3) G(1,4) \tilde{\Gamma}(4,2;3) \tag{2.79}$$

$$W(1,2) = v(1,2) + \int \mathrm{d}(3,4)\, v(1,3) \tilde{\chi}(3,4) W(4,2) \tag{2.80}$$

$$\tilde{\chi}(1,2) = -i \int \mathrm{d}(3,4)\, G(1,3) G(4,1) \tilde{\Gamma}(3,4;2) \tag{2.81}$$

$$\tilde{\Gamma}(1,2;3) = \delta(1,3)\delta(2,3) + \frac{\delta \Sigma(1,2)}{\delta V(3)}. \tag{2.82}$$

This coupled set of equations together with Dyson's equation has to be solved iteratively and is conserving the total energy, the momentum, as well as the angular momentum (Baym & Kadanoff 1961, Baym 1962). In practice, approximations have to be employed, especially to the vertex function.

2.3.3 The GW Approximation

The famous GW approximation (Hedin 1965, Hedin & Lundquist 1969) represents the coarsest approximation to the irreducible vertex function, namely it consists of neglecting the variation of the self-energy with respect to the total classical potential V rendering it into the product of two delta functions

$$\tilde{\Gamma}_{\mathrm{GW}}(1,2;3) = \delta(1,3)\delta(2,3). \tag{2.83}$$

As a consequence, the remaining Hedin's equations reduce to a simpler form, which we shall denote here

$$\Sigma(1,2) = iG(1,2)W(1,2) \tag{2.84}$$

$$W(1,2) = v(1,2) + \int \mathrm{d}(3,4)\, v(1,3) \tilde{\chi}(3,4) W(4,2) \tag{2.85}$$

$$\tilde{\chi}(1,2) = -iG(1,2)G(2,1) \tag{2.86}$$

$$\tilde{\Gamma}_{\mathrm{GW}}(1,2;3) = \delta(1,3)\delta(2,3). \tag{2.87}$$

The self-energy is now simply a product of the Green's function and the screened interaction, therefore called GW approximation (GWA). Arising

from this approximation, the irreducible polarizability is a product of two Green's functions with their arguments interchanged, expressing the *random phase approximation* (RPA) for the latter quantity. It is therefore commonly denoted as $\chi_0(1,2)$.

2.4 Equation of Motion for the Two Particle Green's Function

2.4.1 The Bethe-Salpeter Equation

Having already assessed the equation of motion for the field operators and the one-particle Green's function, we want to extend this idea also to the two-particle Green's function. To this end, the two-particle correlation function L is readily introduced[3]

$$L(1,\mathbf{r}'t;2,\mathbf{r}t^+) = -G_2(1,\mathbf{r}'t;2,\mathbf{r}t^+) + G(1,2)G(\mathbf{r}'t,\mathbf{r}t^+) \tag{2.88}$$

By virtue of Eq. (2.32) we can rewrite this expression for L as a variation of the Green's function

$$L(1,\mathbf{r}'t;2,\mathbf{r}t^+) = \frac{\delta G(1,2)}{\delta u(\mathbf{r},\mathbf{r}',t)}. \tag{2.89}$$

By using the relation Eq. (B.6) and Dyson's equation for the inverse Green's function, we express the correlation function L as

$$\begin{aligned} L(1,\mathbf{r}'t;2,\mathbf{r}t^+) &= -\int \mathrm{d}(3,4)\, G(1,3)G(4,2)\frac{\delta G^{-1}(3,4)}{\delta u(\mathbf{r},\mathbf{r}',t)} \\ &= -\int \mathrm{d}(3,4)\, G(1,3)G(4,2)\frac{\delta}{\delta u(\mathbf{r},\mathbf{r}',t)}\left[G_0^{-1}(3,4) - u(3,4) - \Sigma(3,4)\right] \\ &= -\int \mathrm{d}(3,4)\, G(1,3)G(4,2)\Big[\delta(\mathbf{r},\mathbf{r}_3)\delta(\mathbf{r}',\mathbf{r}_4)\delta(t,t_3)\delta(t_3,t_4) + \frac{\delta\Sigma(3,4)}{\delta u(\mathbf{r},\mathbf{r}',t)}\Big] \\ &= G(1,\mathbf{r}t)G(\mathbf{r}'t,2) + \int \mathrm{d}(3,4)\, G(1,3)G(4,2)\frac{\delta\Sigma(3,4)}{\delta u(\mathbf{r},\mathbf{r}',t)}. \end{aligned} \tag{2.90}$$

[3]Note that the definition for the correlation function is not unique throughout the literature, *e.g.,* the original papers of Baym and Kadanoff (Baym & Kadanoff 1961, Baym 1962) use $L = +G_2 - GG$.

The application of the chain rule for functional differentiation to the variation of Σ yields

$$\frac{\delta\Sigma(3,4)}{\delta u(\mathbf{r},\mathbf{r}',t)} = \int \mathrm{d}(5,6)\,\frac{\delta\Sigma(3,4)}{\delta G(6,5)}\frac{\delta G(6,5)}{\delta u(\mathbf{r},\mathbf{r}',t)}, \tag{2.91}$$

where the variation of G is just the correlation function L. Hence, we can write

$$\begin{aligned} L(1,\mathbf{r}'t;2,\mathbf{r}t^+) &= G(1,\mathbf{r}t)G(\mathbf{r}'t,2) \\ &+ \int \mathrm{d}(3,4,5,6)\,G(1,3)G(4,2)\frac{\delta\Sigma(3,4)}{\delta G(6,5)}L(6,\mathbf{r}'t;5,\mathbf{r}t^+). \end{aligned} \tag{2.92}$$

Because of the topology of the diagrammatic structure of the above equation it does not only hold for the limit of equal times t, t^+ but also arbitrary values t_1', t_2' (Strinati 1988). We proceed to introduce the *effective two-particle interaction* Ξ

$$\Xi(3,5;4,6) = \frac{\delta\Sigma(3,4)}{\delta G(6,5)}. \tag{2.93}$$

With its help the equation of motion for L is expressed as

$$\begin{aligned} L(1,2;1',2') &= G(1,2')G(2,1') \\ &+ \int \mathrm{d}(3,4,5,6)\,G(1,3)G(4,2)\Xi(3,5;4,6)L(6,2;5,2'). \end{aligned} \tag{2.94}$$

This equation is known as the *Bethe-Salpeter* equation for the correlation function L. Historically earlier, the Bethe-Salpeter equation was formulated relativistically in context of nuclear physics for the T-matrix[4] (Salpeter & Bethe 1951). The Bethe-Salpeter equation is an equation of motion for the two-particle correlation- or Green's function and therefore contains all excitation processes caused by two particles, especially the creation and interaction of particle-hole pairs[5]. Since in optical excitations, one electron is transferred to a previously empty state, whereas in the original place of the electron, there is a hole now, these pairs of electrons and holes are interacting with one another and are therefore treated properly with the BSE and not by extracting excitation energies from the single-particle Green's function

[4]The T-matrix is defined as the solution to the equation $T(1,2;1',2') = \Xi(1,2;1',2') + \int \mathrm{d}(3,4,5,6)\,\Xi(1,4;1',3)G(3,6)G(5,4)T(6,2;5,2')$.

[5]Moreover, it contains all information about the linear transport in the system as well (Martin & Schwinger 1959).

only. At the end of this section we draw a relation between the correlation function L and the polarizability χ by inspection of Eqs. (2.88), (2.62) and (2.32)

$$\chi(1,2) = -iL(1,2;1^+,2^+). \tag{2.95}$$

An equivalent expression is found for the corresponding irreducible quantities (see next section)

$$\tilde{\chi}(1,2) = -i\tilde{L}(1,2;1^+,2^+). \tag{2.96}$$

Thus, the polarizability of the system under study is just a degenerate form of the two-particle correlation function.

2.4.2 Irreducible and Non-Interacting Correlation Functions

In order to gain more insight into the two particle effective interaction, Eq. (2.93), we shall split it into a *Hartree part* Ξ_H and an *irreducible part* $\tilde{\Xi}$, describing the correlation effects of the two interacting particles

$$\Xi(1,2;3,4) = \Xi_H(1,2;3,4) + \tilde{\Xi}(1,2;3,4). \tag{2.97}$$

Now, from the expression of the Hartree part of the self-energy, Eq. (2.39), we conclude that

$$\Xi_H(1,2;3,4) = -i\delta(1,3)\delta(2,4)v(1,4). \tag{2.98}$$

The *irreducible* two-particle correlation function $\tilde{L}$ is defined as the solution to the equation

$$\begin{aligned}\tilde{L}(1,2;1',2') &= G(1,2')G(2,1') \\ &+ \int \mathrm{d}(3,4,5,6)\, G(1,3)G(4,1')\tilde{\Xi}(3,5;4,6)\tilde{L}(6,2;5,2'),\end{aligned} \tag{2.99}$$

while it is connected to the full correlation function L by

$$\begin{aligned}L(1,2;1',2') &= \tilde{L}(1,2;1',2') \\ &+ \int \mathrm{d}(3,4,5,6)\, \tilde{L}(1,4;1',3)\Xi_H(3,5;4,6)L(6,2;5,2').\end{aligned} \tag{2.100}$$

The system of the above two equations is equivalent to the original Bethe-Salpeter equation, Eq. (2.94).

By neglecting completely the Coulomb interaction between the two particles, *i.e.*, setting the Hartree-part of the interaction kernel to zero, gives us the irreducible correlation function for two independent particles

$$L_0(1,2;1',2') = G(1,2')G(2,1'). \tag{2.101}$$

With the help of the latter, we recast the Bethe-Salpeter equation, Eq. (2.94) in its final form

$$\begin{aligned} L(1,2;1',2') &= L_0(1,2;1',2') \\ &+ \int \mathrm{d}(3,4,5,6)\, L_0(1,4;1',3)\Xi(3,5;4,6)L(6,2;5,2'). \end{aligned} \tag{2.102}$$

2.4.3 Approximations

As we have seen in the previous sections, the effective two-particle interaction Ξ contains a term which is given by the functional derivative of the self-energy with respect to the Green's function. Since in practice we cannot provide an exact expression for the self-energy, not to mention its dependence on the Green's function, the part $\tilde{\Xi}$ has to be approximated. We know from Hedin's equations that they are conserving in a way that the total number of particles, the total energy and the momentum and angular momentum is conserved (Hedin 1965). The same conserving properties we demand from the correlation function L and the effective interaction Ξ. In fact, one can show (Baym 1962) that if the self-energy is Φ-*derivable*, *i.e.*, there exists a functional Φ such that

$$\Sigma(1,2) = \frac{\delta\Phi}{\delta G(1,2)}, \tag{2.103}$$

the corresponding effective interaction kernel Ξ is a conserving quantity,

$$\Xi(1,2;3,4) = \frac{\delta^2\Phi}{\delta G(1,2)\delta G(4,3)}. \tag{2.104}$$

As a consequence, also the correlation function L obeys the conservation laws.

The simplest approximation to Ξ corresponds to neglecting the variation of the self-energy with respect to the Green's function, *i.e.*, taking only the Hartree part of the interaction kernel. It is therefore referred as the *Hartree*

approximation in the context of the effective two-particle interaction. This approximation is Φ-derivable and in fact the functional takes the simple form

$$\Phi_H = -i \int \mathrm{d}(1,2)\, G(1,1^+) v(1,2) G(2,2^+). \tag{2.105}$$

Analogously, it can be interpreted as the independent motion of particles in an effective potential and is the simplest approximation which is non-perturbative. Because of the presence of the two delta functions in the BSE, Eq. (2.102), only two variables remain to be integrated over and if we contract $1' \to 1^+$ and $2' \to 2^+$ we obtain

$$\begin{aligned} L(1,2;1^+,2^+) &= L_0(1,2;1^+,2^+) \\ &+ \int \mathrm{d}(3,4)\, L_0(1,3;1^+,3) v(3,4) L(4,2;4,2^+). \end{aligned} \tag{2.106}$$

With the help of the relations for the polarizability, Eq. (2.95) and Eq. (2.96) the above equation takes the form

$$\chi(1,2) = \chi_0(1,2) + \int \mathrm{d}(3,4)\, \chi_0(1,3) v(3,4) \chi(4,2), \tag{2.107}$$

where χ_0 is the irreducible polarizability at the Hartree level. Equation (2.107) is now recognized to be the Dyson equation for the polarizability within the random phase approximation (Fetter & Walecka 1971). From the simplest polarization diagram for the RPA in Fig. 2.2 we see that a virtual electron-hole pair is created. Only independent events of virtual electron-hole pairs appear in this approximation. Because the energy and momentum is conserved during the interaction, the quantum-mechanical phase of the electron-hole pair is immediately lost and does not affect another electron-hole pair. This is the reason it is called the "*random phase*" approximation (Zagoskin 1998).

A different kind of approximation is obtained if we consider the self-energy within the GW approximation, $\Sigma = iGW$. The variation of the latter with respect to the Green's function gives us the expression for the irreducible interaction

$$\tilde{\Xi}(1,2;3,4) = i\delta(1,4)\delta(3,2)W(1,2) + iG(1,2)\frac{\delta W(1,2)}{\delta G(4,3)}. \tag{2.108}$$

It contains an attractive interaction between the electron and the hole which is proportional to the screened Coulomb interaction W. In the second term

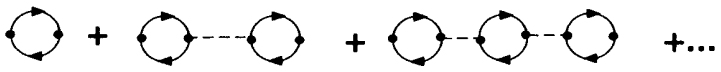

Figure 2.2: Diagrammatic expansion of the polarizability within the RPA. Figure taken from Reference (Zagoskin 1998).

the variation of the screened interaction with respect to the perturbation enters, which only plays a minor role in the description of the electron-hole correlation (Hanke & Sham 1980, Strinati 1982, Strinati 1984). This approximation stemming from the GWA is sometimes called *time-dependent screened Hartree-Fock approximation* for the interaction kernel. This can be understood if we replace the *screened* interaction W by the *bare* interaction v in Eq. (2.108), which would correspond to a time-dependent *unscreened* Hartree-Fock approximation in the original sense. Note that the δ functions in Eq. (2.108) contract different variables than in the expression for the Hartree part of the interaction, Eq. (2.98). Therefore it is not straight forward to map the Bethe-Salpeter equation to a 2-point equation in the presence of the screened Fock- (correlation) term, $-i\delta(1,4)\delta(2,3)W(1,2)$. However, as we will see in Chapt. 5 it is possible to obtain a Dyson-type equation for the 2-point polarizability at the level of the BSE, although at a high price.

If an approximate two-particle interaction of the form

$$\tilde{\Xi}(1,2;3,4) = i\delta(1,4)\delta(2,3)W(1,2), \tag{2.109}$$

is used for the BSE, it is called the *ladder approximation* to the BSE[6]. We arrive at this approximation by taking the first term of an expansion of the irreducible interaction with respect to the screened interaction. In the systems of our interest, namely those with a band gap, the density of electron-hole pairs at the Fermi level is low and it can be shown that only the so-called *ladder diagrams* (Fetter & Walecka 1971, Sham & Rice 1966) in the expansion of the scattering matrix T are dominating. Indeed by using the screened interaction, Eq. (2.109), in place of the irreducible one, we can restrict T to this class of diagrams.

[6]Sometimes this ladder approximation to the BSE is understood as the BSE.

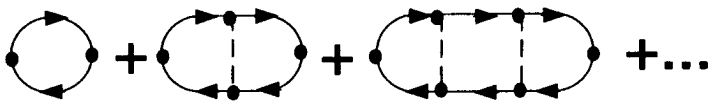

Figure 2.3: Diagrammatic expansion of the polarizability within the ladder approximation. Figure taken from Reference (Zagoskin 1998).

2.5 Linear Response

The functional derivative techniques established and applied in the previous sections deal mostly with first-order changes of the functionals under consideration. In this context the polarizability $\chi(1,2)$, Eq. (2.62), has already been introduced and we have seen its relation to the density-density correlation function, Eq. (2.63). Unfortunately, we cannot directly use this correlation function to obtain information about a perturbation process, which is switched on at a certain time. Under these circumstances, causal boundary conditions have to be used which cannot be described in terms of time-ordered quantities from MBPT. In this section we shall provide a formalism for describing the linear response of a given system, being initially in its ground state, to a time-dependent perturbation. This means we look at the first-order change of the expectation value of an operator with respect to the perturbing part of the Hamiltonian.

Let $\hat{O}(\mathbf{r},t)$ be a time-dependent operator. Then it can be shown that the linear change in its expectation value is given by a *Kubo formula* (Fetter & Walecka 1971, Strinati 1988)

$$\delta\langle\hat{O}(\mathbf{r},t)\rangle = i\int_{-\infty}^{t} \mathrm{d}t' \,\langle[\hat{H}'_I(t'),\hat{O}_I(\mathbf{r},t)]\rangle. \tag{2.110}$$

Here $\hat{H}'_I(t)$ is a perturbing part of the total Hamiltonian in the interaction picture, which is switched on at a certain time, say t_0. Note that also $\hat{O}$ is given in the interaction picture.

As an example we consider an external scalar potential $u(t)$ which is switched on at t_0

$$H'(t) = \int \mathrm{d}^3r\, \hat{n}(\mathbf{r},t)u(\mathbf{r},t), \tag{2.111}$$

where $\hat{n}$ is the density-operator of the unperturbed system. The evaluation of Eq. (2.110) for the expectation value of the density leads us after straightforward algebra to the expression[7]

$$\delta\langle\hat{n}(\mathbf{r},t)\rangle = -i\int \mathrm{d}^3r' \int_{-\infty}^{\infty} \mathrm{d}t' \,\langle[\hat{n}'(\mathbf{r},t),\hat{n}'(\mathbf{r}',t')]\rangle\theta(t-t')u(\mathbf{r}',t'). \quad (2.112)$$

From the equation stated above a *linear* relation between the change in the density and the perturbing potential can be seen. We therefore introduce the *retarded density-density correlation function* or *density-density response function* as[8]

$$\chi^R_{nn}(1,2) = -i\langle[\hat{n}'(1),\hat{n}'(2)]\rangle\theta(t_1-t_2). \quad (2.113)$$

Here, the step function $\theta(t_1-t_2)$ enforces the causality in the perturbation process, since the knowledge of the interaction between the system and the perturbation is only required for times after the perturbation has taken effect. For the time-ordered correlation functions, Eq. (2.62), also the interaction at future times has to be known, rendering it inappropriate for the description of an experimental situation. We can circumvent this issue and still utilize the benefits of MBPT if we compare the corresponding correlation functions to each other in the frequency domain. To this end we introduce the *general correlation function* for time-ordering and causal boundary conditions

$$\chi_{AB}(1,2) = -i\langle T[\hat{A}'(1)\hat{B}'(2)]\rangle \quad (2.114)$$

and

$$\chi^R_{AB}(1,2) = -i\langle[\hat{A}'(1),\hat{B}'(2)]\rangle\theta(t_1-t_2). \quad (2.115)$$

These functions describe the linear change of a physical quantity A due to the coupling of a perturbation to the quantity B. The corresponding operators $\hat{A},\hat{B}$ are assumed to be Hermitian and boson-like. Moreover, the primed symbols denote the deviation character

$$\hat{A}' = \hat{A} - \langle\hat{A}\rangle. \quad (2.116)$$

By Fourier transforming the time-dependence we arrive at the Lehmann representations of the time-ordered and the causal correlation functions

$$\chi_{AB}(\mathbf{r}_1,\mathbf{r}_2,\omega) = \sum_{s\neq 0}\left[\frac{A_s(\mathbf{r}_1)B_s(\mathbf{r}_2)^*}{E_0-E_s+\omega+i\delta} - \frac{A_s(\mathbf{r}_1)^*B_s(\mathbf{r}_2)}{-E_0+E_s+\omega-i\delta}\right] \quad (2.117)$$

[7]Note that this linear change has the meaning of a variation only in the case of a very small $u(t)$.

[8]Sometimes the symbol χ is used for the generalized susceptibility, which is defined as $\chi_{\mathrm{sus}} = \hbar^{-1}\chi$ (Fetter & Walecka 1971).

and

$$\chi^R_{AB}(\mathbf{r}_1, \mathbf{r}_2, \omega) = \sum_{s \neq 0} \left[\frac{A_s(\mathbf{r}_1) B_s(\mathbf{r}_2)^*}{E_0 - E_s + \omega + i\delta} - \frac{A_s(\mathbf{r}_1)^* B_s(\mathbf{r}_2)}{-E_0 + E_s + \omega + i\delta} \right], \quad (2.118)$$

respectively. In these expressions, the index s is labeling the eigenstates of the unperturbed system excluding the ground state. Moreover, the amplitudes, A_s and B_s are defined as the matrix elements of the operators $\hat{A}, \hat{B}$ with respect to the ground state $|N\rangle$ and the s^{th} excited state $|N, s\rangle$

$$A_s(\mathbf{r}) = \langle N | \hat{A}(\mathbf{r}) | N, s \rangle. \quad (2.119)$$

Now, the time-ordered correlation function differs from the causal one only in the sign of the infinitesimal δ in the second denominator. We immediately conclude from the above Eqs. (2.117) and (2.118) the following properties

$$\chi^R_{AB}(\mathbf{r}_1, \mathbf{r}_2, -\omega) = \chi^R_{AB}(\mathbf{r}_1, \mathbf{r}_2, \omega)^* \quad (2.120)$$

for real ω and more importantly

$$\chi_{AB}(\mathbf{r}_1, \mathbf{r}_2, \omega) = \chi^R_{AB}(\mathbf{r}_1, \mathbf{r}_2, \omega) \quad (2.121)$$

$$\chi_{AB}(\mathbf{r}_1, \mathbf{r}_2, -\omega) = \chi_{BA}(\mathbf{r}_2, \mathbf{r}_1, \omega) \quad (2.122)$$

for $\omega > 0$. It is therefore possible to obtain the time-ordered χ from standard many-body techniques for positive frequencies and obtain the retarded χ^R with the help of Eqs. (2.120) and (2.121).

Chapter 3

Density Functional Theory

3.1 Introduction

We have seen in Chapt. 2 that many body perturbation theory provides a systematic way of approximating the interactions to arbitrary order and to obtain the quantities of interest out of the Green's functions. However, there is no guarantee that higher order terms in the approximations will be small. In some cases not only a selected number of diagrams is taken for the approximation but infinite series are summed over without knowledge of their convergence and it is only the agreement with the observation that justifies the initial ansatz.

Another approach to the many-body problem, which is conceptually totally different, is the idea that the framework of calculating observables should not be based upon the complicated N-particle wave-function or Green's functions but rather upon the electron density $n(\mathbf{r})$. A first step towards this idea was taken independently by Thomas and Fermi. They neglected exchange- and correlation effects in the total energy and approximated the kinetic energy by the one for free electrons (the energy density is readily expressed in this case as $\epsilon_{\text{kin}}(n) \sim n^{2/3}$). Unfortunately, this approach had only minor success, but nevertheless it can be considered as the origin of the density functional concept.

Finally, it is due to the work of Hohenberg and Kohn that we understand how fundamental the concept of the electron density in an interacting many-electron system is. The essence of their pioneering work (Hohenberg & Kohn 1964) is the following statement, known as the *Hohenberg-Kohn (HK)*

theorem: *For a bound interacting many electron system there is a one to one correspondence between the external potential and the (ground state) electron density.* This correspondence is given up to a constant which, in turn, would only change the overall phase of the wave-function. As an immediate consequence, the total Hamiltonian of the system is determined by the density, since the operators of the kinetic energy and the Coulomb interaction are universal to a many-electron system. Therefore it is important to note that in principle from the ground state density alone all properties, derivable from the Hamiltonian, are accessible as functionals of the density. For this reason the framework is called *density functional theory* or DFT.

We shall approach the main theorems in a way that is inspired by the original papers of this field. For a mathematically rigorous treatment of density functional theory we refer the reader to the textbooks of Dreizler and Gross (Dreizler & Gross 1990) and, for a review in the spirit of mathematical rigor, including many formulations in terms of functional analysis and the relativistic aspect of DFT, to Eschrig (Eschrig 1996). Other excellent reviews shall be mentioned, namely the ones of Kohn (Kohn 1999), Jones (Jones & Gunnarsson 1989), Capelle (Capelle 2006) and Perdew and Kurth in Ref. (Fiolhais et al. 2003).

3.2 The Hohenberg-Kohn Theorem

Let us start with the proof of the theorem by Hohenberg and Kohn (Hohenberg & Kohn 1964). We assume that the many-electron system under consideration is in its non-degenerate ground state $|\Phi\rangle$ with a corresponding density $n(\mathbf{r}) = \langle\Phi|\hat{n}(\mathbf{r})|\Phi\rangle$, and let N be the total number of electrons. Clearly, the density is a functional of the external potential v_{ext}. The proof of the Hohenberg-Kohn theorem starts with the assumption that two external potentials v_1 and v_2, which differ by more than a constant, lead to the same density. From this assumption a contradiction is derived, which in turn completes the proof of the theorem. Let H_1 be the Hamiltonian subject to the external potential v_1 with a ground state $|\Phi_1\rangle$ and energy E_1. The same notation is applied to the Hamiltonian H_2 stemming from v_2. The total energy

E_1 is given by

$$E_1 = \langle \Phi_1 | \hat{H}_1 | \Phi_1 \rangle \tag{3.1}$$
$$= \int \mathrm{d}^3 r \, v_1(\mathbf{r}) n(\mathbf{r}) + \langle \Phi_1 | \hat{T} + \hat{U} | \Phi_1 \rangle.$$

From the Ritz minimum principle we can now relate the total energies E_1 and E_2

$$E_1 < \langle \Phi_2 | \hat{H}_1 | \Phi_2 \rangle \tag{3.2}$$
$$= \langle \Phi_2 | \hat{H}_2 | \Phi_2 \rangle + \langle \Phi_2 | \hat{H}_1 - \hat{H}_2 | \Phi_2 \rangle \tag{3.3}$$
$$= E_2 + \int \mathrm{d}^3 r \, n(\mathbf{r})[v_1(\mathbf{r}) - v_2(\mathbf{r})]. \tag{3.4}$$

By interchanging the indices 1 and 2 a similar relation is established for E_2

$$E_2 < E_1 + \int \mathrm{d}^3 r \, n(\mathbf{r})[v_2(\mathbf{r}) - v_1(\mathbf{r})]. \tag{3.5}$$

Finally, we arrive at the desired contradiction if we add the last two equations together, leading to

$$E_1 + E_2 < E_1 + E_2, \tag{3.6}$$

which completes the proof. Thus, we are allowed to write the external potential v_{ext} as a functional of the density in a well defined way

$$v_{\mathrm{ext}} = v_{\mathrm{ext}}[n]. \tag{3.7}$$

Note that the HK Theorem has been derived under the assumption of a *non-degenerate* ground state. However, this constraint is not necessary as has been demonstrated by Kohn (Kohn 1985). By looking again at the derivation of the theorem, the inclined reader might have raised two questions. First, the potential as a functional is defined, in principle, for a certain class of functions $n(\mathbf{r})$, for some of them it could be that there is no antisymmetric state $|\Psi\rangle$ reproducing it. This issue is addressed as the *N-representability* problem and it can be shown that all non-negative functions $n(\mathbf{r})$ which are normalized to N are N-representable (Dreizler & Gross 1990, Eschrig 1996). Second, we have assumed that for any given density there exists an external potential reproducing the density through the solution of the Schrödinger equation. Such a density is called *v-representable*, and there are in fact well

behaved densities, adding up to the number of electrons, that do not fulfill this criterion (Levy 1982). However, in practice it has always been possible to achieve v-representability within the desired accuracy.

From the HK theorem it is clear that through the unique relation of the density to the external potential and hence to the total Hamiltonian of the system, the wave-function is (up to an overall phase factor) a functional of the density

$$|\Psi\rangle = |\Psi[n]\rangle. \tag{3.8}$$

Moreover, *the expectation value of every observable is a functional of the ground state density*

$$\langle\Psi|\hat{O}|\Psi\rangle = O[n]. \tag{3.9}$$

Note, that also excited-states energies and wave-functions are (implicit) functionals of the density, since they are accessible through the knowledge of the Hamiltonian. However, in practice, it will be the ground state properties that are available through DFT.

Especially, the sum of the kinetic energy and the energy due to the mutual Coulomb interaction is a *universal* functional of the density, denoted by

$$F[n] = \langle\Phi|\hat{T} + \hat{U}|\Phi\rangle, \tag{3.10}$$

since it is valid for all many electron systems. Another important statement for the total energy is the following: *The total energy is a functional of the density, with its minimum value, the ground state energy, given at the ground state density.* This statement is known as the *Hohenberg Kohn minimum principle* (Hohenberg & Kohn 1964) but shall be demonstrated with the help of the *constrained search method* by Levy and Lieb (Levy 1982). The Ritz minimum principle provides us with the ground state energy E through the minimization of the functional

$$E = \min_{\{\Psi\}} \langle\Psi|\hat{H}|\Psi\rangle. \tag{3.11}$$

In this expression for the total energy, Ψ is the (mathematical) trial wave function. The idea of the constrained search is to decouple the minimization procedure into a step minimizing over all wave-functions that are related to a certain density and another step of minimizing over the densities themselves. Let us denote the set of all wave functions corresponding to a certain density

n as $\{\Psi(n)\}$. We now define a density functional for the total energy as[1]

$$\begin{aligned} E[n] &= \min_{\{\Psi(n)\}} \langle \Psi | \hat{H} | \Psi \rangle \\ &= F[n] + \int \mathrm{d}^3 r \, n(\mathbf{r}) v_{\mathrm{ext}}(\mathbf{r}), \end{aligned} \tag{3.12}$$

where the functional F is given by

$$F[n] = \min_{\{\Psi(n)\}} \langle \Psi | \hat{T} + \hat{U} | \Psi \rangle. \tag{3.13}$$

The total energy of the ground state is then given by minimizing the density functional $E[n]$, introduced above, with respect to the density

$$\begin{aligned} E &= \min_{\{n\}} E[n] \\ &= \min_{\{n\}} \left[F[n] + \int \mathrm{d}^3 r \, n(\mathbf{r}) v_{\mathrm{ext}}(\mathbf{r}) \right]. \end{aligned} \tag{3.14}$$

Thus, Eq. (3.14) expresses the HK minimum principle.

3.3 The Kohn-Sham Equations

Although the knowledge that every observable is a functional of the ground state density alone is an exciting fact from the theoretical point of view, the problem of how to obtain the ground state density in practice has not been addressed so far. It was due to the work of Kohn and Sham (Kohn & Sham 1965) to successfully map the fully interacting many-body problem to a single-particle problem with an effective single-particle potential bearing all the complicated structure of the mutual Coulomb interaction.

The main assumption for this mapping is that for any interacting system, there exists an effective single-particle potential $v_{\mathrm{eff}}(\mathbf{r})$ such that the ground state density of the interacting system equals the one obtained from the auxiliary non-interacting system. Therefore, the density also has to be *non-interacting v-representable*. As a first step towards the single particle

[1] This functional also depends on the explicit external potential, *i.e.*, $E = E[n, v_{\mathrm{ext}}]$.

equations, we make use of the HK minimum principle including the constraint of a constant number of particles by means of a Lagrange multiplier

$$\begin{aligned}\delta E[n] &= \int \mathrm{d}^3 r \, \frac{\delta}{\delta n(\mathbf{r})} \left[E[n] - \left(\varepsilon \int \mathrm{d}^3 r' \, n(\mathbf{r}') - N \right) \right] \delta n(\mathbf{r}) \\ &= \int \mathrm{d}^3 r \, \left[\frac{\delta E[n]}{\delta n(\mathbf{r})} - \varepsilon \right] \delta n(\mathbf{r}) = 0.\end{aligned} \tag{3.15}$$

It is now convenient to express the total energy of the interacting system in the following way

$$E[n] = T'[n] + \int \mathrm{d}^3 r \int \mathrm{d}^3 r' \, n(\mathbf{r}) v(\mathbf{r}, \mathbf{r}') n(\mathbf{r}') + \int \mathrm{d}^3 r \, v_{\mathrm{ext}}(\mathbf{r}) n(\mathbf{r}) + E_{\mathrm{xc}}[n], \tag{3.16}$$

where $T'[n]$ is the kinetic energy of the non-interacting system and E_{xc} is the so-called *exchange-correlation energy* which is defined by Eq. (3.16). Inserting Eq. (3.16) into Eq. (3.15) leads to

$$\int \mathrm{d}^3 r \, \left[\frac{\delta T'[n]}{\delta n(\mathbf{r})} + v_{\mathrm{eff}}(\mathbf{r}) - \varepsilon \right] \delta n(\mathbf{r}) = 0, \tag{3.17}$$

where the effective single-particle potential v_{eff} is defined as

$$v_{\mathrm{eff}}(\mathbf{r}) = v_{\mathrm{ext}}(\mathbf{r}) + v_H(\mathbf{r}) + v_{\mathrm{xc}}(\mathbf{r}). \tag{3.18}$$

In Eq. (3.18) the Hartree potential is clearly given by

$$v_H(\mathbf{r}) = \int \mathrm{d}^3 r \, v_{\mathrm{ext}}(\mathbf{r}) n(\mathbf{r}), \tag{3.19}$$

whereas the *exchange-correlation (xc) potential* $v_{\mathrm{xc}}(\mathbf{r})$ is given by

$$v_{\mathrm{xc}}(\mathbf{r}) = \left. \frac{\delta E_{\mathrm{xc}}[n']}{\delta n'(\mathbf{r})} \right|_{n'=n}. \tag{3.20}$$

In Eq. (3.20) the *xc*-energy functional has to be evaluated at the ground state density $n(\mathbf{r})$. Since for a non-interacting system subject to a single-particle potential $v_{\mathrm{eff}}(\mathbf{r})$ exactly the same variational equation, Eq. (3.17) can be derived, Kohn and Sham concluded that the ground state density of the interacting system can be obtained through the solution of the following single-particle Schrödinger equations

$$\left[-\frac{1}{2} \nabla^2 + v_{\mathrm{eff}}(\mathbf{r}) \right] \phi_j(\mathbf{r}) = \varepsilon_j \phi_j(\mathbf{r}). \tag{3.21}$$

Since the many-particle wave function for a non-interacting system is just a single Slater determinant, the density is readily expressed as (see Appendix C)

$$n(\mathbf{r}) = \sum_{j=1}^{N} |\phi_j(\mathbf{r})|^2. \tag{3.22}$$

The effective single-particle equations (3.21) are the *Kohn-Sham equations* which have to be solved self-consistently together with Eq. (3.22). The procedure of finding a solution to the Kohn-Sham equations is the following: We start from an initial guess for the effective potential. As a next step, Eq. (3.21) is solved from which the single-particle wave functions ϕ_j and energies ε_j are obtained. From these wave functions the density is calculated via Eq. (3.22) and again a new effective potential is constructed. Again, Eq. (3.21) is solved and this procedure is repeated until we arrive at a converged density. With the help of the ground state density, obtained from the Kohn-Sham equations the total energy may be expressed as

$$E = \sum_{j=1}^{\mathrm{N(occ.)}} \varepsilon_j - \frac{1}{2}\int \mathrm{d}^3r \int \mathrm{d}^3r'\, n(\mathbf{r})v(\mathbf{r},\mathbf{r}')n(\mathbf{r}') - \int \mathrm{d}^3r\, v_{\mathrm{xc}}(\mathbf{r})n(\mathbf{r}) + E_{\mathrm{xc}}[n]. \tag{3.23}$$

With the Kohn-Sham method it is possible to obtain the exact density, however, the success of this method depends on how well the *xc*-potential can be approximated as a functional of the density. Since it is the functional derivative of the *xc*-energy one has to find suitable approximations to it which are also not to complicated for the sake of a practical application.

3.4 The Local Density Approximation

A very simple approximation for the *xc*-energy functional is the *local density approximation* (LDA)

$$E_{\mathrm{xc}}^{\mathrm{LDA}}[n] = \int \mathrm{d}^3r\, \epsilon_{\mathrm{xc}}^{\mathrm{heg}}(n(\mathbf{r}))n(\mathbf{r}). \tag{3.24}$$

Here, $\epsilon_{\mathrm{xc}}^{\mathrm{heg}}$ is the *xc*-energy density (*i.e.,* the *xc*-energy per particle) of the homogeneous electron gas. Its exchange part is known analytically and the correlation part is also known exactly for the limit of high densities.

For arbitrary densities, Quantum Monte Carlo simulations have been performed and a parametrization of the correlation part is obtained by Ceperly (Ceperly 1978) and Ceperly and Alder (Ceperly & Alder 1980). Trivially, the LDA functional is exact for the homogeneous electron gas and also expected to be a good approximation only for the case of the nearly free electron gas, *i.e.,* for slowly varying densities as are present in metals. However, the LDA gives ionization energies of atoms and dissociation energies of molecules, both systems with a not too slowly varying density, within an accuracy of about 10-20%. And more surprisingly, the LDA gives bond lengths and geometries of molecules and solids typically with a quite high accuracy of about 1% (Kohn 1999). Shortly, in the next sections, we will give a hint why the LDA performs so well in these aspects.

3.5 The Total Energy

In this section we shall derive an expression for the total energy of an interacting many-electron system and relate this expression to the results obtained from DFT. Starting from the obvious expression of the total energy in terms of the constituting operators in the Hamiltonian we obtain

$$\begin{aligned} E &= \langle\Psi|\hat{T}|\Psi\rangle + \langle\Psi|\hat{U}|\Psi\rangle + \int \mathrm{d}^3r\, v_{\mathrm{ext}}(\mathbf{r})n(\mathbf{r}) \\ &= T + U + E_{\mathrm{ext}}. \end{aligned} \tag{3.25}$$

Now, the framework of density matrices[2] (see Appendix C) permits us to express the expectation values of the kinetic energy operator as

$$T = -\frac{1}{2}\int \mathrm{d}^3r \lim_{\mathbf{r}'\to\mathbf{r}} \nabla^2_{\mathbf{r}} n_1(\mathbf{r},\mathbf{r}'). \tag{3.26}$$

The contribution of the Coulomb part of the total energy on the other hand is given with the help of the pair correlation function (see Appendix C) as

$$U = \frac{1}{2}\int \mathrm{d}^3r \int \mathrm{d}^3r'\, n(\mathbf{r})n(\mathbf{r}')g(\mathbf{r},\mathbf{r}')v(\mathbf{r},\mathbf{r}'). \tag{3.27}$$

We proceed to introduce the *exchange-correlation (xc) hole*

$$n_{\mathrm{xc}}(\mathbf{r},\mathbf{r}') = n(\mathbf{r}')\left[g(\mathbf{r},\mathbf{r}') - 1\right], \tag{3.28}$$

[2]We could equally well use the concept of the Green's function, but following the approach of density matrices shall be more natural here.

which can be interpreted as a hole within the average density $n(\mathbf{r}')$ if an electron is present at $\mathbf{r}$. From the properties of the two-particle density matrix an important sum rule for the xc-hole can be derived

$$\int \mathrm{d}^3 r' \, n_{\mathrm{xc}}(\mathbf{r}, \mathbf{r}') = -1. \tag{3.29}$$

This sum rule expresses that the lack of charge in the vicinity of the electron at position $\mathbf{r}$ is exactly the charge of one electron. In this context, it is commonly believed that an important reason for the success of the LDA lies in the exact fulfillment of this sum rule. By means of the xc-hole the Coulomb part of the total energy can now be split into a Hartree part E_H and an xc-part U_{xc}

$$\begin{aligned} U &= \frac{1}{2} \int \mathrm{d}^3 r \int \mathrm{d}^3 r' \, n(\mathbf{r}) n(\mathbf{r}') v(\mathbf{r}, \mathbf{r}') + \frac{1}{2} \int \mathrm{d}^3 r \int \mathrm{d}^3 r' \, n(\mathbf{r}) n_{\mathrm{xc}}(\mathbf{r}, \mathbf{r}') v(\mathbf{r}, \mathbf{r}') \\ &= E_H + U_{\mathrm{xc}}. \end{aligned} \tag{3.30}$$

Summarizing the above findings, the expression for the total energy for the interacting system is given by

$$E = T + E_{\mathrm{ext}} + E_H + U_{\mathrm{xc}}. \tag{3.31}$$

Now, we want to draw a connection to the total energy of the non-interacting system by means of the Hellman-Feynman theorem. The mutual Coulomb interaction of the electrons shall now be scaled with a parameter λ and at the same time an external potential $v_{\mathrm{ext}}^{(\lambda)}$ is chosen in a way that the electron density of the system remains the same. Note that for $\lambda = 1$ the fully interacting system is recovered, whereas for $\lambda = 0$ the Kohn-Sham system is obtained. The change of the total energy subject to the λ-dependent potential is now given by virtue of the Hellman-Feynman theorem as

$$\frac{\partial E_\lambda}{\partial \lambda} = \int \mathrm{d}^3 r \, \frac{\partial v_{\mathrm{ext}}^{(\lambda)}(\mathbf{r})}{\partial \lambda} n(\mathbf{r}) + E_H + U_{\mathrm{xc}}^{(\lambda)}. \tag{3.32}$$

Here, the xc-part of U depends on λ through the xc-hole. An integration with respect to the interaction strength λ leads to

$$E - E' = \int \mathrm{d}^3 r \, \left[v_{\mathrm{ext}}(\mathbf{r}) - v_{\mathrm{ext}}^{(0)}(\mathbf{r}) \right] + E_H + \bar{U}_{\mathrm{xc}}, \tag{3.33}$$

where the E' denotes the total energy of the non-interacting system and $v_{\text{ext}}^{(0)}(\mathbf{r})$ corresponds to the Kohn-Sham effective potential. The xc-part $\bar{U}_{\text{xc}}$ is given in terms of an xc-hole which is averaged over all values of the interaction strength λ.

$$\bar{n}_{\text{xc}}(\mathbf{r},\mathbf{r}') = \int_0^1 \mathrm{d}\lambda\, n_{\text{xc}}^{(\lambda)}(\mathbf{r},\mathbf{r}'). \tag{3.34}$$

With the help of Eq. (3.16) and the total energy E' of the Kohn-Sham system we establish the important relation for the xc-energy

$$E_{\text{xc}}[n] = \frac{1}{2}\int \mathrm{d}^3r \int \mathrm{d}^3r'\, n(\mathbf{r})\bar{n}_{\text{xc}}(\mathbf{r},\mathbf{r}')v(\mathbf{r},\mathbf{r}'). \tag{3.35}$$

This relation was found independently by Harris and Jones (Harris & Jones 1974), Langreth and Perdew (Langreth & Perdew 1975) and Gunnarson and Lundquist (Gunnarsson & Lundqvist 1976). Finally, a comparison of the expressions for the total energy, Eqs. (3.16) and (3.33) yields

$$E_{\text{xc}} = \bar{U}_{\text{xc}} = U_{\text{xc}} + T_{\text{xc}}, \tag{3.36}$$

where $T_{\text{xc}} = T - T'$. From this relation the xc-energy is composed of a part containing exchange and correlation effects related to the Coulomb interaction and one being the difference of the kinetic energies of the interacting and non-interacting systems. For the pair correlation function entering U_{xc} it is not difficult to find good approximations, but it is the quite large contribution of the xc-part of the kinetic energy which has turned out to be difficult to approximate (von Barth 2004).

3.6 Beyond LDA

Besides the most obvious and simple approximation to the xc-energy, the LDA, one can think of a local functional using not only the density but also the spatial variations of the latter. Such an approximation is called a *generalized gradient approximation* (GGA), formally given in terms of the density and its gradients

$$E_{\text{xc}}^{\text{GGA}}[n] = \int \mathrm{d}^3r\, g(n(\mathbf{r}), |\nabla n(\mathbf{r})|, \ldots)n(\mathbf{r}). \tag{3.37}$$

Already in the work of HOHENBERG and KOHN (Hohenberg & Kohn 1964) a simpler version of such a general approximation is found. There, the energy is not only expanded in the density itself but also a term $|\nabla n|^2$ taking into account its variation is used. This kind of gradient expansion is called the *gradient expansion approximation* (GEA), however, it did not substantially improve over the LDA in its practical application. What is actually called the GGA is related to a second order expansion of the average *xc*-hole surrounding an electron. There are various parametrizations of the GGA available, among them we mention the PERDEW-WANG functional (Perdew & Wang 1992) and as an improvement over the latter, the one proposed by PERDEW, BURKE and ERNZERHOF (Perdew et al. 1998). The latter functional is known to improve the accuracy of bond-lengths and atomization energies compared to the LDA (Kohn 1958).

Other attempts towards approximating E_{xc} result into the exact treatment of the exchange-part of the total energy, E_{x}, since it is known analytically (see Ref. (Fiolhais et al. 2003) for details). The corresponding functional is called *exact exchange* or EXX functional. The advantage of the EXX is the fact that it is self-interaction free, *i.e.,* the self-interaction part of the Hartree energy is exactly counterbalanced by a corresponding part in the expression for the exchange part. This is, for instance, known to be not the case for the LDA. On the other hand, the correlation part has to be taken from another ansatz rendering the total expression for E_{xc} somewhat heterogeneous. Finally, we mention the existence of so-called *hybrid functionals*, being mostly a combination of the exact exchange functional and the GGA functional, where the weights of the individual parts are determined by a fitting parameter. In this work we shall, however, only use the LDA functional for the *xc*-potential.

3.7 The Role of the Kohn-Sham Energies

In Sect. 3.3 we used an auxiliary, non-interacting system in order to obtain the density and the total energy of the real, interacting system by means of the Kohn-Sham equations. There, the single-particle wave functions and energies are purely mathematical without any ad-hoc relation to the real system. The KS wave functions $\phi_j(\mathbf{r})$ are not the same as the quasi-particle wave functions in MBPT and the KS energies ε_j can not be used for the calculation of electron removal energies as this is the case in the Hartree-

Fock theory, *i.e.,* there is no Koopman's theorem in DFT. Nevertheless, the Kohn-Sham energies are frequently used for the band structure of real solids with remarkable success, except for the description of the band gap in insulators and semiconductors. In these systems the gap is usually twice as large as obtained from a DFT calculation.

We shall now investigate how the band gap is related to the Kohn-Sham energies and what difficulties will arise in this context. The definition of the band gap E_{gap} is given for a system of N particles by the difference of the ionization potential I and the electron affinity A

$$E_{\mathrm{gap}}(N) = I(N) - A(N) \tag{3.38}$$
$$I(N) = E(N-1) - E(N) \tag{3.39}$$
$$A(N) = E(N) - E(N+1). \tag{3.40}$$

By inspection of the expression for the band gap, it is seen to be a ground state quantity, depending on the total energy of systems with N, $N-1$ and $N+1$ particles. The relation between the differences in the total energy and the Kohn-Sham energies is established through *Janak's theorem*, which is discussed shortly now. The theorem states that for a Kohn-Sham orbital ϕ_j the corresponding energy ε_j is related to the change in the total energy with respect to the occupation number f_j by (Janak 1978)

$$\frac{\partial E(f_j)}{\partial f_j} = \varepsilon_N(f_j), \tag{3.41}$$

or in integral form

$$E(f_j) - E(f_j - 1) = \int_0^1 \mathrm{d}f\, \varepsilon_j(f_j + f - 1). \tag{3.42}$$

For an extended system where the number of particles is very large the Kohn-Sham energy of the highest occupied level will be independent of adding or removing an extra particle (Perdew & Levy 1983) and hence an application of Janak's theorem yields

$$-I(N) = \epsilon_N(N - \delta) \tag{3.43}$$
$$-A(N) = \epsilon_{N+1}(N + \delta), \tag{3.44}$$

where δ denotes a positive, infinitesimal fraction of a particle being added to or subtracted from the N-particle system. Consequently, we are able to

express the band gap (at least partially) in terms of Kohn-Sham energies

$$E_{\mathrm{gap}}(N) = \Delta\varepsilon(N) + \Delta_{\mathrm{xc}}(N). \tag{3.45}$$

Here, $\Delta\varepsilon(N)$ is the Kohn-Sham gap of the N-particle system and $\Delta_{\mathrm{xc}}(N)$ is the so-called *xc* derivative discontinuity

$$\Delta_{\mathrm{xc}}(N) = \varepsilon_N(N+\delta) - \varepsilon_N(N-\delta). \tag{3.46}$$

It is given in terms of the *xc*-energy by (Sham & Schlüter 1983)

$$\Delta_{\mathrm{xc}}(N) = \left.\frac{\delta E_{\mathrm{xc}}}{\delta n(\mathbf{r})}\right|_{N+\delta} - \left.\frac{\delta E_{\mathrm{xc}}}{\delta n(\mathbf{r})}\right|_{N-\delta}. \tag{3.47}$$

As a consequence of the discontinuity, the exchange-correlation potential shows a step each time the total number of particles passes an integer number. Moreover, it is possible to draw a relation to many body perturbation theory and express the discontinuity in terms of the self-energy (Sham & Schlüter 1983). Finally, it was shown by Godby that the underestimation of the band gap within the LDA is partially due to this discontinuity (Godby et al. 1986).

Chapter 4

Time-Dependent DFT

4.1 Introduction

Time-dependent DFT is based on the statement that the time-dependent (*td*) density of an interacting quantum many-particle system determines its external potential and hence the Hamiltonian up to a purely *td* function. This fact is known as the Runge–Gross theorem (Runge & Gross 1984, Gross et al. 1996). As a consequence, every observable is a functional of the *td* density of the many-body system. Moreover, it is possible to derive an effective single-particle Schrödinger equation from an action principle yielding the same density as the original interacting system. The effective potential entering this time-dependent version of the Schrödinger equation contains now a time-dependent exchange-correlation potential, which has to be approximated as in the case of a static *xc*-potential.

The field of application of TDDFT is mainly divided into two different categories. These are non-perturbative regimes (Marques & Gross 2004) and the linear (or higher order) response framework which is valid for weak external potentials. Within the linear response the so-called *exchange-correlation kernel* will play a central role, which is given by the variation of the *xc*-potential with respect to the density. Such an approach allows for the calculation of quantities related to various spectroscopic experiments, including optical spectroscopy (Reining et al. 2002), EELS, and dynamical structure factors (Onida et al. 2002) for instance. In this work, we will specialize in the latter approach of linear response.

Finally, we mention various review articles on which this chapter is based

on. These are the ones by Gross and co-workers (Gross et al. 1996), Gross and Kohn (Gross & Kohn 1990), Burke and Gross (Burke & Gross 1998), Maitra and co-workers (Maitra et al. 2002) and Marques and Gross (Marques & Gross 2004). A recent and very comprehensive work including a basic introduction as well as advanced topics is found in Ref. (Marques et al. 2006).

4.2 The Runge-Gross Theorem

The ground state formulation of DFT, which states that there is a one-to-one correspondence between densities and potentials, is derived from the Rayleigh-Ritz minimum principle for the total energy. A straight forward extension of the Hohenberg-Kohn theorem based on this principle to time-dependent densities and potentials is not possible, since there is no minimum principle available in that case. However, we are able to prove a theorem similar to the one of Hohenberg and Kohn which is not based on a minimum principle. This theorem, which is known as the *Runge-Gross theorem* states that the time-dependent density $n(\mathbf{r}, t)$ uniquely determines the time-dependent external potential $v_{\text{ext}}(\mathbf{r}, t)$ up to a purely time-dependent function. For this one-to-one correspondence between densities and potentials, however, two assumptions have to be taken. First, only densities are considered that evolve from a common *initial state* $|\Psi_0\rangle$ at an initial (finite) time t_0

$$|\Psi_0\rangle = |\Psi(t_0)\rangle, \tag{4.1}$$

which need not necessarily be the ground state or an eigenstate of the initial potential $v^0_{\text{ext}}(\mathbf{r}) = v_{\text{ext}}(\mathbf{r}, t_0)$. Second, the class of potentials is limited to those being expandable in a Taylor series around the initial time

$$v_{\text{ext}}(\mathbf{r}, t) = \sum_{j=0}^{\infty} \frac{1}{j!} v_j(\mathbf{r})(t - t_0)^j. \tag{4.2}$$

In this series, the $v_j(\mathbf{r})$ are the Taylor coefficients, depending on the spatial variable $\mathbf{r}$. These assumptions explicitly exclude potentials, that are switched on adiabatically at $t_0 = -\infty$.

For the proof of the Runge-Gross theorem we follow the ideas of the original paper by Runge and Gross (Runge & Gross 1984) and to some

extent GROSS and KOHN (Gross & Kohn 1990) and GROSS ET. AL, (Gross et al. 1996). We start from the time-dependent Schrödinger equation

$$i\frac{\partial}{\partial t}|\Psi(t)\rangle = \hat{H}(t)|\Psi(t)\rangle, \tag{4.3}$$

together with the initial condition Eq. (4.1), where the Hamiltonian $\hat{H}(t)$ is given by a combination of Eqs. (A.37) and (A.1) (see Chapt. 2) but with a *time-dependent* external single-particle potential $v_{\text{ext}}(\mathbf{r},t)$. For the following, we drop the explicit subscript of v_{ext} for convenience. We assume now that for two external potentials $v(\mathbf{r},t)$ and $v'(\mathbf{r},t)$ which differ by more than a purely time-dependent function the corresponding time-dependent densities $n(\mathbf{r},t)$ and $n'(\mathbf{r},t)$ are different. Since both external potentials are expandable in a Taylor series and differ by more than a purely time-dependent function, some of the expansion coefficients $v_j(\mathbf{r})$ and $v'_j(\mathbf{r})$ differ by more than a constant. As a consequence, there exists a smallest index $k \geq 0$ such that

$$v_k(\mathbf{r}) - v'_k(\mathbf{r}) = \frac{\partial^k}{\partial t^k}\left[v_k(\mathbf{r},t) - v'_k(\mathbf{r},t)\right]\big|_{t=t_0} \neq \text{const.} \tag{4.4}$$

This inequality shall be the basis to show that the current densities $\mathbf{j}(\mathbf{r},t)$ and $\mathbf{j}'(\mathbf{r},t)$ belonging to $v(\mathbf{r},t)$ and $v'(\mathbf{r},t)$ are different, and second, that the densities themselves are different. But first, we study the time evolution of the current density by means of the equation of motion

$$i\frac{\partial}{\partial t}\langle\Psi(t)|\hat{O}(t)|\Psi(t)\rangle = \langle\Psi(t)|\left(\frac{\partial}{\partial t}\hat{O}(t) + [\hat{O}(t),\hat{H}(t)]\right)|\Psi(t)\rangle. \tag{4.5}$$

By combining the equations of motion for $j(\mathbf{r},t)$ and $j'(\mathbf{r},t)$ we obtain (see Appendix D.1)

$$i\frac{\partial}{\partial t}\left[\mathbf{j}(\mathbf{r},t) - \mathbf{j}'(\mathbf{r},t)\right]\big|_{t=t_0} = in_0(\mathbf{r})\nabla[v(\mathbf{r},t_0) - v'(\mathbf{r},t_0)], \tag{4.6}$$

where $n_0(\mathbf{r}) = n(\mathbf{r},t_0)$. If the condition Eq. (4.4) is satisfied for $k=0$, the right hand side of Eq. (4.6) cannot vanish identically, and hence the currents become different at times infinitesimally later than t_0. For $k>0$ we have to apply the equation of motion k times. After some algebra (see Appendix D.2) we obtain

$$\left(i\frac{\partial}{\partial t}\right)^{k+1}\left[\mathbf{j}(\mathbf{r},t) - \mathbf{j}'(\mathbf{r},t)\right]\big|_{t=t_0} = in_0(\mathbf{r})\nabla\left\{\left(i\frac{\partial}{\partial t}\right)^{k}\left[v(\mathbf{r},t) - v'(\mathbf{r},t)\right]\big|_{t=t_0}\right\}. \tag{4.7}$$

From the above equation we see that also for $k > 0$ the currents evolve differently in time, starting from t_0. So far we have shown that the current densities stemming from two different external potentials are different. Now, based on these findings, we shall see that also the corresponding densities are different. To this end, we use the continuity equation

$$\frac{\partial}{\partial t} n(\mathbf{r}, t) + \nabla \mathbf{j}(\mathbf{r}, t) = 0, \tag{4.8}$$

take its $k+1$st derivative and use Eq. (4.7) to obtain

$$\left(\frac{\partial}{\partial t}\right)^{k+2} [n(\mathbf{r}, t) - n'(\mathbf{r}, t)]|_{t=t_0} = -\nabla \left[n_0(\mathbf{r}) \nabla w_k(\mathbf{r})\right], \tag{4.9}$$

where

$$w_k(\mathbf{r}) = \frac{\partial^k}{\partial t^k} \left[v(\mathbf{r}, t) - v'(\mathbf{r}, t)\right]|_{t=t_0}. \tag{4.10}$$

It remains to show that the right hand side of Eq. (4.9) cannot vanish identically. By assuming the contrary we will now deduce a contradiction. Doing so, we obtain the vanishing integral

$$I = \int \mathrm{d}^3 r \, n_0(\mathbf{r}) [\nabla w_k(\mathbf{r})]^2 = 0. \tag{4.11}$$

By virtue of the Green's theorem (see Appendix D.3) the integral is rewritten as

$$I = -\int \mathrm{d}^3 r \, w_k(\mathbf{r}) \nabla [n_0(\mathbf{r}) \nabla w_k(\mathbf{r})] + \oint \mathrm{d}\mathbf{S} \, [n_0(\mathbf{r}) w_k(\mathbf{r}) \nabla w_k(\mathbf{r})]. \tag{4.12}$$

For realistic potentials stemming from some external charge density it can be shown that they decay faster than $1/r$ and hence the surface integral in Eq. (4.12) vanishes (Gross & Kohn 1990). Now the first integral in Eq. (4.12) vanishes because of our assumption $\nabla [n_0(\mathbf{r}) \nabla w_k(\mathbf{r})] = 0$, and consequently also the integral in Eq. (4.11) has to be zero. This is a contradiction, since the density $n_0(\mathbf{r})$ is assumed to be non vanishing and positive, and $w_k(\mathbf{r}) \neq$ const., and hence the proof is complete.

Let us summarize what we have proved so far. Given two external, time-dependent potentials, which differ by more than an additive and purely time-dependent function, and a common initial state, the time-dependent densities subject to the two different potentials are different. Hence, the

time-dependent density uniquely determines the time-dependent potential up to a purely time-dependent function. The effect on the wave function of adding a purely time-dependent function to the external potential would show up as an additional time-dependent phase factor, which cancels out in the construction of any expectation value. As an immediate consequence, *in the presence of a time-dependent external potential, each observable is a unique functional of the time-dependent density.* The difference to a time-dependent version of the Hohenberg-Kohn theorem is located first, in the restriction to the class of Taylor-expandable potentials and second, in the fact that the correspondence between potentials and densities depends on the initial state. However, for a system evolving from its ground state, the initial state itself is by virtue of the Hohenberg-Kohn theorem a functional of the ground state density such that in this case the dependence on the initial state is lifted.

4.3 The Time Dependent Kohn-Sham Equations

As in the case of ground state DFT, in practice we need an auxiliary non-interacting system to calculate the electron density. For the time-dependent case this system now obeys the *time-dependent Kohn-Sham equations*, given by

$$i\frac{\partial}{\partial t}\phi_j(\mathbf{r},t) = \left[-\frac{1}{2}\nabla^2 + v_{\text{eff}}[n](\mathbf{r},t)\right]\phi_j(\mathbf{r},t) \tag{4.13}$$

where the $\phi_j(\mathbf{r},t)$ denote the Kohn-Sham orbitals and the density $n(\mathbf{r},t)$ is given by

$$n(\mathbf{r},t) = \sum_j^{\text{occ.}} |\phi_j(\mathbf{r},t)|^2. \tag{4.14}$$

By virtue of the Runge-Gross theorem, now the effective potential $v_{\text{eff}}[n](\mathbf{r},t)$ is a unique functional of the density $n(\mathbf{r},t)$. We then define the *time-dependent exchange-correlation potential* $v_{\text{xc}}[n](\mathbf{r},t)$ through the following equation

$$v_{\text{eff}}[n](\mathbf{r},t) = v_{\text{ext}}(\mathbf{r},t) + \int \mathrm{d}^3r' \, \frac{n(\mathbf{r}',t)}{|\mathbf{r}-\mathbf{r}'|} + v_{\text{xc}}[n](\mathbf{r},t). \tag{4.15}$$

This exchange-correlation potential has a functional dependence on the density of the system at the current and at all previous times, hence including its whole history. In principle, it also depends on the initial state $|\Psi\rangle$ (which comes into play through the Runge-Gross theorem) and the initial Kohn-Sham state $|\Phi\rangle$. Hence, the knowledge of this functional would solve all time-dependent (externally driven) Coulomb problems (Marques et al. 2006). In the ground state DFT we have seen that the exchange-correlation potential is the functional derivative of $E_{\mathrm{xc}}[n]$ with respect to the density. For the time-dependent *xc*-potential such a generating functional would be the *exchange-correlation action* $A_{\mathrm{xc}}[n]$. A possible expression for it has already been discussed in (Runge & Gross 1984)

$$A_{\mathrm{xc}} = \int_{t_0}^{t_1} \mathrm{d}t \, \langle \Psi(t) | i\frac{\partial}{\partial t} - \hat{H}(t) | \Psi(t) \rangle, \tag{4.16}$$

where the state $|\Psi(t)\rangle$ and the Hamiltonian $\hat{H}(t)$ are functionals of the time-dependent density and so is the action. Consequently, the *xc*-potential is expressed as (Runge & Gross 1984)

$$v_{\mathrm{xc}}(\mathbf{r}, t) = \frac{\delta A_{\mathrm{xc}}}{\delta n(\mathbf{r}, t)}. \tag{4.17}$$

However, it has been shown that such an action functional leads to an exchange-correlation kernel that violates causality (Gross et al. 1994) (see next subsection).

For the practical applicability of the time-dependent Kohn-Sham scheme an approximation to the exchange-correlation potential has to be used, as we already mentioned. The simplest and straight forward approximation is the *time-dependent* or *adiabatic* LDA (TDLDA or ALDA)[1]. Therein, the exchange-correlation functional of the traditional Hohenberg-Kohn density functional theory is used and evaluated at the time-dependent density

$$v_{\mathrm{xc}}^{\mathrm{ALDA}}[n](\mathbf{r}, t) = v_{\mathrm{xc}}^{\mathrm{LDA}}(n(\mathbf{r}, t)) = \frac{\mathrm{d}}{\mathrm{d}n} \left[n\epsilon_{\mathrm{xc}}^{heg}(n) \right] \Big|_{n=n(\mathbf{r},t)}. \tag{4.18}$$

This functional depends in a very simple manner on the exchange-correlation energy density $\epsilon_{\mathrm{xc}}^{heg}(n)$ being already present in the *xc*-energy of ground state DFT, Eq. (3.24).

[1]Both abbreviations are used in literature for the *xc*-potential in the context of the Kohn-Sham equations as well as for the *xc* kernel in the context of linear response (see next section).

4.4 Linear Response

For weak external potentials like present in optical spectroscopy a perturbative approach is more suitable than the direct solution of the *td* Kohn-Sham equations. From Sect 2.5 we know that the density-density response function which is due to an external potential

$$v_{\text{ext}}(1) = v^0_{\text{ext}}(\mathbf{r}_1) + \theta(t_1 - t_0)\delta v_{\text{ext}}(1) \tag{4.19}$$

being switched on at an initial time t_0 is given by

$$\chi^R_{nn}(1,2) = -i\theta(t_1 - t_2)\langle[\hat{n}'(1), \hat{n}'(2)]\rangle = \left.\frac{\delta n[v_{\text{ext}}](1)}{\delta v_{\text{ext}}(2)}\right|_{v_{\text{ext}}=v^0_{\text{ext}}}. \tag{4.20}$$

This means that the density responds linearly to a change in the perturbing potential δv_{ext} through the (density-density) response function χ:

$$\delta n(1) = \int \mathrm{d}(2)\, \chi^R_{nn}(1,2)\delta v_{\text{ext}}(2). \tag{4.21}$$

From now on we skip the explicit superscript for the retarded response function as well as the highlighting of the density-density correlation character unless it is necessary. As indicated in the above equation, the density is clearly a functional of the external or total potential through the solution of the time-dependent Schrödinger equation. Now, we want to relate the response function of the interacting system to the one of the associated non-interacting Kohn-Sham system by means of the chain rule of functional calculus

$$\chi(1,2) = \int \mathrm{d}(3)\, \left.\frac{\delta n(1)}{\delta v_{\text{eff}}(3)}\right|_{v_{\text{eff}}[v^0_{\text{ext}}]} \left.\frac{\delta v_{\text{eff}}(3)}{\delta v_{\text{ext}}(2)}\right|_{v^0_{\text{ext}}}. \tag{4.22}$$

The variation of the effective potential with respect to the external potential is guaranteed to exist by means of the Runge-Gross theorem and the assumption of non-interacting v-representability[2]: The effective potential is a functional of the density, which in turn, is a functional of the external potential. Inserting the expression for the effective potential, Eq. (4.15), into the

[2] As in the case of the ground state DFT it is assumed that there exists a potential for the non-interacting Kohn-Sham system which reproduces the density of the interacting system.

above equation and carrying out the derivative with respect to the external potential yields in combination with Eq. (2.67)

$$\chi(1,2) = \chi_{\mathrm{KS}}(1,2) + \int \mathrm{d}(3)\chi_{\mathrm{KS}}(1,3)\left.\frac{\delta[v_H(3)+v_{\mathrm{xc}}(3)]}{\delta v_{\mathrm{ext}}(2)}\right|_{v^0_{\mathrm{ext}}}, \tag{4.23}$$

where $\chi_{\mathrm{KS}}(1,2)$ denotes the irreducible response function $\tilde{\chi}(1,2)$ of the Kohn-Sham system and is given by

$$\chi_{\mathrm{KS}}(1,2) = \left.\frac{\delta n(1)}{\delta v_{\mathrm{eff}}(2)}\right|_{v_{\mathrm{eff}}[v^0_{\mathrm{ext}}]}. \tag{4.24}$$

Once again, we make use of the chain rule, as we again include a variation with respect to the density

$$\chi(1,2) = \chi_{\mathrm{KS}}(1,2) + \int \mathrm{d}(3,4)\chi_{\mathrm{KS}}(1,3)\left.\frac{\delta[v_H(3)+v_{\mathrm{xc}}(3)]}{\delta n(4)}\right|_{n_0}\left.\frac{\delta n(4)}{\delta v_{\mathrm{ext}}(2)}\right|_{v^0_{\mathrm{ext}}}. \tag{4.25}$$

Further evaluation of the variation of v_H and v_{xc} with respect to the density finally leads to the expression (Gross & Kohn 1985, Petersilka et al. 1996)

$$\chi(1,2) = \chi_{\mathrm{KS}}(1,2) + \int \mathrm{d}(3,4)\chi_{\mathrm{KS}}(1,3)[v(3,4)+f_{\mathrm{xc}}(3,4)]\chi(4,2), \tag{4.26}$$

where we have introduced the so-called *exchange-correlation kernel* $f_{\mathrm{xc}}(1,2)$ which is defined as the variation of the *xc*-potential with respect to the density, evaluated at the ground state density $n_0(\mathbf{r})$

$$f_{\mathrm{xc}}(1,2) = \left.\frac{\delta v_{\mathrm{xc}}[n](1)}{\delta n(2)}\right|_{n=n_0}. \tag{4.27}$$

The equation for the response function, Eq. (4.26) is also called the Dyson-type equation of linear response, because of its similarity to the Dyson equation for the polarizability with MBPT, Eq. (2.68). The only difference to that equation is the presence of the Kohn-Sham response function in place of the independent-particle one, and the appearance of an additional term in the kernel of the integral, namely the exchange-correlation kernel. As a functional, it depends *only* on the ground state density and contains all many-body effects up to first order in the density. As in the case of the *xc*-potential for the ground state, it has to be approximated in practice.

An explicit expression for the xc kernel is, however, obtained by a formal inversion of Eq. (4.26)

$$f_{\mathrm{xc}}(1,2) = \chi_{\mathrm{KS}}^{-1}(1,2) - \chi^{-1}(1,2) - v(1,2). \tag{4.28}$$

Investigations on the invertability of the response functions result into the statement that for time-dependent potentials which are switched on at a certain time t_0 the response function is invertible, given that the potential is Laplace-transformable (van Leeuwen 2006). This condition is much weaker than requiring the potential to be analytic at the switch-on time as in the case of the Runge-Gross theorem.

Looking at the Dyson equation of TDDFT, Eq. (4.26) we notice that the response functions χ_{KS} and χ are retarded quantities. It can be shown that in such a case, the xc kernel cannot be symmetric with respect to its arguments. However, if we think of the xc-potential as a variation of an xc action with respect to the density (see Eq. (4.17)) we obtain the xc kernel as a second variation

$$f_{\mathrm{xc}}(1,2) = \frac{\delta^2 A_{\mathrm{xc}}}{\delta n(1)\delta n(2)}, \tag{4.29}$$

which clearly is symmetric. This problem has been solved by VAN LEEUWEN by defining an action functional in the Keldysh formalism, where the xc kernel is symmetric with respect to the Keldysh pseudo-time (van Leeuwen 1998).

In view of the further outline of this thesis we switch to an explicit formulation in terms of $\mathbf{r}$ and t and apply a partial Fourier transform to the Dyson equation with respect to the time

$$\begin{aligned}\chi(\mathbf{r},\mathbf{r}';\omega) = \chi_{\mathrm{KS}}(\mathbf{r},\mathbf{r}';\omega) + \int \mathrm{d}^3x \int \mathrm{d}^3x'\, \chi_{\mathrm{KS}}(\mathbf{r},\mathbf{x};\omega) \\ \times[v(\mathbf{x}-\mathbf{x}') + f_{\mathrm{xc}}(\mathbf{x},\mathbf{x}',\omega)]\chi(\mathbf{x}',\mathbf{r}';\omega).\end{aligned} \tag{4.30}$$

In the frequency domain the Kohn-Sham response function can be worked out purely in terms of Kohn-Sham orbitals ϕ_i and energies ε_i by means of standard many-body techniques (Schöne 2001)

$$\chi_{\mathrm{KS}}(\mathbf{r},\mathbf{r}';\omega) = \sum_{i,j}(f_i - f_j)\frac{\phi_i^*(\mathbf{r})\phi_j(\mathbf{r})\phi_j^*(\mathbf{r}')\phi_i(\mathbf{r}')}{\varepsilon_i - \varepsilon_j + \omega + i\delta}, \tag{4.31}$$

where the f_i are the occupation numbers $f_i = \theta(\varepsilon_F - \varepsilon_i)$. Finally, the Dyson equation within TDDFT (4.30) can also be seen as a generalization of the case of the random phase approximation where $f_{\mathrm{xc}} \equiv 0$.

4.5 The xc Kernel

4.5.1 The Adiabatic LDA

Choosing the LDA functional for the time-dependent xc-potential leads us to the *adiabatic* LDA kernel (ALDA kernel) (Gross et al. 1996), which is local in space and time. In configuration space it is given by

$$f_{\mathrm{xc}}^{\mathrm{ALDA}}(\mathbf{r},t;\mathbf{r}',t') = \delta(\mathbf{r}-\mathbf{r}')\delta(t-t')\left.\frac{\mathrm{d}v_{\mathrm{xc}}^{\mathrm{LDA}}(n)}{\mathrm{d}n}\right|_{n=n_0(\mathbf{r})}. \tag{4.32}$$

A Fourier transform of the expression for the ALDA kernel from the time to the frequency variable gives

$$f_{\mathrm{xc}}^{\mathrm{ALDA}}(\mathbf{r},\mathbf{r}';\omega) = \delta(\mathbf{r}-\mathbf{r}')\left.\frac{\mathrm{d}v_{\mathrm{xc}}^{\mathrm{LDA}}(n)}{\mathrm{d}n}\right|_{n=n_0(\mathbf{r})}, \tag{4.33}$$

expressing the static (energy-independent) property of the ALDA. The combination of the LDA for the xc-potential and the ALDA kernel is sometimes called the *time dependent local density approximation* (TDLDA).

Although being a very simple approximation the ALDA kernel gives remarkably good results for the excitation spectra of isolated atoms, molecules and clusters (Marques et al. 2006). This kind of magic (which is also present to some extent in the LDA of the static DFT) is not fully understood yet. However, for the application to periodic systems, this approximation is not the method of choice as it has no long-range behavior.

4.5.2 Other Approximations

Besides the ALDA kernel, which is a pure density functional through its dependence on the LDA exchange-correlation potential, there exist many other approximations. Among them we mention the *PGG* kernel an approximation to a general TDOEP-kernel, derived by Petersilka, Grossmann and Gross in the context of exact exchange and time-dependent optimized effective potentials (Petersilka et al. 1996). It is an orbital functional and frequency-independent. Furthermore, there are attempts for a self-interaction correction to the ALDA kernel resulting into the development of the TDOEP-SIC, which should combine the advantages of the ALDA and TDOEP. For a detailed review of possible xc kernels we refer the reader to

the review article of Onida (Onida et al. 2002). A second class of approximation is obtained through a comparison to the equations of many body perturbation theory. The discussion of this kind of kernels shall, however, be shifted to the next chapter, since the formalism of TDDFT and MBPT will be strongly linked.

Chapter 5

Linking TDDFT and BSE

5.1 Introduction

In this chapter we shall investigate the relation between the TDDFT linear response equation and the BSE leading to approximations for the xc kernel. Before drawing these relations we briefly look at the connection between ground state DFT and many-body perturbation theory. It is the Sham-Schlüter equation which relates the exchange-correlation potential v_{xc} to the Green's function and the self-energy of MBPT (Sham 1985, Sham & Schlüter 1985)

$$\int \mathrm{d}(3,4) G_{\mathrm{KS}}(1,3)[\Sigma(3,4) - v_{\mathrm{xc}}(3)\delta(3,4)]G(4,1^+) = 0. \tag{5.1}$$

In practice, the equation is linearized, *i.e.,* the true Green's function is approximated by the Kohn-Sham one. In combination with the GW approximation to the self-energy this equation has been applied in order to study the xc-potential.

There are several attempts to use many-body perturbation theory in order to obtain an expression for f_{xc} reproducing the macroscopic dielectric function at the BSE level in a best possible way. They rely on either fully solving the BSE (Del Sole et al. 2003), or by assuming f_{xc} to be static (Reining et al. 2002) which can be lifted by imposing the equality of the four-point polarizabilites from TDDFT and BSE (Sottile et al. 2003). Furthermore, a many-body analog to the xc kernel is found by equating the two-point polarizabilities of BSE and TDDFT (Adragna et al. 2003, Marini et al. 2003).

5.2 The Role of f_{xc} in MBPT and TDDFT

In the work of Bruneval and co-workers a very general relation between the xc kernel of TDDFT and the quantities of MBPT is established (Bruneval et al. 2005, Bruneval 2005) which is reflected in the so-called ρ/G-approach. The same "tricks" that have been applied in Chapt. 2 are used for the derivation of an explicit expression for the xc kernel with the help of functional derivative techniques. Hereby, the xc-potential and the effective Kohn-Sham potential are made explicit in the Dyson equation for the Green's function. As central quantity the variation of the self-energy is not taken with respect to the Green's function as in the case of the Bethe-Salpeter equation but the variation is performed with respect to the density, which is possible due to the Runge-Gross theorem. Without derivation (Bruneval 2005) we note the relation of the xc kernel to the quantities of TDDFT linear response and MBPT

$$\begin{aligned} f_{\mathrm{xc}}(1,2) = \chi_{\mathrm{KS}}^{-1}(1,2) - \chi_0^{-1}(1,2) \\ - i \int \mathrm{d}(3,4,5)\chi_0^{-1}(1,5)G(5,3)G(4,5)\frac{\delta\Sigma(3,4)}{\delta n(2)}. \end{aligned} \tag{5.2}$$

From the structure of Eq. (5.2) the expression for f_{xc} is often split into two parts, called $f_{\mathrm{xc}}^{(1)}$ and $f_{\mathrm{xc}}^{(2)}$ (Stubner et al. 2004, Stubner 2005). The first part is given by

$$f_{\mathrm{xc}}^{(1)}(1,2) = \chi_{\mathrm{KS}}^{-1}(1,2) - \chi_0^{-1}(1,2). \tag{5.3}$$

which transforms the Dyson equation of TDDFT, Eq. (4.26), into the RPA version of MBPT, Eq. (2.107). This can be seen by insertion into Eq. (4.26). The first part has therefore the role of a gap-correction part of the kernel. The second part is responsible for the particle-hole correlations in a similar way as the part $\tilde{\Xi}$ of the Bethe-Salpeter kernel. It is purely expressed in terms of MBPT quantities (not the Kohn-Sham ones)

$$f_{\mathrm{xc}}^{(2)}(1,2) = -i \int \mathrm{d}(3,4,5)\chi_0^{-1}(1,5)G(5,3)G(4,5)\frac{\delta\Sigma(3,4)}{\delta n(2)}. \tag{5.4}$$

It is now the variation of the self-energy with respect to the density which plays the central role for the xc kernel. Again, by using the functional-derivative techniques of MBPT an equation for the determination of $\delta\Sigma/\delta\rho$ is found (Bruneval 2005). Using

$$\lambda = \delta(1,3)f_{\mathrm{xc}}^{(2)}(1,2) - \frac{\delta\Sigma(1,3)}{\delta n(2)} \tag{5.5}$$

as a coupling parameter, one obtains for the 0-th order in λ

$$f_{\mathrm{xc}}^{(2),0}(1,2) = 0 \tag{5.6}$$

which means that it leads to the RPA equation, as mentioned above. The first-order result with respect to λ is given by

$$\begin{aligned} f_{\mathrm{xc}}^{(2),1}(1,2) = &- i \int \mathrm{d}(3,4,5,7,8,9)\chi_0^{-1}(1,5)G(5,3)G(4,5)\Xi(3,8;4,7) \\ &\times G(7,9)G(9,8)\chi_0^{-1}(9,2) \end{aligned} \tag{5.7}$$

for the general interaction kernel Ξ. In combination with the GW-approximation for Σ and hence for Ξ the latter result is simplified to

$$\begin{aligned} f_{\mathrm{xc}}^{(2),1}(1,2) = &\int \mathrm{d}(3,4,5,9)\chi_0^{-1}(1,5)G(5,3)G(4,5)W(3,4) \\ &\times G(3,9)G(9,4)\chi_0^{-1}(9,2). \end{aligned} \tag{5.8}$$

Since the above expression contains the inverse of the quasi-particle response function, it has proven useful to not directly work with $f_{\mathrm{xc}}^{(2),1}$ but with the related quantity $T_{\mathrm{xc}}^{(2),1}$ which is defined by[1]

$$T_{\mathrm{xc}}^{(2),1}(1,2) = \int \mathrm{d}(3,4)\chi_0(1,3)f_{\mathrm{xc}}^{(2),1}(3,4)\chi_0(4,2). \tag{5.9}$$

Consequently, $T_{\mathrm{xc}}^{(2),1}$ is expressed more simply in first order as (see Eq. (2.101))

$$T_{\mathrm{xc}}^{(2),1}(1,2) = \int \mathrm{d}(3,4)G(1,3)G(4,1)W(3,4)G(3,2)G(2,4) \tag{5.10}$$

$$= \int \mathrm{d}(3,4)L_0(1,4;1^+,3)W(3,4)L_0(3,2;4,2^+). \tag{5.11}$$

For the sake of completeness another relation of the xc kernel to MBPT, which arises naturally, shall be mentioned. In the so-called ρ/G-approach (Bruneval et al. 2005) the part of the kernel $f_{\mathrm{xc}}^{(2)}$ plays the role of a two-point kernel in a Dyson equation for the irreducible polarizability[2]

$$\tilde{\chi} = \chi_0 + \chi_0 f_{\mathrm{xc}}^{(2)}\tilde{\chi} \tag{5.12}$$

[1] The usage of the symbol T is inspired by the work of Sottile which shall be partly discussed at a later point in this chapter.

[2] We allow to suppress the integrations in favor of a compact notation, where it is clear which variables are to be integrated over.

which is not difficult to derive from Hedin's equation (2.58) and with the help of the Runge-Gross theorem.

Now we summarize these findings with respect to their impact on the Dyson equation for TDDFT linear response. On the RPA-level the two equations are equivalent

$$\chi = \chi_{\text{KS}} + \chi_{\text{KS}}(v + f_{\text{xc}}^{(1)})\chi \tag{5.13}$$
$$\chi = \chi_0 + \chi_0 v \chi, \tag{5.14}$$

and for the exact response function the following two equations

$$\chi = \chi_{\text{KS}} + \chi_{\text{KS}}(v + f_{\text{xc}}^{(1)} + f_{\text{xc}}^{(2)})\chi \tag{5.15}$$
$$\chi = \chi_0 + \chi_0(v + f_{\text{xc}}^{(2)})\chi \tag{5.16}$$

and their inverse formulations

$$\chi_{\text{KS}}^{-1} = \chi^{-1} + v + f_{\text{xc}}^{(1)} + f_{\text{xc}}^{(2)} \tag{5.17}$$
$$\chi_0^{-1} = \chi^{-1} + v + f_{\text{xc}}^{(2)} \tag{5.18}$$

hold.

The considerations taken so far lay a very general framework for approximations to the xc kernel in terms of MBPT quantities and provide important insight for other methods of approximating the xc kernels.

5.3 A Perturbative Expansion of f_{xc}

A different approach to an expression for f_{xc} (to be more precise, for $f_{\text{xc}}^{(2)}$) is taken by Marini and co-workers (Marini et al. 2003). They impose the existence of an $f_{\text{xc}}^{(2)}$ which reproduces the BSE-polarizability. In the following we omit the superscript (2) when it is not of immediate importance. The irreducible polarization is now split into two parts

$$\tilde{\chi} = \chi_0 + \delta\tilde{\chi}, \tag{5.19}$$

where

$$\delta\tilde{\chi} = \chi_0 f_{\text{xc}} \tilde{\chi} \tag{5.20}$$
$$f_{\text{xc}} = \chi_0^{-1} \delta\tilde{\chi}\tilde{\chi}^{-1}. \tag{5.21}$$

By using Eq. (5.18) and Eq. (5.19) we obtain with the help of the above equation

$$\chi_0 f_{\mathrm{xc}} \chi_0 = \delta\tilde{\chi} - \delta\tilde{\chi} f_{\mathrm{xc}} \chi_0. \tag{5.22}$$

The quantities $\delta\tilde{\chi}$ and f_{xc} are now written as series in the order of W

$$\delta\tilde{\chi} = \sum_j \delta\tilde{\chi}^{[j]} \tag{5.23}$$

$$f_{\mathrm{xc}} = \sum_j f_{\mathrm{xc}}^{[j]}. \tag{5.24}$$

We are using the square brackets for indicating the order of the expansion of f_{xc} with respect to W, in contrast to the previous section, where the expansion index in the round brackets was referring to the coupling parameter λ (see Eq. (5.5)). From Eq. (5.22) and the latter series expansions, an iterative scheme for the determination of f_{xc} as an expansion in terms of W is obtained (Marini et al. 2003, Marini 2003)

$$f_{\mathrm{xc}}^{[n]} = \chi_0^{-1} \left[\delta\tilde{\chi}^{[n]} \chi_0^{-1} - \sum_{j=0}^{n-1} \delta\tilde{\chi}^{[j]} f_{\mathrm{xc}}^{[n-j]} \right], \tag{5.25}$$

with $\delta\tilde{\chi}^{[0]} = 0$. If we write down the above scheme explicitly for the orders 1 and 2 we obtain

$$f_{\mathrm{xc}}^{[1]} = \chi_0^{-1} \delta\tilde{\chi}^{[1]} \chi_0^{-1} \tag{5.26}$$

$$f_{\mathrm{xc}}^{[2]} = \chi_0^{-1} [\delta\tilde{\chi}^{[2]} - \delta\tilde{\chi}^{[1]} \chi_0^{-1} \delta\tilde{\chi}^{[1]}] \chi_0^{-1}. \tag{5.27}$$

The first order result stated above has also been found previously by Reining (Reining et al. 2002), Adragna and co-workers (Adragna et al. 2003) and Sottile (Sottile et al. 2003, Sottile 2003) and is exactly given by (see Eq. (5.10))

$$\delta\tilde{\chi}^{[1]}(1,2) = T_{\mathrm{xc}}^{(2),1}(1,2). \tag{5.28}$$

Higher order results for $\delta\tilde{\chi}^{[n]}$ are found more easily in Fourier space in terms of the correlation function L_0 and the matrix elements transforming from the transition space to the **G** space. Such higher order expressions will be mentioned in a later chapter being more specialized to the treatment of TDDFT linear response in Fourier space.

These first and second order approximations have been successfully applied in the study of the optical absorption as well as the electron energy

loss spectroscopy (EELS) of LiF and reproduce (at least in the second order approximation) the result of a BSE calculation quite accurately (Marini et al. 2003). All these expressions that we have seen so far are despite their correct behavior with respect to the description of the electron hole interaction quite difficult to evaluate. The question arises if there are simpler xc kernels bearing the same physics. The answer is both, yes and no, as we will see in the following.

5.4 Model Kernels

From a direct comparison of the TDDFT equations to the Bethe Salpeter equation it can be shown there that the long-range behavior of the exact xc kernel has the proportionality (Reining et al. 2002)

$$f_{\mathrm{xc}}(\mathbf{q},\omega) \sim -\alpha(\omega)\frac{1}{q^2}, \tag{5.29}$$

for small vectors $\mathbf{q}$. With an approximation of $\alpha(\omega) \equiv 0.2$ for instance, the continuum excitonic effects in bulk silicon are described very well. This kernel which is given in real space for a frequency-independent α as

$$f_{\mathrm{xc}}(\mathbf{r},\mathbf{r}') = -\frac{\alpha}{4\pi}v(\mathbf{r},\mathbf{r}'), \tag{5.30}$$

is also called the *RORO*-kernel named after the authors of the original paper Reining, Olevano, Rubio and Onida. It is important to note that this long-range term $1/q^2$ is not present in the ALDA, which explains why it does not work for extended systems.

This idea has been developed further by Botti and co-workers (Botti et al. 2004) in order to relate the (frequency dependent) parameter $\alpha(\omega)$ to macroscopic quantities of the system under study. In a static approach, α is related to the macroscopic dielectric constant ϵ_∞ and the kernel is called the static long-range contribution (LRC) kernel. It was found that for a series of simple semi-conductors, including Si and GaAs, an empirical law can be established, relating the parameter α to the dielectric constant,

$$\alpha = \frac{4.615}{\epsilon_M(0)} - 0.213. \tag{5.31}$$

The fitting parameters of the above equation are determined through a comparison to the results from the solution of the BSE. A more sophisticated approach targets towards a frequency-dependent model-kernel. Starting from

the model of a single Lorentz oscillator for the Kohn-Sham response function an expression for the xc kernel of the form

$$\alpha(\omega) = \alpha' + \beta'\omega^2 \tag{5.32}$$

is derived. It is called the dynamical LRC kernel (Botti et al. 2005). Again, the parameters α' and β' are related to macroscopic properties of the system, namely the dielectric constant ϵ_∞ and the plasmon frequency ω_p. As in the case of the static LRC kernel, through fitting the parameters for several systems to the results obtained from a solution of the BSE the following empirical law is established

$$\alpha' = 104.5\frac{\omega_g}{\epsilon_M(0)\omega_p^2} \tag{5.33}$$

$$\beta' = \frac{\alpha'}{\omega_g^2}, \tag{5.34}$$

where ω_g is an average value for the gap of the system and is to be placed in the middle of the absorption range (Botti et al. 2005). This dynamical model partially allows for the description of the strongly bound exciton in LiF. The strong peak related to this exciton is present, however, at higher energies. The price to pay for the capturing of the bound exciton is that the overall structure of the spectrum for higher energies is completely lost. We will present more details in one of the following chapters.

Following this way of modeling the kernel, a pure (ab-initio) expression is dropped in favor of a very simple kernel which indeed corresponds to a simple (frequency-dependent) rescaling of the Coulomb interaction. In general, we cannot expect such a kernel to work equally well for all systems, since it is purely proportional to the bare Coulomb potential.

Chapter 6

Optical Properties of Solids

In this chapter, we provide a description for the optical response for solids in the linear regime. Starting from basic electrodynamics, the path to the macroscopic dielectric properties based on the wave functions and energies of a single-particle band structure calculation is displayed. The dielectric function has been studied from first principles within the random phase approximation by Ehrenreich and Cohen (Ehrenreich & Cohen 1959), Adler and Wiser (Adler 1962) and Nozieres and Pines (Nozieres & Pines 1958*b*, Nozieres & Pines 1958*a*, Nozieres & Pines 1958*c*) and their main results are shown.

In the remaining part of this chapter, we go beyond the RPA involving electron-hole correlations which are important for the excitonic effects in semiconductors and insulators. We provide the Bethe-Salpeter equation for periodic solids following mainly the work of Strinati (Strinati 1984), Albrecht (Albrecht et al. 1998) and Rohlfing (Rohlfing & Louie 2000).

6.1 The Dielectric Function in Solids

We know from the Maxwell equations (see for instance (Jackson 1998)) that the electric displacement $\mathbf{D}$ is related to the electric field $\mathbf{E}$ through the polarization $\mathbf{P}$ as $\mathbf{D} = \mathbf{E} + \mathbf{P}$. In the linear or dipole approximation we connect the electric field and the electric displacement linearly

$$\mathbf{D}(\mathbf{r}, t) = \int \mathrm{d}t \int \mathrm{d}^3 r' \epsilon(\mathbf{r}, t; \mathbf{r}', t') \mathbf{E}(\mathbf{r}', t'). \tag{6.1}$$

In Eq. (6.1) the microscopic dielectric function $\epsilon(\mathbf{r}, t; \mathbf{r}', t')$ is in general a tensor of rank two except the case of cubic symmetry where it is a scalar. Since we restrict our study to solids now, a perfect crystal is assumed, the dielectric function is symmetric with respect to a translation of both spatial variables $\mathbf{r}$ and $\mathbf{r}'$ (see Eq. (E.18)), and it is homogeneous in time, which is expressed by its dependence on the time-difference $t - t'$

$$\epsilon(\mathbf{r} + \mathbf{R}, \mathbf{r}' + \mathbf{R}; t - t') = \epsilon(\mathbf{r}, \mathbf{r}'; t - t'). \tag{6.2}$$

By Fourier transforming Eq. (6.1) we obtain

$$\mathbf{D}_{\mathbf{G}}(\mathbf{q}, \omega) = \sum_{\mathbf{G}'} \epsilon_{\mathbf{G}\mathbf{G}'}(\mathbf{q}, \omega) \mathbf{E}_{\mathbf{G}'}(\mathbf{q}, \omega), \tag{6.3}$$

which is a matrix equation depending on the crystal momentum $\mathbf{q}$ and the frequency ω. The quantity $\epsilon_{\mathbf{G}\mathbf{G}'}$ is therefore called the *dielectric matrix*.

It has to be mentioned in this context that we are studying a system which is perturbed by a light wave which clearly constitutes a transverse field. Therefore one has to insert a vector potential $A(\mathbf{r}, t)$ into the kinetic part of the Hamiltonian $\mathbf{p} \rightarrow \mathbf{p} + \mathbf{A}(\mathbf{r}, \mathbf{t})/c$. By taking only the linear terms in $1/c$ a term $\mathbf{A}(\mathbf{r}, t) \cdot \mathbf{p}$ remains then as a perturbation in the total Hamiltonian, and the dielectric properties would have to be evaluated using correlations between currents and densities. Another complication in inhomogeneous solids is the fact that a purely longitudinal (transversal) electric field induces longitudinal *and* transverse currents which cannot be captured by the longitudinal-longitudinal and transverse-transverse dielectric functions alone. However, in the limit of very small $\mathbf{q}$ vectors a longitudinal perturbation given by a scalar potential leads to the same result as a transverse one. This fact was shown by Ambegaokar and Kohn (Ambegaokar & Kohn 1960) for crystals with cubic symmetry and by del Sole and Fiorino (Del Sole & Fiorino 1984) for systems with arbitrary symmetry.

6.2 The Self-Consistent Field Method

Here we want to review the results for the longitudinal dielectric response of periodic solids in the independent particle approximation (Adler 1962, Nozieres & Pines 1958*b*, Nozieres & Pines 1958*a*, Nozieres & Pines 1958*c*). Within this approximation, the electrons and holes are treated as *independent*

particles which is reflected in the self-consistent potential being the sum of an external potential and an induced screening potential which is purely electrostatic and does not bare any exchange and correlation effects. Additionally, the external potential is assumed to vary only on a macroscopic scale, hence have vanishing Fourier coefficients for $\mathbf{G} \neq 0$. This treatment is equivalent to the random phase approximation in MBPT for the polarizability.

Let us consider an electronic system given by a Hamiltonian

$$\begin{aligned} \hat{H}(t) &= \hat{H}_0 + \hat{V}(t) \\ \hat{V}(t) &= \hat{V}_{\text{ext}}(t) + \hat{V}_{\text{scr}}(t) \end{aligned} \tag{6.4}$$

subject to an external potential $v_{\text{ext}}(\mathbf{r}, t)$ and an induced screening potential $v_{\text{scr}}(\mathbf{r}, t)$. For the derivation of the polarizability within the independent particle approximation the Liouville equation for the density operator is then linearized with respect to the density change. For the unperturbed system, the electrons are assumed to be described by an effective single-particle potential

$$\hat{H}_0|n\mathbf{k}\rangle = \varepsilon_{n\mathbf{k}}|n\mathbf{k}\rangle, \tag{6.5}$$

whereas for the external perturbation we assume a monochromatic wave with a time-dependence

$$v_{\text{ext}} \sim e^{-i(\omega+i\delta)t} \tag{6.6}$$

which is switched on adiabatically due to the infinitesimal δ. We denote the result for the polarizability χ_0 in terms of the single-particle states $|n\mathbf{k}\rangle$, energies $\varepsilon_{n\mathbf{k}}$, and occupation numbers $f_{n\mathbf{k}}$ which are given by the Fermi-Dirac distribution at zero temperature. If transformed to Fourier space, χ_0 is given by

$$\chi^0_{\mathbf{G}\mathbf{G}'}(\mathbf{q}, \omega) = \frac{1}{V} \sum_{nm\mathbf{k}} \frac{f_{n\mathbf{k}} - f_{m\mathbf{k}+\mathbf{q}}}{\varepsilon_{n\mathbf{k}} - \varepsilon_{m\mathbf{k}+\mathbf{q}} + \omega + i\delta} M_{nm\mathbf{k}}(\mathbf{q}, \mathbf{G}) M^*_{nm\mathbf{k}}(\mathbf{q}, \mathbf{G}'), \tag{6.7}$$

where the states m and n run over both spins. In similarity to the Lehmann representation of the response function, Eq. (2.118), the pole structure is spotted in the denominators and the whole spectrum is a superposition of Lorentzian peaks at the single-particle energy differences $\varepsilon_{n\mathbf{k}} - \varepsilon_{m\mathbf{k}+\mathbf{q}}$. The quantities $M_{nm\mathbf{k}}(\mathbf{q} + \mathbf{G})$ which appear in Eq. (6.7) are defined as the $\mathbf{q}$-dependent matrix elements between the single-particles states $|n\mathbf{k}\rangle$

$$M_{nm\mathbf{k}}(\mathbf{q}, \mathbf{G}) = \langle n\mathbf{k}|e^{-i(\mathbf{q}+\mathbf{G})\mathbf{r}}|m\mathbf{k} + \mathbf{q}\rangle \tag{6.8}$$

In this formulation the *local field effects* are already included. They are explained in the following way. An external potential which varies only on a macroscopic scale can nevertheless induce a screening field which varies on a microscopic (atomic) scale for an inhomogeneous system. These local-field effects are accounted for in the formalism since the whole Fourier representation of the induced screening potential v_{scr} is used in the derivation of Eq. (6.7) and not only the 00 component. With the help of the relation Eq. (2.71) in Fourier space a relation between the total and the external potential is established

$$v_{\mathbf{0}}^{\mathrm{tot}}(\mathbf{q},\omega) = \epsilon_{\mathbf{00}}^{-1}(\mathbf{q},\omega) v_{\mathbf{0}}^{\mathrm{ext}}(\mathbf{q},\omega), \tag{6.9}$$

which is valid since $v_{\mathbf{G}}^{\mathrm{ext}}(\mathbf{q},\omega) = v_{\mathbf{0}}^{\mathrm{ext}}(\mathbf{q},\omega)\delta_{\mathbf{G},\mathbf{0}}$. From Eq. (6.9) it is seen that the 00 Fourier coefficient of the inverse *microscopic* dielectric matrix relates the *macroscopic* external and self-consistent potentials. Therefrom and from the definition of the dielectric function, Eq. (2.60), the *macroscopic dielectric function* ϵ_M is given by (Adler 1962)

$$\epsilon_M(\mathbf{q},\omega) = \frac{1}{\epsilon_{\mathbf{00}}^{-1}(\mathbf{q},\omega)}. \tag{6.10}$$

It is therefore not the spatial average of the microscopic dielectric function itself, but the inverse of the average inverse microscopic dielectric function which connects the macroscopic external and self-consistent fields. This relation, Eq. (6.10), is one of the key results of this chapter since it allows for the determination of a macroscopic quantity, which can be measured by experiments, from a microscopic and fully ab-initio description of a crystal. With the help of the macroscopic dielectric function a variety of other spectroscopically measurable quantities are obtained. Among them we mention the loss function $L(\mathbf{q},\omega)$ defined by

$$L(\mathbf{q},\omega) = -\mathrm{Im}\frac{1}{\epsilon_M(\mathbf{q},\omega)}, \tag{6.11}$$

which describes, for instance, the EELS.

If we neglect the induced local fields in the screening potential on the other hand, we can denote a very simple expression for the macroscopic dielectric function in terms of the independent-particle response function χ_0

$$\epsilon_M(\mathbf{q},\omega) = 1 + v(\mathbf{q})\chi_0(\mathbf{q},\omega). \tag{6.12}$$

The insertion of Eq. (6.7) into Eq. (6.12) finally gives an explicit expression for the macroscopic dielectric function in the absence of local fields

$$\epsilon_M(\mathbf{q},\omega) = 1+\frac{4\pi}{Vq^2}\sum_{nm\mathbf{k}}\frac{f_{n\mathbf{k}}-f_{m\mathbf{k}+\mathbf{q}}}{\varepsilon_{n\mathbf{k}}-\varepsilon_{m\mathbf{k}+\mathbf{q}}+\omega+i\delta}M_{nm\mathbf{k}}(\mathbf{q},0)M^*_{nm\mathbf{k}}(\mathbf{q},0), \quad (6.13)$$

where V denotes the crystal volume.

6.3 The Long Wavelength Limit

Since we are mostly interested in *optical* perturbations having wavelengths that are much larger compared to the size of the crystal unit cell, the associated momentum $\mathbf{q}$ is very small and can be treated in the limit of $\mathbf{q} \to 0$. This limit has, however, to be taken analytically in the expression for the macroscopic dielectric function since the Coulomb potential becomes singular in this case and has to be compensated by χ_0. First, we investigate the matrix elements $M_{nm\mathbf{k}}(\mathbf{q} \to 0, 0)$ within this limit. From $\mathbf{k}\cdot\mathbf{p}$ perturbation theory we obtain for non-degenerate states

$$M_{nm\mathbf{k}}(\mathbf{q}\to 0,0) = \delta_{nm} + \frac{q\hat{\mathbf{\Omega}}_q\mathbf{P}_{nm\mathbf{k}}}{\epsilon_{m\mathbf{k}}-\epsilon_{n\mathbf{k}}}(1-\delta_{nm}), \quad (6.14)$$

where $\hat{\mathbf{\Omega}}_\mathbf{q}$ is the unit vector in the direction of $\mathbf{q}$ and

$$\mathbf{P}_{nm\mathbf{k}} = \langle n\mathbf{k}|\hat{\mathbf{v}}|n\mathbf{k}\rangle \quad (6.15)$$

are the matrix elements of the velocity operator, defined as $\hat{\mathbf{v}} = -i[\hat{H},\hat{\mathbf{r}}]$. This velocity operator reduces to $\hat{\mathbf{v}} = \hat{\mathbf{p}}/m$ for a Hamiltonian with a local (multiplicative) potential (Levine & Allen 1989, Levine & Allen 1991, Del Sole & Girlanda 1993). By using the analytical properties of Eqs. (6.7) and (6.12) and the relation $\mathrm{Im}[1/(x+i\delta)] = \mathcal{P}[1/x] - i\pi\delta(x)$ we obtain for the macroscopic dielectric tensor for $\mathbf{q} \to 0$ without the inclusion of local fields

$$\begin{aligned}\epsilon_M^{\alpha\beta}(\omega) = \delta_{\alpha\beta} &+ \frac{4\pi}{V}{\sum_{nm\mathbf{k}}}'\frac{f_{n\mathbf{k}}-f_{m\mathbf{k}}}{(\varepsilon_{m\mathbf{k}}-\varepsilon_{n\mathbf{k}})^2}\frac{P^\alpha_{nm\mathbf{k}}[P^\beta_{nm\mathbf{k}}]^*}{\varepsilon_{n\mathbf{k}}-\varepsilon_{m\mathbf{k}}+\omega} \\ &- i\frac{4\pi}{\omega^2 V}{\sum_{nm\mathbf{k}}}'(f_{n\mathbf{k}}-f_{m\mathbf{k}})P^\alpha_{nm\mathbf{k}}[P^\beta_{nm\mathbf{k}}]^*\delta(\varepsilon_{n\mathbf{k}}-\varepsilon_{m\mathbf{k}}+\omega).\end{aligned} \quad (6.16)$$

The primed summation symbol in the above equation accounts for omitting the intra-band contributions $m = n$. Such a contribution is usually only important for systems without a gap and shall not be further discussed here. The fact that we obtain a tensor quantity $\epsilon_M^{\alpha\beta}$ starting from considerations of a longitudinal response is justified only, as pointed out earlier, in the $\mathbf{q} \to 0$ limit (Ambegaokar & Kohn 1960, Del Sole & Fiorino 1984).

The matrix elements of the momentum operator will depend naturally on the actual choice of the single particle states. One possible choice would be the Kohn-Sham states from DFT, another one, the quasi-particle states obtained from the Dyson equation, Eq. (2.56). Sometimes, the wave functions of DFT and the quasi-particle ones are assumed to be almost identical and the quasi-particle energies $E_{n\mathbf{k}}$ are related to the DFT ones $\varepsilon_{n\mathbf{k}}$ only through a simple scissors shift. This means that the conduction band energies are rigidly shifted upwards by a constant value. In such a case, one would expect to simply substitute $\varepsilon_{n\mathbf{k}}$ by $E_{n\mathbf{k}}$ in the expression Eq. (6.16) for the dielectric function. However, this is not sufficient, since the self-energy operator is non-local in any case, such that the matrix elements of the momentum operator have to be rescaled (Levine & Allen 1989, Levine & Allen 1991, Del Sole & Girlanda 1993) in the following way

$$\langle n\mathbf{k}|\hat{\mathbf{p}}|m\mathbf{k}\rangle_{\mathrm{QP}} = \frac{E_{n\mathbf{k}} - E_{m\mathbf{k}}}{\varepsilon_{n\mathbf{k}} - \varepsilon_{m\mathbf{k}}} \langle n\mathbf{k}|\hat{\mathbf{p}}|m\mathbf{k}\rangle_{\mathrm{KS}}. \tag{6.17}$$

The above relation is valid for general quasi-particle energies $E_{n\mathbf{k}}$ and for the case of a scissors shift the resulting dielectric function is shifted with respect to the energy argument.

Another peculiarity which is related to the long wavelength limit is the appearance of a divergent Fourier coefficient of the Coulomb potential in the Dyson equation for the polarizability, Eq. (2.68). This problem can be lifted in defining a modified polarizability $\bar{\chi}$ for which the polarization process including the long-range part is neglected (Ambegaokar & Kohn 1960). In doing so, a Dyson equation for the modified polarizability is found

$$\bar{\chi} = \tilde{\chi} + \tilde{\chi}\bar{v}\bar{\chi}, \tag{6.18}$$

where a modified Coulomb potential $\bar{v}$ is used according to

$$\bar{v}_{\mathbf{G}}(\mathbf{q}) = \begin{cases} 0, & \mathbf{G} = 0 \\ v_{\mathbf{G}}(\mathbf{q}), & \text{otherwise} \end{cases} \tag{6.19}$$

Finally, a combination of the Dyson equations for the full polarizability χ and the modified one $\bar{\chi}$ yields an expression for the macroscopic dielectric function, different but still equivalent to the one of ADLER and WISER, Eq. (6.10)

$$\epsilon_M(\mathbf{q},\omega) = 1 - v(\mathbf{q})\bar{\chi}_{\mathbf{00}}(\mathbf{q},\omega). \tag{6.20}$$

We will see in the following that the above expression for the macroscopic dielectric function is favorable in the context of the Bethe-Salpeter equation.

6.4 Excitonic Effects via the BSE

So far, the dielectric response to the external perturbation was only treated in the random phase approximation, *i.e.,* the correlation between the electrons and the holes has been neglected. Furthermore, we note that the Hartree approximation to the interaction kernel of the Bethe-Salpeter equation just gives the RPA result as we have seen in Sect. 2.4.3. In utilizing the BSE in the ladder approximation we will now include such correlations. The adoption of the BSE in the context of a periodic solid has been reported many times (Strinati 1984, Strinati 1988, Albrecht et al. 1998, Rohlfing & Louie 2000, Arnaud 2000, Puschnig 2002) already and shall be sketched very briefly in the following.

It has been shown already long time ago that the two-particle correlation function L contains information about the excitation energies $\mathcal{E}_\lambda$ which are caused by charge-neutral excitations of bosonic character of a bound N-particle system (Gell-Mann & Low 1951, Sham & Rice 1966). This very general two-particle correlation function $L(1,2;1',2')$ contains various correlations between electrons (e) and holes (h), namely e-e, h-h and e-h correlations. However, only 2 out of 6 possible combinations of splitting the time-ordering of the field operators in Eq. (2.88) contribute to the singularities at the exact excitation energies of the N particle system[1], $\mathcal{E}_\lambda$, if L is transformed to Fourier space. Due to the appearance of the time variables in combination with the excitation energies there is finally only one frequency variable which is important. We arrive at this situation by first pairing the time variables as in Eq. (2.95) and then taking the Fourier transform with respect to the resulting relative time (Strinati 1988). In doing so, we obtain

[1]For other combinations, the energies related to the $N \pm 2$ particle system appear which are not relevant for neutral excitation processes, or do not lead to a pole-structure.

a frequency-dependent correlation function $L(\mathbf{r}_1, \mathbf{r}_2, \mathbf{r}'_1, \mathbf{r}'_2; \omega)$. Furthermore, we need to select the correlations associated to a (small) momentum transfer vector $\mathbf{q}$ (Sham & Rice 1966), denoted by $L_\mathbf{q}(\mathbf{r}_1, \mathbf{r}_2, \mathbf{r}'_1, \mathbf{r}'_2; \omega)$ (or short $L_\mathbf{q}(\omega)$), which establishes the Bloch periodicity in each variable. The total correlation function is hence given as a sum over all $\mathbf{q}$ vectors

$$L(\mathbf{r}_1, \mathbf{r}_2, \mathbf{r}'_1, \mathbf{r}'_2; \omega) = \sum_\mathbf{q} L_\mathbf{q}(\mathbf{r}_1, \mathbf{r}_2, \mathbf{r}'_1, \mathbf{r}'_2; \omega). \tag{6.21}$$

The same considerations apply to the correlation function L^0 and the interaction kernel Ξ. Now the Bethe-Salpeter equation can be written in a form depending explicitly on the $\mathbf{q}$ vector and the frequency

$$L_\mathbf{q}(\omega) = L^0_\mathbf{q}(\omega) + L^0_\mathbf{q}(\omega)\Xi^0_\mathbf{q}(\omega)L_\mathbf{q}(\omega), \tag{6.22}$$

where the spatial integrations in Eq. (6.22) are the same as in Eq. (2.102). The special treatment of the long-range term of the Coulomb interaction can also be introduced in the context of the interaction kernel Ξ of the Bethe-Salpeter equation. In that case it will be defined with respect to the modified Coulomb interaction Eq. (6.19) which we assume for the following discussion. As a next step the terms in the BSE, Eq. (6.22), are expanded in terms of quasi-particle wave functions $\psi_j(\mathbf{r})$. Such an expansion for a general, Bloch-periodic 4-point quantity is given by

$$K_\mathbf{q}(\mathbf{r}_1, \mathbf{r}_2, \mathbf{r}_3, \mathbf{r}_4) = \sum_{i_1,i_2,i_3,i_4} \psi^*_{i_1}(\mathbf{r}_1)\psi_{i_2}(\mathbf{r}_2)\psi_{i_3}(\mathbf{r}_3)\psi^*_{i_4}(\mathbf{r}_4)K^\mathbf{q}_{i_1 i_2, i_3 i_4}, \tag{6.23}$$

where

$$K^\mathbf{q}_{i_1 i_2, i_3 i_4} = \int \mathrm{d}^3 r_1 \mathrm{d}^3 r_2 \mathrm{d}^3 r_3 \mathrm{d}^3 r_4 \psi_{i_1}(\mathbf{r}_1)\psi^*_{i_2}(\mathbf{r}_2)\psi^*_{i_3}(\mathbf{r}_3)\psi_{i_4}(\mathbf{r}_4)K_\mathbf{q}(\mathbf{r}_1, \mathbf{r}_2, \mathbf{r}_3, \mathbf{r}_4). \tag{6.24}$$

The Bloch vectors $\mathbf{k}_j$ associated to the indices i_j obey the relation (Arnaud 2000)

$$i_1 = (n_1, \mathbf{k}_1), i_2 = (n_2, \mathbf{k}_1 - \mathbf{q}), i_3 = (n_3, \mathbf{k}_3), i_4 = (n_4, \mathbf{k}_3 - \mathbf{q}), \tag{6.25}$$

and the numbers n_j denote the indices of the corresponding bands. In the following, we limit our discussion to the case of $\mathbf{q} \to 0$ since we are mostly interested in optical excitations. Without derivation we provide the expansion coefficients of the correlation function L_0 in terms of single-particle states

$$L^0_{i_1 i_2, i_3 i_4}(\omega) = -i\frac{f_{i_1} - f_{i_2}}{E_{i_1} - E_{i_2} + \omega + i\delta}\delta_{i_1 i_3}\delta_{i_3 i_4}. \tag{6.26}$$

Here, the result for the retarded L_0 is given, whereas the time-ordered one is needed in MBPT. However, for positive frequencies all following considerations will remain valid[2]. Now we transform the Bethe-Salpeter equation, Eq. (6.22), to transition space with the help of Eq. (6.24) and write it in a compact matrix form where the indices of the matrices consist of pairs $(i_a i_b)$

$$L(\omega) = K(\omega) L_0(\omega). \tag{6.27}$$

Here, the linear transformation K is given by[3]

$$K(\omega) = [1 - L_0(\omega)\Xi]^{-1}. \tag{6.28}$$

Due to the occupation number difference $f_{i_1} - f_{i_2}$ in L^0, Eq. (6.26), the expression for the correlation function can be expressed as

$$L(\omega) = i[H^{\text{eff}} - \omega]^{-1} \operatorname{diag}(\Delta f), \tag{6.29}$$

with

$$H^{\text{eff}} = \operatorname{diag}(\Delta E) - i \operatorname{diag}(\Delta f)\Xi. \tag{6.30}$$

Here, $\operatorname{diag}(\Delta f)_{(i_1 i_2),(i_3 i_4)} = \Delta f_{(i_1 i_2)} \delta_{(i_1 i_2),(i_3 i_4)}$ is a diagonal matrix constructed from the difference in occupation numbers, $\Delta f_{(i_1 i_2)} = f_{i_2} - f_{i_1}$ and $\Delta E_{(i_1 i_2)} = E_{i_2} - f_{i_1}$. The frequency argument is now made explicit in the latter expression for L, and the spectral theorem (see Eq. (F.17) in Appendix F) is employed for a representation of L in terms of eigenvalues and eigenvectors of H^{eff} which are given by

$$H^{\text{eff}} A^\lambda = \mathcal{E}^\lambda A^\lambda. \tag{6.31}$$

The resulting expression is given by

$$L_{i_1 i_2, i_3 i_4}(\omega) = i \sum_{\lambda\lambda'} \frac{A^\lambda_{i_1 i_2} M^{-1}_{\lambda\lambda'} [A^{\lambda'}_{i_3 i_4}]^*}{\mathcal{E}^\lambda - \omega} (f_{i_4} - f_{i_3}). \tag{6.32}$$

As a next step, a back-transform to configuration space with the help of Eq. (6.23), a subsequent pairing of the variables as in Eq. (2.95), and a Fourier transform to $\mathbf{G}$ space provides us with $\bar{\chi}_{\mathbf{G}\mathbf{G}'}(\mathbf{q}, \omega)$. Finally, from

[2]For a time-ordered expression we refer the reader to Ref. (Strinati 1988).

[3]We now assume the general interaction kernel Ξ to be static which is valid, for instance, in the *GW* approximation in combination with a static screening.

Eq. (6.20) we obtain the expression for the macroscopic dielectric function (Albrecht et al. 1998)

$$\begin{aligned} \epsilon_M(\mathbf{q},\omega) &= 1 - \frac{v(\mathbf{q})}{V}\sum_{\lambda}\frac{x_\lambda z_\lambda}{\mathcal{E}_\lambda - \omega} \\ x_\lambda &= \sum_{i_1 i_2} M_{i_1 i_2}(\mathbf{q}) A^{\lambda}_{i_1 i_2} \\ y_\lambda &= \sum_{i_1 i_2} M_{i_1 i_2}(\mathbf{q}) A^{\lambda}_{i_1 i_2}(f_{i_2} - f_{i_1}) \\ z_\lambda &= \sum_{\lambda'} M^{-1}_{\lambda\lambda'}[y_{\lambda'}]^*, \end{aligned} \tag{6.33}$$

where the $\mathbf{q}$-dependent matrix elements (see Eq. (6.8)) are given by

$$M_{i_1 i_2}(\mathbf{q}+\mathbf{G}) = \langle i_1 | e^{-i(\mathbf{q}+\mathbf{G})\mathbf{r}} | i_2 \rangle. \tag{6.34}$$

The Bloch indices $\mathbf{k}(i)$ in the wave functions of these matrix elements reflect the momentum transfer vector $\mathbf{q}$ since the following equality holds[4]

$$M_{i_1 i_2}(\mathbf{q}+\mathbf{G}) = \langle i_1 | e^{-i(\mathbf{q}+\mathbf{G})\mathbf{r}} | i_2 \rangle \delta_{\mathbf{q},\mathbf{k}(i_2)-\mathbf{k}(i_1)}. \tag{6.35}$$

A similar expression is found for the long wavelength limit $\mathbf{q} \to 0$

$$\begin{aligned} \epsilon^{\alpha\beta}_M(\omega) &= 1 - \frac{4\pi}{V}\sum_{\lambda}\frac{x_\lambda z_\lambda}{\mathcal{E}_\lambda - \omega} \\ x_\lambda &= \sum_{i_1 i_2} \frac{P^{\alpha}_{i_1 i_2}}{E_{i_2} - E_{i_1}} A^{\lambda}_{i_1 i_2} \\ y_\lambda &= \sum_{i_1 i_2} \frac{P^{\alpha}_{i_1 i_2}}{E_{i_2} - E_{i_1}} A^{\lambda}_{i_1 i_2}(f_{i_2} - f_{i_1}) \\ z_\lambda &= \sum_{\lambda'} M^{-1}_{\lambda\lambda'}[y_{\lambda'}]^*. \end{aligned} \tag{6.36}$$

Here, the matrix elements $P^{\alpha}_{i_1 i_2}$ (see Eq. (6.15)) are defined as

$$P^{\alpha}_{i_1 i_2} = \langle i_1 | \hat{v}_\alpha | i_2 \rangle, \tag{6.37}$$

[4]The δ function relating both $\mathbf{k}$ vectors to the $\mathbf{q}$ vector is defined modulo a reciprocal lattice vector.

and they only give a non-zero contribution for equal Bloch vectors $\mathbf{k}(i)$

$$P^{\alpha}_{i_1 i_2} = \langle i_1 | \hat{v}_\alpha | i_2 \rangle \delta_{\mathbf{k}(i_1),\mathbf{k}(i_2)}. \tag{6.38}$$

The E_{i_j} which appear in Eq. (6.36) are the single-particle energies. The expressions for the macroscopic dielectric function, Eqs. (6.33) and (6.36), are the most important ones of this chapter and are valid in a very general context. For a choice of DFT single particle states $|i_j\rangle$ and energies ε_{i_j} the rescaling of $P^{\alpha}_{i_1 i_2}$ has to be considered according to Eq. (6.17).

A second aspect comes into play for systems with a gap, where the transitions are limited to the combinations of occupied (v) and unoccupied (c) bands only. In this case, the size of the original Hamiltonian matrix, Eq. (6.30), is reduced by a factor of 2, because of vanishing differences in occupation numbers. We see this fact in considering the block structure of the BSE Hamiltonian

$$H^{\text{eff}} = H^{\text{eff}} \begin{pmatrix} v_1c_2, v_3c_4{}^{(+)} & v_1c_2, c_3v_4{}^{(\#)} & v_1c_2, v_3v_4 & v_1c_2, c_3c_4 \\ c_1v_2, v_3c_4{}^{(\#')} & c_1v_2, c_3v_4{}^{(-)} & c_1v_2, v_3v_4 & c_1v_2, c_3c_4 \\ [v_1v_2, v_3c_4] & [v_1v_2, c_3v_4] & (v_1v_2, v_3v_4) & [v_1v_2, c_3c_4] \\ [c_1c_2, v_3c_4] & [c_1c_2, c_3v_4] & [c_1c_2, v_3v_4] & (c_1c_2, c_3c_4) \end{pmatrix}, \tag{6.39}$$

which we write in a compact form to highlight the index combinations. The blocks for which the first two indices are of the same type (valence or conduction bands) vanish (indicated by square brackets) or are diagonal matrices (indicated by round brackets), which we see from Eq. (6.30). Hence, the Hamiltonian matrix is upper block diagonal and so is the matrix for the correlation function $L_{i_1 i_2, i_3 i_4}(\omega)$, Eq. (6.29). Because of the term $\Delta f_{i_1 i_2}$ in the expression for the correlation function, Eq. (6.29), only the blocks corresponding to the index combinations $(i_1 i_2, i_3 i_4) = (v_1c_2, v_3c_4)$, (v_1c_2, c_3v_4), (c_1v_2, v_3c_4), (c_1v_2, c_3v_4) survive in the expression for L. Therefore, only those blocks of H^{eff} marked with $(+), (-), (\#)$ and $(\#')$ are relevant, since they correspond to the equivalent blocks of L[5]. They denote the resonant part $(+)$ and the anti-resonant part $(-)$ which can be shown to be Hermitian, as well as the coupling parts $(\#), (\#')$ which are symmetric. The Hamiltonian matrix now takes the form

$$H^{\text{eff}} = \begin{pmatrix} H^{(+)}_{v_1c_2, v_3c_4} & H^{(\#)}_{v_1c_2, c_3v_4} \\ H^{(\#')}_{c_1v_2, v_3c_4} & H^{(-)}_{c_1v_2, c_3v_4} \end{pmatrix}. \tag{6.40}$$

[5]This can be seen by investigating the inversion of a 2×2 block matrix.

Another aspect concerning the size of the effective Hamiltonian is related to the so-called *Tamm-Dancoff* approximation (Fetter & Walecka 1971)[6]. Therein, the excited state $|N, \lambda\rangle$ is expanded only in electron-hole states as

$$|N, \lambda\rangle = \sum_{\lambda} A^{\lambda}_{vc} |vc\rangle, \tag{6.41}$$

where

$$|vc\rangle = a^{\dagger}_{v} b^{\dagger}_{c} |N\rangle, \tag{6.42}$$

and $a^{\dagger}_{v}$ and $b^{\dagger}_{c}$ create an electron in the state v and a hole in the state c, respectively. This procedure is justified for systems with a gap which is, larger as the average electron-hole interaction strength. The coupling between $|vc\rangle$ and $|cv\rangle$ states lacks a diagonal contribution ΔE in the Hamiltonian, Eq. (6.30), and therefore would be small (Rohlfing & Louie 2000). If we neglect the coupling blocks $H^{(\#)}_{v_1 c_2, c_3 v_4}$ and $H^{(\#')}_{c_1 v_2, v_3 c_4}$ the effective Hamiltonian can be block-diagonalized and the size of the eigenvalue problem is, again, reduced by a factor of two.

6.4.1 The Electron-Hole Interaction

Right now, we want to approximate the effective two-particle interaction Ξ by the ladder approximation, *i.e.,* using the first order term in the screened interaction W (see Eq. (2.109)), which we assume to be statically screened. This procedure has been applied frequently and it is claimed that the dynamical effects of the screening and of the one-particle Green's function cancel each other (Bechstedt et al. 1997). The conjecture of such a cancellation effect is, however, by no means proved in general. The effective Hamiltonian, Eq. (6.30) splits now into two parts

$$H^{\text{eff}} = H^{\text{diag}} + H^{\text{x}} + H^{\text{dir}}, \tag{6.43}$$

[6]For a more detailed discussion of the Tamm-Dancoff approximation see (Rohlfing & Louie 2000) and references therein.

where the individual parts are obtained from a combination of Eqs. (6.24), (2.109) and (6.30)

$$H^{\text{diag}}_{i_1 i_2, i_3 i_4} = (E_{i_2} - E_{i_1})\delta_{i_1 i_3}\delta_{i_2 i_4} \tag{6.44}$$

$$H^{\text{x}}_{i_1 i_2, i_3 i_4} = \int \mathrm{d}^3 r \mathrm{d}^3 r' \psi_{i_1}(\mathbf{r})\psi^*_{i_2}(\mathbf{r})\bar{v}(\mathbf{r},\mathbf{r}')\psi^*_{i_3}(\mathbf{r}')\psi_{i_4}(\mathbf{r}') \tag{6.45}$$

$$H^{\text{dir}}_{i_1 i_2, i_3 i_4} = -\int \mathrm{d}^3 r \mathrm{d}^3 r' \psi_{i_1}(\mathbf{r})\psi^*_{i_2}(\mathbf{r}')W(\mathbf{r},\mathbf{r}')\psi^*_{i_3}(\mathbf{r})\psi_{i_4}(\mathbf{r}'). \tag{6.46}$$

In the above equations, H^{diag} denotes a term which is diagonal and only contains differences in the single-particle energies, E_j, H^{x} is the repulsive exchange term, and H^{dir} is the *attractive* term describing the electron-hole correlations of the system.

We now proceed to sketch the spin-structure of the Bethe-Salpeter equation, which has been thoroughly discussed by Strinati (Strinati 1988) and Rohlfing and Louie (Rohlfing & Louie 2000). If the spin-orbit interaction of the system is weak and therefore neglected in the Hamiltonian, the spins of the electron and the hole can be treated separately, resulting into four subspaces

$$\{|v_\uparrow c_\uparrow\rangle\}, \{|v_\uparrow c_\downarrow\rangle\}, \{|v_\downarrow c_\uparrow\rangle\}, \{|v_\downarrow c_\downarrow\rangle\}, \tag{6.47}$$

according to the pairings of the spins for the electron-hole pairs. The block structure of the BSE Hamiltonian now splits into 4x4 blocks according to the subspaces of the spin-combinations, and some of these blocks vanish. Finally, two decoupled Bethe-Salpeter equations are obtained for the so-called *spin-singlet* and *spin-triplet* configurations. Thereby, the spin-singlet corresponds to the subspace

$$\left\{\frac{1}{\sqrt{2}}(|v_\uparrow c_\uparrow\rangle - |v_\downarrow c_\downarrow\rangle)\right\}, \tag{6.48}$$

whereas the spin-triplet configuration corresponds to the combination of three subspaces

$$\left\{\frac{1}{\sqrt{2}}(|v_\uparrow c_\uparrow\rangle + |v_\downarrow c_\downarrow\rangle), |v_\uparrow c_\downarrow\rangle, |v_\downarrow c_\uparrow\rangle\right\}, \tag{6.49}$$

Without derivation we denote the Hamiltonians for the singlet and triplet subspaces

$$H^{\text{singlet}} = H^{\text{diag}} + 2H^{\text{x}} + H^{\text{dir}} \tag{6.50}$$

$$H^{\text{triplet}} = H^{\text{diag}} + H^{\text{dir}}, \tag{6.51}$$

where a factor of 2 now appears in front of the exchange term for the singlet subspace, whereas it is absent for the triplet subspace. For a comparison to the excitation spectra obtained from TDDFT, mostly the spin-singlet will be of interest.

6.5 Excitonic Effects via TDDFT

In the case of time-dependent DFT, the formulation of the equation for linear response (the Dyson like equation), Eq. (4.30) is readily written in Fourier space

$$\begin{aligned}\chi_{\mathbf{G}\mathbf{G}'}(\mathbf{q},\omega) &= \chi^{\mathrm{KS}}_{\mathbf{G}\mathbf{G}'}(\mathbf{q},\omega) \\ &+ \sum_{\mathbf{G}_1\mathbf{G}_2} \chi^{\mathrm{KS}}_{\mathbf{G}\mathbf{G}_1}(\mathbf{q},\omega)[v_{\mathbf{G}_1}(\mathbf{q})\delta_{\mathbf{G}_1\mathbf{G}_2} + f^{\mathrm{xc}}_{\mathbf{G}_1\mathbf{G}_2}(\mathbf{q},\omega)]\chi_{\mathbf{G}_2\mathbf{G}'}(\mathbf{q},\omega).\end{aligned} \tag{6.52}$$

The response functions χ and χ^{KS} as well as the xc kernel are determined according to the expansion Eq. (E.12). The xc kernel in Eq. (6.52) is frequency dependent, not only for the exact expression but also for the one of Eq. (5.2), reproducing the dielectric function on the level of the Bethe-Salpeter equation even already in the first order GW approximation with static screening (Eq.(5.8)). In contrast, the corresponding two-particle interaction kernel of the BSE is a static quantity (for a static screening).

For the expressions of the Kohn-Sham response function basically the same considerations as in Sec. 6.2 apply with the difference that the single-particle states and energies are the Kohn-Sham ones

$$\chi^{\mathrm{KS}}_{\mathbf{G}\mathbf{G}'}(\mathbf{q},\omega) = \frac{1}{V}\sum_{n m \mathbf{k}} \frac{f_{n\mathbf{k}} - f_{m\mathbf{k}+\mathbf{q}}}{\varepsilon_{n\mathbf{k}} - \varepsilon_{m\mathbf{k}+\mathbf{q}} + \omega + i\delta} M_{nm\mathbf{k}}(\mathbf{q},\mathbf{G}) M^*_{nm\mathbf{k}}(\mathbf{q},\mathbf{G}'). \tag{6.53}$$

The matrix elements are the ones from Eq. (6.8) based upon Kohn-Sham wave functions. The considerations for the long wavelength limit in Sec. 6.3 apply in the context of TDDFT as well. Consequently, Dyson's equation is immediately given by Eq. (6.18) with the modified Coulomb potential from Eq. (6.19). The Kohn-Sham response function on the other hand is given with the help of the corresponding matrix elements from Eqs. (6.8) and (6.17), where again the Kohn-Sham wave functions and energies are used. The long wavelength limit of the xc kernel strongly depends on the adopted

approximationand will be discussed separately. Finally, the macroscopic dielectric function ϵ_M is obtained in the same way as in the case of the BSE, since in both theories, it is related to the full polarizability or interacting response function, in the language of TDDFT linear response.

Chapter 7

The LAPW Method

7.1 Introduction

There are different ways to solve the Kohn-Sham equations in general. Since we are treating periodic solids a possible choice of a basis set would be plane waves. The advantages of the latter are located in the orthogonality and the analytical simplicity. However, the size of the basis set would be too large when approaching the vicinity of the atomic nuclei in a crystal. Therefore, the Coulomb potential of the nuclei is often approximated by "pseudopotentials" which employ a shape approximation and thus do not have such singularities. The pseudopotential approach is quite popular in the field of electronic structure calculations, but suffers from the disadvantage, that it is an approximation giving rise to an unphysical behavior in the vicinity of the nuclei.

An early attempt for a precise description of the Kohn-Sham wave function in the entire unit cell has been proposed by Slater and is called the APW-method (Slater 1937). It stands for *augmented plane wave* method, and therein plane waves are augmented by sets of atomic-like functions. The original APW method has the drawback of energy-dependent basis functions and therefore, leads to a non-linear eigenvalue problem, rendering its solution computationally very demanding. As a way out of this situation, several APW-derived methods have been established, going to energy-independent basis functions and hence linearizing the eigenvalue problem. This is the reason why they are called *linearized* APW (LAPW) methods.

7.2 The Eigenvalue Problem

In order to solve the Kohn-Sham eigenvalue equations, Eq. (3.21), we reformulate them in terms of a general basis for the wave function ϕ with the help of basis functions ϕ_j. To this end we write the wave function as

$$\phi(\mathbf{r}) = \sum_j c_j \phi_j(\mathbf{r}). \tag{7.1}$$

The eigenvalue problem is now given, by virtue of Ritz's variational principle, as generalized matrix eigenvalue problem

$$\sum_j H_{ij} c_j^{(n)} = \varepsilon^{(n)} \sum_j S_{ij} c_j^{(n)}, \tag{7.2}$$

which is called the *secular equation* of the system. In this equation, the $c^{(n)}$ are the eigenvectors and the $\varepsilon^{(n)}$ the eigenvalues. The Hamiltonian matrix H_{ij} and the overlap matrix S_{ij} are given by the following expressions

$$H_{ij} = \langle \phi_i | \hat{h}(\mathbf{r}) | \phi_j \rangle \tag{7.3}$$

$$S_{ij} = \langle \phi_i | \phi_j \rangle, \tag{7.4}$$

where $\hat{h}(\mathbf{r})$ is the Kohn-Sham single-particle Hamiltonian consisting of the kinetic energy operator and the Kohn-Sham effective potential, Eq. (3.18). The overlap matrix accounts for the case of non-orthogonal basis functions.

7.3 The Basis Set

The main characteristics of the APW method and related methods is to divide the crystal in two different types of regions. The first one, called the muffin-tin region, consists of spheres centered around the atoms while the remaining part of the unit cell is called the interstitial region. Inside the muffin-tin spheres, the basis consists of atomic-like functions to account for the rapid changes of the wave function in this area. In contrast, in the interstitial region at some distance from the atomic sites the wave function changes only slowly and hence plane waves are appropriate.

We proceed now to describe the APW-like basis set which we present in the general form

$$\phi^{\mathrm{APW}}_{\mathbf{k}+\mathbf{G}}(\mathbf{r}) = \begin{cases} \frac{1}{\sqrt{V}} e^{i(\mathbf{k}+\mathbf{G})\mathbf{r}}, & \mathbf{r} \in \text{interstitial} \\ \sum\limits_{\alpha,lm} f^{\alpha,lm}_{\mathbf{k}+\mathbf{G}}(r_\alpha) Y_{lm}(\hat{\mathbf{r}}_\alpha), & \mathbf{r} \in \text{muffin-tin} \end{cases} \tag{7.5}$$

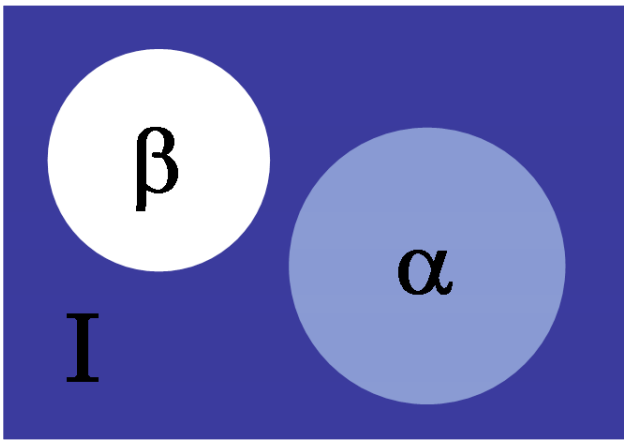

Figure 7.1: The partition of the unit cell into muffin-tin spheres (α, β) and an interstitial region (I).

where $\mathbf{r}_\alpha = \mathbf{r} - \mathbf{R}_\alpha$ and $\mathbf{R}_\alpha$ is the center of the muffin-tin sphere related to atom α. The lm-expansion coefficients $f^{\alpha,lm}_{\mathbf{k}+\mathbf{G}}(r_\alpha)$ are given in terms of the radial functions $u^\alpha_{lp}(r_\alpha, E_l)$ and so-called matching coefficients $A^\alpha_{lmp}(\mathbf{k}+\mathbf{G})$

$$f^{\alpha,lm}_{\mathbf{k}+\mathbf{G}}(r_\alpha) = \sum_{p=0}^{p_{\max}} A^\alpha_{lmp}(\mathbf{k}+\mathbf{G}) u^\alpha_{lp}(r_\alpha, E_l). \tag{7.6}$$

In the above equation, $u^\alpha_{lp}(r_\alpha, E_l)$ denotes the p-th derivative of the radial wave function $u^\alpha_l(r_\alpha, E_l)$ with respect to the *energy*. The radial wave functions are the solutions of the radial, scalar-relativistic Schrödinger equation (Koelling & Harmon 1977) in the radial-symmetric potential of the respective sphere.

Now, it was the idea of Andersen (Andersen 1975) (see also Reference (Ambrosch-Draxl 2004) for details) to use $p_{\max} = 1$, *i.e.*, , the radial function $u^\alpha_l(r_\alpha, E_l)$ and its derivative with respect to the energy, $\dot{u}^\alpha_l(r_\alpha, E_l)$ at a fixed chosen energy E_l, called *linearization energy*. This way, the radial function at the exact, at present unknown, energy E can be seen in the spirit of a first order Taylor expansion

$$u^\alpha_l(r_\alpha, E) = u^\alpha_l(r_\alpha, E_l) + (E - E_l)\dot{u}^\alpha_l(r_\alpha, E_l). \tag{7.7}$$

For higher values of $p_{\max}$ the so-called *SLAPW-3* and *SLAPW-4* methods are obtained (Singh & Krakauer 1991). It has to be pointed out that the

linearization energies E_l are neither the eigenvalues of the radial Schrödinger equation, nor of the secular equation as it is the case in the original APW method. They merely enter the radial equation as parameters, although physically meaningful ones. In practice they are usually set in the middle of the band with the corresponding l character.

The afore mentioned matching coefficients are determined by the requirement that the basis function has to be continuous at the boundary of the muffin-tin sphere up to the order $p_{\max}$. The coefficients are then obtained through the set of equations

$$\sum_{q=0}^{p_{\max}} \frac{\mathrm{d}^p}{\mathrm{d}r^p} u_{lq}^{\alpha}(r, E_l)\bigg|_{r=R_{\alpha}^{\mathrm{MT}}} A_{lmp}^{\alpha}(\mathbf{k}') = \frac{4\pi}{\sqrt{V}} i^l e^{i\mathbf{k}'\mathbf{R}_{\alpha}} Y_{lm}^*(\hat{\mathbf{k}}') \left.\frac{\mathrm{d}^p}{\mathrm{d}r^p} j_l(k'r)\right|_{r=R_{\alpha}^{\mathrm{MT}}} \tag{7.8}$$

for $p = 0, \ldots, p_{\max}$, where $\mathbf{k}' = \mathbf{k} + \mathbf{G}$.

The set of APW-related basis functions can be made more flexible by the addition of so-called local orbitals $\phi_L^{\mathrm{lo}}(\mathbf{r})$, which are defined as

$$\phi_L^{\mathrm{lo}}(\mathbf{r}) = \begin{cases} 0, & \mathbf{r} \in \text{interstitial} \\ v_L^{\alpha}(r_{\alpha}) Y_{lm}(\hat{\mathbf{r}}_{\alpha}), & \mathbf{r} \in \text{muffin-tin of atom } \alpha, \end{cases} \tag{7.9}$$

where the overall index L comprises the angular momentum lm as well as the atom index α and the matching order $p_{\max}$. The functions $v_s^{\alpha}(r_{\alpha})$ are again linear superpositions of radial functions $u_{lp}^{\alpha}(r_{\alpha})$ (and their derivatives with respect to the energy)

$$v_L^{\alpha}(r) = \sum_{b=0}^{p_{\max}} A_b^{\alpha} u_{lp_b}^{\alpha}(r, E_b). \tag{7.10}$$

The matching coefficients A_b^{α} are obtained in a similar manner as the APW functions. A possible implementation of such conditions is given as follows

$$\sum_{c=0}^{p_{\max}} \frac{\mathrm{d}^b}{\mathrm{d}r^b} u_{lp_c}^{\alpha}(r, E_c)\bigg|_{r=R_{\alpha}^{\mathrm{MT}}} A_c^{\alpha} = e^{i\mathbf{k}\mathbf{R}_{\alpha}} \delta_{b,p_{\max}}, \tag{7.11}$$

where $b = 0, \ldots, p_{\max}$.

Local orbitals are utilized to increase the flexibility of the basis set in two different ways. The first one is to describe low-lying valence states (semi-core states) properly by choosing one of the linearization energies close to the one

of the semi-core state (Singh 1994). Adding, on the other hand, a local orbital with the expansion energy of the APW basis function (Sjöstedt et al. 2000) provides a way of linearizing the secular equation. This so-called APW+lo method is an alternative to the well-known LAPW method. It is even a more favorable choice, since it is computationally less expensive. For further details of the basis set we refer the reader to Refs. (Singh 1994, Ambrosch-Draxl 2004).

The expansion of the Bloch wave function $\phi_{n\mathbf{k}}(\mathbf{r})$ in terms of the basis including APW-like basis functions and local orbitals is now given by

$$\phi_{n\mathbf{k}}(\mathbf{r}) = \sum_{\mathbf{G}} c_{n\mathbf{k}+\mathbf{G}} \phi^{\mathrm{APW}}_{\mathbf{k}+\mathbf{G}}(\mathbf{r}) + \sum_{L} c_{n\mathbf{k},L} \phi^{\mathrm{lo}}_{L}(\mathbf{r}), \tag{7.12}$$

where the coefficients $c_{n\mathbf{k}+\mathbf{G}}$ and $c_{n\mathbf{k},L}$ enter in place of the general coefficients $c_j^{(n)}$ from Eq. (7.2).

7.4 The Density and the Potential

Not only the wave function is expanded using the dual basis inside the muffin-tin spheres and the interstitial region in order to account for the chosen partition of the unit cell. Also the density and the effective potential are represented in the same way. Since they have the periodicity of the unit cell it is sufficient to expand them in a Fourier series similar to the one of Eq. (E.14). The expansion of the valence density of the electrons is given by

$$n_{\mathrm{val}}(\mathbf{r}) = \begin{cases} \sum\limits_{\mathbf{G}} n_{\mathbf{G}} e^{i\mathbf{G}\mathbf{r}}, & \mathbf{r} \in \text{interstitial} \\ \sum\limits_{\alpha lm} n^{\alpha}_{lm}(r_\alpha) Y_{lm}(\hat{\mathbf{r}}_\alpha), & \mathbf{r} \in \text{muffin-tin.} \end{cases} \tag{7.13}$$

For the core electrons, only the spherically symmetric part of the density is considered, and it is assumed to vanish outside the muffin-tin spheres

$$n_{\mathrm{cor}}(\mathbf{r}) = \begin{cases} 0, & \mathbf{r} \in \text{interstitial} \\ \sum\limits_{\alpha} n^{\alpha}_{00}(r_\alpha) Y_{00}(\hat{\mathbf{r}}_\alpha), & \mathbf{r} \in \text{muffin-tin.} \end{cases} \tag{7.14}$$

The core states of the system from which the core density is constructed, is obtained from a solution to the Dirac equation (Greiner 2000, Itzykson & Zuber 1980). The total density is given as a sum of the valence and the core density.

In virtually the same way, the effective Kohn-Sham potential is expanded

$$v(\mathbf{r}) = \begin{cases} \sum\limits_{\mathbf{G}} v_{\mathbf{G}} e^{i\mathbf{G}\mathbf{r}}, & \mathbf{r} \in \text{interstitial} \\ \sum\limits_{\alpha lm} v_{lm}^{\alpha}(r_\alpha) Y_{lm}(\hat{\mathbf{r}}_\alpha), & \mathbf{r} \in \text{muffin-tin.} \end{cases} \tag{7.15}$$

With the help of the latter representations of the wave function on the one side and the density and the potential on the other side, the Hamiltonian matrix elements can be obtained analytically in a straight forward way (Singh 1994). For further details on the implementation of an LAPW scheme can be found in the book of Singh (Singh 1994).

Chapter 8

Implementation

In this chapter the focus is set on the implementation of the Bethe-Salpeter equation and the TDDFT linear response formalism into the all-electron LAPW code `EXC!TiNG` (Dewhurst et al. 2005, Ambrosch-Draxl et al. 2009). The most important quantities from the implementation point of view are the matrix elements of a plane wave, which we will also refer to as **q**-dependent matrix element, and the ones of the momentum operator. They are involved from the aspect of the analytic expression, and they distinguish our actual implementations of BSE and TDDFT from other codes. Starting from the expressions for the above mentioned matrix elements, Eqs. (6.8), (6.15) the dielectric matrix, the screened Coulomb interaction as well as the parts of the effective Hamiltonian matrix, Eqs. (6.46), (6.45) are displayed for the BSE. For the TDDFT implementation, the frequency-dependent Kohn-Sham response function, Eq. (6.7), as well as the xc kernels, Eqs. (4.33), (5.11) are discussed. Additionally, some peculiarities concerning the solution of the Dyson equation are shown.

8.1 Matrix Elements of the Momentum Operator

For the calculation of the macroscopic dielectric function in various approximations within both, TDDFT and BSE, the matrix elements of the momentum operator, Eq. (6.15), need to be calculated. They are given by the following expression

$$P^{j}_{nm\mathbf{k}} = \langle n\mathbf{k}|-i\nabla_j|m\mathbf{k}\rangle. \tag{8.1}$$

The evaluation of these matrix elements with the APW-like basis is obtained with the help of vector spherical harmonics (Arfken & Weber 2005) and is summarized in the following. By virtue of Eq. (7.12) the basis coefficients of the wave functions can be pulled out of the matrix elements

$$\begin{aligned} P^j_{nm\mathbf{k}} = N_\Omega \sum_{\mathbf{G}'\mathbf{G}''} c^*_{n\mathbf{k}+\mathbf{G}'} c_{m\mathbf{k}+\mathbf{G}''} P^j_{\mathbf{G}'\mathbf{G}''\mathbf{k}} \\ + N_\Omega \sum_{\mathbf{G}'L''} c^*_{n\mathbf{k}+\mathbf{G}'} c_{m\mathbf{k},L''} P^j_{\mathbf{G}'L''\mathbf{k}} \\ + N_\Omega \sum_{L'\mathbf{G}''} c^*_{n\mathbf{k},L'} c_{m\mathbf{k}+\mathbf{G}''} P^j_{L'\mathbf{G}''\mathbf{k}} \\ + N_\Omega \sum_{L'L''} c^*_{n\mathbf{k},L'} c_{m\mathbf{k},L''} P^j_{L'L''\mathbf{k}}, \end{aligned} \tag{8.2}$$

where the $\mathbf{G}$ vector acts as an index for the APW function and the L index points to a local orbital. The quantities $P^j_{\mathbf{G}'\mathbf{G}''\mathbf{k}}$, $P^j_{\mathbf{G}'L''\mathbf{k}}$, $P^j_{L'\mathbf{G}''\mathbf{k}}$ and $P^j_{L'L''\mathbf{k}}$ in the above equation are defined as

$$\begin{aligned} P^j_{\mathbf{G}'\mathbf{G}''\mathbf{k}} &= \langle \phi_{\mathbf{k}+\mathbf{G}'} \mid -i\nabla_j \mid \phi_{\mathbf{k}+\mathbf{G}''} \rangle_\Omega \\ P^j_{\mathbf{G}'L''\mathbf{k}} &= \langle \phi_{\mathbf{k}+\mathbf{G}'} \mid -i\nabla_j \mid \phi_{\mathbf{k},L''} \rangle_\Omega \\ P^j_{L'\mathbf{G}''\mathbf{k}} &= \langle \phi_{\mathbf{k}L'} \mid -i\nabla_j \mid \phi_{\mathbf{k}+\mathbf{G}''} \rangle_\Omega \\ P^j_{L'L''\mathbf{k}} &= \langle \phi_{\mathbf{k},L'} \mid -i\nabla_j \mid \phi_{\mathbf{k},L''} \rangle_\Omega. \end{aligned} \tag{8.3}$$

Now, these matrix elements can be split into contributions from the interstitial and the muffin-tin region

$$P^j_{ab\mathbf{k}} = P^{j,\mathrm{I}}_{ab\mathbf{k}} + P^{j,\mathrm{MT}}_{ab\mathbf{k}}, \tag{8.4}$$

where $a, b \in \{\mathbf{G}', \mathbf{G}'', L', L''\}$. Here, the interstitial term is straight forwardly given by

$$P^{j,\mathrm{I}}_{ab\mathbf{k}} = (\mathbf{k}+\mathbf{G}')\tilde{\theta}_I(\mathbf{G}-\mathbf{G}'). \tag{8.5}$$

In this expression, $\tilde{\theta}_I(\mathbf{G})$ denotes the Fourier transform of the Heaviside step function, which will be provided in more detail in the next subsection. The contribution of the muffin-tin spheres is obtained as

$$\begin{aligned} P^{j,\mathrm{MT}}_{\mathbf{G}'\mathbf{G}''\mathbf{k}} &= \sum_\alpha \sum_{lmp} A^\alpha_{l'm'p'}(\mathbf{k}+\mathbf{G}')^* \sum_{l''m''p''} A^\alpha_{l''m''p''}(\mathbf{k}+\mathbf{G}'') \zeta^{\alpha,j}_{l'm'p',l''m''p''} \\ \zeta^{\alpha,j}_{l'm'p',l''m''p''} &= \int_0^{R^{\mathrm{MT}}_\alpha} \mathrm{d}r\, r^2 u^\alpha_{l'p'}(r) u^{\alpha,j}_{l''m''p'',l'm'}(r). \end{aligned} \tag{8.6}$$

The quantities $u^{\alpha,j}_{l'm'p',lm}(r)$ are the expansion coefficients of the gradient of a radial function and a spherical harmonic

$$\nabla_j[u^{\alpha}_{lp}(r)Y_{lm}(\hat{\mathbf{r}})] = \sum_{l''m''} u^{\alpha,j}_{lmp,l''m''}(r)Y_{l''m''}(\hat{\mathbf{r}}). \tag{8.7}$$

They can be worked out utilizing the analytical properties of spherical harmonics (Arfken & Weber 2005) as

$$\begin{aligned} u^{\alpha,j}_{l''m''p'',l'm'}(r) = &- \left[\frac{l''+1}{2l''+1}\right]^{\frac{1}{2}} \left[\frac{\mathrm{d}}{\mathrm{d}r} - \frac{l''}{r}\right] u^{\alpha}_{l''p''}(r) C^{j}_{l''m'',l'm'}\delta_{l',l''+1} \\ &+ \left[\frac{l''}{2l''+1}\right]^{\frac{1}{2}} \left[\frac{\mathrm{d}}{\mathrm{d}r} + \frac{l''+1}{r}\right] u^{\alpha}_{l''p''}(r) C^{j}_{l''m'',l'm'}\delta_{l',l''-1}. \end{aligned} \tag{8.8}$$

The coefficients $C^{j}_{lm,l'm'}$ are related to the Clebsch-Gordon coefficients $C(l_1l_2l_3|m_1m_2m_3)$ as follows

$$\begin{aligned} C^{1}_{lm,l'm'} &= \frac{1}{\sqrt{2}}[C(l'1l|m'-1m) - C(l'1l|m'1m)] \\ C^{2}_{lm,l'm'} &= \frac{-i}{\sqrt{2}}[C(l'1l|m'-1m) + C(l'1l|m'1m)] \\ C^{3}_{lm,l'm'} &= C(l'1l|m'0m). \end{aligned} \tag{8.9}$$

For the other combinations of APW functions and local orbitals or for the case of two local orbitals in Eq. (8.3) we summarize the results below. The case of an APW function and a local orbital is given as

$$\begin{aligned} P^{j,\mathrm{MT}}_{\mathbf{G}'L''\mathbf{k}} &= \sum_{l'm'p'} A^{\alpha''}_{l'm'p'}(\mathbf{k}+\mathbf{G}'')\zeta^{\alpha'',j}_{l'm'p',s''m''} \\ \zeta^{\alpha'',j}_{l'm'p',s''m''} &= \int_0^{R^{\mathrm{MT}}_{\alpha''}} \mathrm{d}r\, r^2 u^{\alpha''}_{l'p'}(r) v^{\alpha'',j}_{s''m'',l'm'}(r) \\ v^{\alpha'',j}_{s''m'',l'm'}(r) &= - \left[\frac{l''+1}{2l''+1}\right]^{\frac{1}{2}} \left[\frac{\mathrm{d}}{\mathrm{d}r} - \frac{l''}{r}\right] v^{\alpha''}_{s''}(r) C^{j}_{l''m'',l'm'}\delta_{l',l''+1} \\ &\quad + \left[\frac{l''}{2l'+1}\right]^{\frac{1}{2}} \left[\frac{\mathrm{d}}{\mathrm{d}r} + \frac{l''+1}{r}\right] v^{\alpha''}_{s''}(r) C^{j}_{l''m'',l'm'}\delta_{l',l''-1}. \end{aligned} \tag{8.10}$$

The corresponding expressions for swapping the APW function and the local orbital in the matrix element results from the Hermiticity of the momentum

operator. Finally, for the case of two local orbitals we obtain

$$\begin{aligned} P^{j,\mathrm{MT}}_{L'L''\mathbf{k}} &= \zeta^{\alpha',j}_{s'm',s''m''}\delta_{\alpha',\alpha''} \\ \zeta^{\alpha',j}_{s'm',s''m''} &= \int_0^{R^{\mathrm{MT}}_{\alpha'}} \mathrm{d}r\, r^2 v^{\alpha'}_{s'}(r) v^{\alpha'',j}_{s''m'',l'm'}(r). \end{aligned} \tag{8.11}$$

We note that in the expressions for the matrix elements given above, the local orbital index L determines the indices α, the local orbital index for the radial function s, and the m index. All such indices which are not summed over, are hence determined by the L index on the left hand side of the equations. The expressions for the matrix elements of the momentum operator are given here in the most general form including basis function matching to arbitrary order. They have been worked out for the LAPW and APW+lo scheme already and can be found in Refs. (Abt 1997, Ambrosch-Draxl & Sofo 2006).

8.2 Matrix Elements of the Plane Wave

The key-ingredients of the whole BSE and TDDFT formalism are the $\mathbf{q}$ dependent matrix elements, Eq. (6.8). They are given by a plane wave $e^{-i(\mathbf{q}+\mathbf{G})\mathbf{r}}$ which is sandwiched between two Bloch functions $\phi_{n\mathbf{k}}$ and $\phi_{m\mathbf{k}+\mathbf{q}}$

$$M_{nm\mathbf{k}}(\mathbf{q}+\mathbf{G}) = \langle \phi_{n\mathbf{k}} \mid e^{-i(\mathbf{q}+\mathbf{G})\mathbf{r}} \mid \phi_{m\mathbf{k}+\mathbf{q}} \rangle. \tag{8.12}$$

Because of the Bloch property, this expression for $M_{nm\mathbf{k}}(\mathbf{q}+\mathbf{G})$ can be written either in terms of the periodic part of the wave functions only as a simple Fourier transform

$$M_{nm\mathbf{k}}(\mathbf{q}+\mathbf{G}) = N_\Omega \int_\Omega \mathrm{d}^3 r\, e^{-i\mathbf{G}\mathbf{r}} u^*_{n\mathbf{k}}(\mathbf{r}) u_{m\mathbf{k}+\mathbf{q}}(\mathbf{r}) \tag{8.13}$$

with $N_\Omega = V/\Omega$ being the number of unit cells Ω in the crystal volume V (which is the same as the number of $\mathbf{k}$ vectors), where the periodic parts $u_{n\mathbf{k}}$ are given by

$$\phi_{n\mathbf{k}}(\mathbf{r}) = u_{n\mathbf{k}}(\mathbf{r}) e^{i\mathbf{k}\mathbf{r}}. \tag{8.14}$$

Alternatively they can be expressed as

$$\begin{aligned} M_{nm\mathbf{k}}(\mathbf{q}+\mathbf{G}) &= N_\Omega \int_\Omega \mathrm{d}^3 r\, \phi^*_{n\mathbf{k}}(\mathbf{r}) e^{-i(\mathbf{q}+\mathbf{G})\mathbf{r}} \phi_{m\mathbf{k}+\mathbf{q}}(\mathbf{r}) \\ &\equiv N_\Omega \langle \phi_{n\mathbf{k}} \mid e^{-i(\mathbf{q}+\mathbf{G})\mathbf{r}} \mid \phi_{m\mathbf{k}+\mathbf{q}} \rangle_\Omega. \end{aligned} \tag{8.15}$$

Using Eq. (7.5) the basis coefficients can be pulled out of the integration

$$\begin{aligned} M_{nm\mathbf{k}}(\mathbf{q}+\mathbf{G}) = N_\Omega \sum_{\mathbf{G}'\mathbf{G}''} c^*_{n\mathbf{k}+\mathbf{G}'} c_{m\mathbf{k}+\mathbf{q}+\mathbf{G}''} M_{\mathbf{G}'\mathbf{G}''\mathbf{k}}(\mathbf{q}+\mathbf{G}) \\ + N_\Omega \sum_{\mathbf{G}'L''} c^*_{n\mathbf{k}+\mathbf{G}'} c_{m\mathbf{k}+\mathbf{q},L''} M_{\mathbf{G}'L''\mathbf{k}}(\mathbf{q}+\mathbf{G}) \\ + N_\Omega \sum_{L'\mathbf{G}''} c^*_{n\mathbf{k},L'} c_{m\mathbf{k}+\mathbf{q}+\mathbf{G}''} M_{L'\mathbf{G}''\mathbf{k}}(\mathbf{q}+\mathbf{G}) \\ + N_\Omega \sum_{L'L''} c^*_{n\mathbf{k},L'} c_{m\mathbf{k}+\mathbf{q},L''} M_{L'L''\mathbf{k}}(\mathbf{q}+\mathbf{G}) \end{aligned} \tag{8.16}$$

with

$$\begin{aligned} M_{\mathbf{G}'\mathbf{G}''\mathbf{k}}(\mathbf{q}+\mathbf{G}) &= \langle \phi_{\mathbf{k}+\mathbf{G}'} \mid e^{-i(\mathbf{q}+\mathbf{G})\mathbf{r}} \mid \phi_{\mathbf{k}+\mathbf{q}+\mathbf{G}''} \rangle_\Omega \\ M_{\mathbf{G}'L''\mathbf{k}}(\mathbf{q}+\mathbf{G}) &= \langle \phi_{\mathbf{k}+\mathbf{G}'} \mid e^{-i(\mathbf{q}+\mathbf{G})\mathbf{r}} \mid \phi_{\mathbf{k}+\mathbf{q},L''} \rangle_\Omega \\ M_{L'\mathbf{G}''\mathbf{k}}(\mathbf{q}+\mathbf{G}) &= \langle \phi_{\mathbf{k}L'} \mid e^{-i(\mathbf{q}+\mathbf{G})\mathbf{r}} \mid \phi_{\mathbf{k}+\mathbf{q}+\mathbf{G}''} \rangle_\Omega \\ M_{L'L''\mathbf{k}}(\mathbf{q}+\mathbf{G}) &= \langle \phi_{\mathbf{k},L'} \mid e^{-i(\mathbf{q}+\mathbf{G})\mathbf{r}} \mid \phi_{\mathbf{k}+\mathbf{q},L''} \rangle_\Omega . \end{aligned} \tag{8.17}$$

The integral can be split into contributions from the interstitial and the muffin-tin region

$$M_{ab\mathbf{k}}(\mathbf{q}+\mathbf{G}) = M^{\mathrm{I}}_{ab\mathbf{k}}(\mathbf{q}+\mathbf{G}) + M^{\mathrm{MT}}_{ab\mathbf{k}}(\mathbf{q}+\mathbf{G}) \tag{8.18}$$

where $a, b \in \{\mathbf{G}', \mathbf{G}'', L', L''\}$.

We proceed to evaluate the interstitial contribution:

$$\begin{aligned} M^{\mathrm{I}}_{\mathbf{G}'\mathbf{G}''\mathbf{k}}(\mathbf{q}+\mathbf{G}) &= N_\Omega \frac{1}{V} \int_\Omega \mathrm{d}^3 r\, \theta_I(\mathbf{r}) e^{-i(\mathbf{k}+\mathbf{G}')\mathbf{r}} e^{-i(\mathbf{q}+\mathbf{G})\mathbf{r}} e^{i(\mathbf{k}+\mathbf{G}'')\mathbf{r}} \\ &= N_\Omega \frac{1}{V} \int_\Omega \mathrm{d}^3 r\, \theta_I(\mathbf{r}) e^{-i(\mathbf{G}'-\mathbf{G}''-\mathbf{G})\mathbf{r}} \\ &= \frac{1}{\Omega} \int_\Omega \mathrm{d}^3 r\, \theta_I(\mathbf{r}) e^{-i(\mathbf{G}'-\mathbf{G}''-\mathbf{G})\mathbf{r}} \\ &= \tilde{\theta}_I(\mathbf{G}'-\mathbf{G}''-\mathbf{G}) \end{aligned} \tag{8.19}$$

yielding the Fourier transform of the step function of the interstitial $\tilde{\theta}_I(\mathbf{G})$ evaluated at the sum of $\mathbf{G}$ vectors, stemming from the APW expansions and from the exponential factor. The latter expression is analytically known as

$$\tilde{\theta}_I(\mathbf{G}) = \begin{cases} 1 - \sum_\alpha \frac{4\pi R_\alpha^3}{3\Omega} & \mathbf{G} = 0 \\ -\sum_\alpha \frac{4\pi R_\alpha^3}{3\Omega} \frac{j_1(|\mathbf{G}|R_\alpha)}{|\mathbf{G}|R_\alpha} 3 e^{i\mathbf{G}\mathbf{R}_\alpha} & \mathbf{G} \neq 0. \end{cases} \tag{8.20}$$

$M^{\mathrm{I}}_{\mathbf{G}'L''\mathbf{k}}(\mathbf{q}+\mathbf{G})$, $M^{\mathrm{I}}_{L'\mathbf{G}''\mathbf{k}}(\mathbf{q}+\mathbf{G})$ and $M^{\mathrm{I}}_{L'L''\mathbf{k}}(\mathbf{q}+\mathbf{G})$ are zero because the local orbital basis functions vanish in the interstitial.

In order to evaluate the muffin-tin contribution we note the following identity:

$$\int_{\mathbb{MT}} \mathrm{d}^3 r \sum_{\alpha} f_\alpha(\mathbf{r}-\mathbf{R}_\alpha) e^{i\mathbf{kr}} = \sum_{\alpha} e^{i\mathbf{kR}_\alpha} \int_{\mathbb{MT}_\alpha} \mathrm{d}^3 r\, f_\alpha(\mathbf{r}) e^{i\mathbf{kr}} \tag{8.21}$$

with the centered muffin-tin sphere $\mathbb{MT}_\alpha$ given by all $\mathbf{r}$ with $r < R^{\mathrm{MT}}_\alpha$, and remembering the Rayleigh expansion (Rayleigh 1870) of a plane wave in terms of spherical harmonics and spherical Bessel functions of first kind

$$e^{i\mathbf{gr}} = 4\pi \sum_{lm} i^l j_l(gr) Y_{lm}(\hat{\mathbf{r}}) Y^*_{lm}(\hat{\mathbf{g}}). \tag{8.22}$$

Alternatively, this expression can be rewritten in terms of $-\mathbf{g}$ instead of $\mathbf{g}$ as

$$e^{i(-\mathbf{g})\mathbf{r}} = 4\pi \sum_{lm} (-i)^l j_l(gr) Y_{lm}(\hat{\mathbf{r}}) Y^*_{lm}(\hat{\mathbf{g}}). \tag{8.23}$$

Using Eqs. (8.21) and (8.23) it is straightforward to derive the following expressions for $M^{\mathrm{MT}}_{\mathbf{G}'\mathbf{G}''\mathbf{k}}(\mathbf{q}+\mathbf{G})$

$$\begin{aligned} M^{\mathrm{MT}}_{\mathbf{G}'\mathbf{G}''\mathbf{k}}(\mathbf{q}+\mathbf{G}) = 4\pi \sum_{\alpha} S^*_\alpha(\mathbf{q}+\mathbf{G}) \sum_{l'm'p'} A^\alpha_{l'm'p'}(\mathbf{k}+\mathbf{G}')^* \\ \sum_{l''m''p''} A^\alpha_{l''m''p''}(\mathbf{k}+\mathbf{G}'') X^\alpha_{l'm'p',l''m''p''}(\mathbf{q}+\mathbf{G}). \end{aligned} \tag{8.24}$$

The structure factors

$$S_\alpha(\mathbf{q}+\mathbf{G}) = e^{i(\mathbf{q}+\mathbf{G})\mathbf{R}_\alpha}, \tag{8.25}$$

occur due to Eq. (8.21) and we define the quantities X and R as follows

$$\begin{aligned} X^\alpha_{l'm'p',l''m''p''}(\mathbf{q}+\mathbf{G}) &= \sum_l (-i)^l R^\alpha_{l'p'l''p''l}(\mathbf{q}+\mathbf{G}) \sum_m Y_{lm}(\widehat{\mathbf{q}+\mathbf{G}})^* C^{l'm'}_{lml''m''} \\ R^\alpha_{l'p'l''p''l}(\mathbf{q}+\mathbf{G}) &= \int_0^{R^{\mathrm{MT}}_\alpha} \mathrm{d}r\, r^2 u^\alpha_{l'p'}(r) j_l(|\mathbf{q}+\mathbf{G}|r) u^\alpha_{l''p''}(r), \end{aligned} \tag{8.26}$$

where the $C^{l'm'}_{lml''m''}$ denote the Gaunt coefficients (Gaunt 1929). We proceed to evaluate the expressions $M^{\mathrm{MT}}_{\mathbf{G}'L''\mathbf{k}}(\mathbf{q}+\mathbf{G})$, $M^{\mathrm{MT}}_{L'\mathbf{G}''\mathbf{k}}(\mathbf{q}+\mathbf{G})$ and $M^{\mathrm{MT}}_{L'L''\mathbf{k}}(\mathbf{q}+$

G) (which now contain contributions from the local orbitals). By following straightforwardly the way in which Eq. (8.24) was derived, we obtain for a combination of one local orbital and one APW-function

$$\begin{aligned} M^{\mathrm{MT}}_{\mathbf{G}'L''\mathbf{k}}(\mathbf{q}+\mathbf{G}) &= 4\pi \sum_{\alpha} S^{*}_{\alpha}(\mathbf{q}+\mathbf{G}) \sum_{l'm'p'} A^{\alpha}_{l'm'p'}(\mathbf{k}+\mathbf{G}')^{*} X^{\alpha}_{l'm'p',s''}(\mathbf{q}+\mathbf{G}) \\ X^{\alpha}_{l'm'p',s''}(\mathbf{q}+\mathbf{G}) &= \sum_{l} (-i)^{l} R^{\alpha}_{l'p's''l}(\mathbf{q}+\mathbf{G}) \sum_{m} Y_{lm}(\widehat{\mathbf{q}+\mathbf{G}})^{*} C^{l'm'}_{lml''m''} \\ R^{\alpha}_{l'p's''l}(\mathbf{q}+\mathbf{G}) &= \int_{0}^{R^{\mathrm{MT}}_{\alpha}} \mathrm{d}r\, r^{2} u^{\alpha}_{l'p'}(r) j_{l}(|\mathbf{q}+\mathbf{G}|r) v^{\alpha}_{s''}(r) \delta_{\alpha,\alpha''} \end{aligned} \tag{8.27}$$

and

$$\begin{aligned} M^{\mathrm{MT}}_{L'\mathbf{G}''\mathbf{k}}(\mathbf{q}+\mathbf{G}) &= 4\pi \sum_{\alpha} S^{*}_{\alpha}(\mathbf{q}+\mathbf{G}) \sum_{l''m''p''} A^{\alpha}_{l''m''p''}(\mathbf{k}+\mathbf{G}'') \\ &\quad \times X^{\alpha}_{s',l''m''p''}(\mathbf{q}+\mathbf{G}) \\ X^{\alpha}_{s',l''m''p''}(\mathbf{q}+\mathbf{G}) &= \sum_{l} (-i)^{l} R^{\alpha}_{s'l''p''l}(\mathbf{q}+\mathbf{G}) \sum_{m} Y_{lm}(\widehat{\mathbf{q}+\mathbf{G}})^{*} C^{l'm'}_{lml''m''} \\ R^{\alpha}_{s'l''p''l}(\mathbf{q}+\mathbf{G}) &= \int_{0}^{R^{\mathrm{MT}}_{\alpha}} \mathrm{d}r\, r^{2} v^{\alpha}_{s'}(r) j_{l}(|\mathbf{q}+\mathbf{G}|r) u^{\alpha}_{l''p''}(r) \delta_{\alpha,\alpha'}. \end{aligned} \tag{8.28}$$

Finally, for the case of two local orbitals, we arrive at

$$\begin{aligned} M^{\mathrm{MT}}_{L',L''\mathbf{k}}(\mathbf{q}+\mathbf{G}) &= 4\pi \sum_{\alpha} S^{*}_{\alpha}(\mathbf{q}+\mathbf{G}) X^{\alpha}_{s',s''}(\mathbf{q}+\mathbf{G}) \\ X^{\alpha}_{s',s''}(\mathbf{q}+\mathbf{G}) &= \sum_{l} (-i)^{l} R^{\alpha}_{s's''l}(\mathbf{q}+\mathbf{G}) \sum_{m} Y_{lm}(\widehat{\mathbf{q}+\mathbf{G}})^{*} C^{l'm'}_{lml''m''} \\ R^{\alpha}_{s's''l}(\mathbf{q}+\mathbf{G}) &= \int_{0}^{R^{\mathrm{MT}}_{\alpha}} \mathrm{d}r\, r^{2} v^{\alpha}_{s'}(r) j_{l}(|\mathbf{q}+\mathbf{G}|r) v^{\alpha}_{s''}(r) \delta_{\alpha,\alpha'} \delta_{\alpha,\alpha''}. \end{aligned} \tag{8.29}$$

In the last three equations we used Eq. (7.9) and the fact that all indices l, m, p and s that occur without a sum depend on the corresponding L value for the local orbitals, e.g.

$$l' = l'(L'),\ m' = m'(L'),\ p' = p'(L'),\ s' = s'(L').$$

The calculation of these matrix elements consumes a very large, if not the largest amount of computation time for the TDDFT and especially for the BSE part of the implementation. It is therefore desirable to exploit the symmetries of the system under consideration to reduce the actual number of matrix elements to be calculated. This strategy is easily worked out (Puschnig 2002) and applied partially for the calculation of the $\mathbf{q}$ dependent dielectric matrix.

8.3 Dielectric Matrix and Kohn-Sham Response Function

The dielectric matrix at the independent quasi-particle level and the Kohn-Sham response function are conceptually different quantities, since they involve the quasi-particle wave functions and energies and the Kohn-Sham ones, respectively. Since, we are using the Kohn-Sham wave functions throughout the formalism as an approximation, and correct the quasi-particle energies by a simple scissor's shift the dielectric matrix and the Kohn-Sham response function can be discussed simultaneously. The dielectric matrix is given with the help of Eq. (6.7) and Eq. (2.69)

$$\epsilon_{\mathbf{G}\mathbf{G}'}(\mathbf{q},\omega) = \delta_{\mathbf{G}\mathbf{G}'} - \chi^0_{\mathbf{G}\mathbf{G}'}(\mathbf{q},\omega) v_{\mathbf{G}'}(\mathbf{q}) \tag{8.30}$$

in reciprocal space. Since we are using a static screening for the BSE, the dielectric matrix is calculated for $\omega = 0$ only, which we will denote as $\epsilon_{\mathbf{G}\mathbf{G}'}(\mathbf{q})$. For the Kohn-Sham response function $\chi^{\mathrm{KS}}_{\mathbf{G}\mathbf{G}'}(\mathbf{q},\omega)$, Eq. (6.53) can be immediately evaluated.

The inclined reader my have noticed that the Kohn-Sham response function for the TDDFT formalism, as well as the independent quasi-particle polarizability for the case of the BSE has some vanishing Fourier coefficients for the long wavelength limit $\mathbf{q} \to 0$. The parts χ^0_{00} as well as $\chi^0_{0\mathbf{G}}$ and $\chi^0_{\mathbf{G}0}$, which are called *head* and *wings* of the corresponding matrix in Fourier space, are vanishing for $\mathbf{q} \to 0$ and $\mathbf{G} \neq 0$. This fact has been pointed out already by Pick, Cohen and Martin (Pick et al. 1970) who showed that

$$\chi^0_{00}(\mathbf{q}) \sim q^2 \tag{8.31}$$

$$\chi^0_{0\mathbf{G}}(\mathbf{q}), \chi^0_{\mathbf{G}0}(\mathbf{q}) \sim q \tag{8.32}$$

for $\mathbf{G} \neq 0$. On the other hand the Coulomb potential is singular in reciprocal space for $\mathbf{q} \to 0$. This counterbalances the vanishing head of the polarizability, however, one of the wings, $\chi^0_{0\mathbf{G}}$, diverges as $1/q$. Consequently, the dielectric matrix has divergent terms and is non-Hermitian. It is therefore common to use the concept of the so-called *symmetrized dielectric matrix* (Rohlfing et al. 1995), $\tilde{\epsilon}_{\mathbf{GG'}}(\mathbf{q})$, which we introduce as

$$\tilde{\epsilon}_{\mathbf{GG'}}(\mathbf{q}) = \sum_{\mathbf{G}_1\mathbf{G}_2} v^{-\frac{1}{2}}_{\mathbf{GG}_1}(\mathbf{q}) \epsilon_{\mathbf{G}_1\mathbf{G}_2}(\mathbf{q}) v^{\frac{1}{2}}_{\mathbf{G}_2\mathbf{G'}}(\mathbf{q}). \tag{8.33}$$

The "square root" of the Coulomb potential, $v^{\frac{1}{2}}_{\mathbf{GG'}}(\mathbf{q})$, has the meaning of a matrix square root and is given by

$$v^{\frac{1}{2}}_{\mathbf{GG'}}(\mathbf{q}) = \sqrt{v_{\mathbf{GG'}}(\mathbf{q})} = \frac{\sqrt{4\pi}}{|\mathbf{q}+\mathbf{G}|}\delta_{\mathbf{GG'}}. \tag{8.34}$$

It corresponds to

$$v^{\frac{1}{2}}(\mathbf{r}, \mathbf{r'}) = \frac{\pi^{-\frac{3}{2}}}{|\mathbf{r}-\mathbf{r'}|^2} \tag{8.35}$$

in real space (Rohlfing et al. 1995). The symmetrized dielectric matrix obtained in this way is Hermitian and remains finite for $\mathbf{q} \to 0$. It is used for inversion to obtain $\epsilon^{-1}_{\mathbf{GG'}}(\mathbf{q})$ and subsequently the screened Coulomb interaction $W_{\mathbf{GG'}}(\mathbf{q})$ as a prerequisite for the BSE.

For the Kohn-Sham response function, χ^{KS}, a similar symmetrization procedure is used to get rid of vanishing components for the head and wings of the corresponding matrix in Fourier space. To this end, we introduce the *symmetrized Kohn-Sham response function*

$$\tilde{\chi}^{\mathrm{KS}}_{\mathbf{GG'}}(\mathbf{q}, \omega) = \sum_{\mathbf{G}_1\mathbf{G}_2} v^{\frac{1}{2}}_{\mathbf{GG}_1}(\mathbf{q}) \chi^{\mathrm{KS}}_{\mathbf{G}_1\mathbf{G}_2}(\mathbf{q}, \omega) v^{\frac{1}{2}}_{\mathbf{G}_2\mathbf{G'}}(\mathbf{q}) \tag{8.36}$$

in order to exactly counterbalance the vanishing components of χ^{KS}. This strategy will also become clear when applying this procedure to the Dyson equation. We skip the tilde as label for the symmetrization in the following, unless it is important.

For practical calculations it shall be mentioned that the dielectric matrix as well as the Kohn-Sham response function converge very slowly with respect to the number of $\mathbf{k}$ points used in the summation. This is particularly true for

the head and the wings. The convergence of the body (the remaining part of the matrix besides the head and the wings) does not depend crucially on the **k**-point sampling. This finding has also been reported previously (Puschnig 2002). This convergence problem is associated with the pole structure of the dielectric matrix or response function. Especially, the terms

$$\frac{1}{\varepsilon_{n\mathbf{k}} - \varepsilon_{m\mathbf{k}+\mathbf{q}} + \omega + i\delta} \tag{8.37}$$

vary rapidly with respect to the **k** point. Since the **k**-point sampling has to be moderate in view of the time consumption of the subsequent steps towards the solution of the BSE or TDDFT response equation, an interpolation method is desirable. One possible way of interpolation is the *linear tetrahedron method* (Lehmann & Taut 1972) where the sub-cells of a regular **k** mesh are divided into tetrahedra and the function is interpolated linearly inside these tetrahedra. We have optionally employed this method using an implementation by Li and Gomez-Abal (Gomez-Abal et al. 2009) based on Ref. (Blöchl et al. 1994). With the help of the tetrahedron method it is possible to determine the onset of the response function (the optical gap) quite accurately, whereas for a summation including a finite broadening the onset gets smeared out. However, the physical interpretation of a broadening in terms of a lifetime gets lost. A second way of improving the convergence of the response function is to employ analytic continuation techniques. They are especially useful if a finite broadening gives strong oscillations in the response function (Ku & Eguiluz 1999). One possible way of performing the analytic continuation is to apply a Wick rotation to the frequency plane and calculate $\chi^{\mathrm{KS}}_{\mathbf{GG}'}(\mathbf{q}, i\omega)$ now at the purely imaginary frequencies $i\omega$. The functions obtained that way are in general very smooth and well behaved. We have implemented an analytic continuation scheme by using N-point Padé approximants (Vidberg & Serene 1977) which have been used originally in the context of finite temperature Eliashberg equations. This method has proven especially powerful in the determination of the loss function (Lee & Chang 1996, Ku & Eguiluz 1999) and is also implemented mainly for this purpose.

8.4 Bethe-Salpeter Equation

This section is targeted to the screened Coulomb interaction on the one hand and the detailed formalism of the effective Hamiltonian matrix for

the Bethe-Salpeter equation on the other hand. The representation of the dielectric function in terms of the eigenvalues and eigenvectors of the BSE Hamiltonian is explicitly given within the approximations chosen for the actual implementation.

8.4.1 The Screened Coulomb Interaction

We start to evaluate the screened Coulomb interaction with the help of the symmetrized dielectric matrix

$$W_{\mathbf{GG'}}(\mathbf{q}) = \epsilon^{-1}_{\mathbf{GG'}}(\mathbf{q}) v_{\mathbf{G'}}(\mathbf{q}) \tag{8.38}$$

$$= v^{\frac{1}{2}}_{\mathbf{G'}}(\mathbf{q}) \tilde{\epsilon}^{-1}_{\mathbf{GG'}}(\mathbf{q}) v^{\frac{1}{2}}_{\mathbf{G'}}(\mathbf{q}). \tag{8.39}$$

This expression is, however, singular for $\mathbf{q} = 0$ if at least one of the $\mathbf{G}$ vectors vanishes. It will be the aim now to find a way to treat this singularity without altering the BSE formalism. One very general idea is to replace the value of $W_{\mathbf{GG'}}(\mathbf{q})$ by the corresponding average $W'_{\mathbf{GG'}}(\mathbf{q})$ over the sub-cell $V_{\mathbf{q}}$, which is centered at the $\mathbf{q}$ point and extends between the neighboring $\mathbf{q}$ points of the mesh[1]

$$\begin{aligned} W'_{\mathbf{GG'}}(\mathbf{q}) &= \frac{1}{V_q} \int_{V_{\mathbf{q}}} \mathrm{d}^3 p W_{\mathbf{GG'}}(\mathbf{p}) \\ &= \frac{1}{V_q} \int_{V_{\mathbf{q}}} \mathrm{d}^3 p \frac{\sqrt{4\pi} \epsilon^{-1}_{\mathbf{GG'}}(\mathbf{p}) \sqrt{4\pi}}{|\mathbf{p}+\mathbf{G}||\mathbf{p}+\mathbf{G'}|}. \end{aligned} \tag{8.40}$$

The volume of this sub-cell $V_{\mathbf{q}}$ is given by $V_q = (2\pi)^3/V$. We have implemented such a scheme using either an extrapolation technique in order to find the value of the integral, Eq. (8.40), for a vanishing volume element in $\mathbf{q}$ space (Rohlfing & Louie 2000), or using a Monte-Carlo integration technique (Marini et al. 2009). The detailed description of these methods goes, however, beyond the scope of this thesis.

In practical calculations, it is too time-consuming to average all $\mathbf{GG'}$ components of the screened Coulomb interaction. Only those being singular at the Γ-point are treated this way. Additionally, for the integral in Eq. (8.40) the inverse dielectric matrix has to be known in dependence of $\mathbf{p}$ throughout the sub-cell. From its analytical properties we know the angular dependence

[1] We again omit the tilde for the symmetrized dielectric matrix from now on.

at the Γ point. It is therefore more favorable to split the integration into an angular part and a radial part

$$\begin{aligned}\int_{V_{\mathbf{q}}} \mathrm{d}^3p\, f(\mathbf{p}) &= \int_{V_\Gamma = V_{\mathbf{q}} - \mathbf{q}} \mathrm{d}^3p\, f(\mathbf{q}+\mathbf{p}) \\ &= \int \mathrm{d}\hat{\Omega}_{\mathbf{p}} \int \mathrm{d}p \lambda_{\mathbf{q}}(p, \hat{\Omega}_{\mathbf{p}})\, f(\mathbf{q}+\mathbf{p}).\end{aligned} \tag{8.41}$$

Here $\lambda_{\mathbf{q}}(p, \hat{\Omega}_{\mathbf{p}})$ denotes the characteristic function of the sub-cell V_Γ. We will specialize our investigations for this reason to the case of $\mathbf{q} = 0$ and follow the findings of Ref. (Freysoldt et al. 2007). As further approximation we take into account only the angular dependence of the inverse dielectric matrix

$$W'_{\mathbf{G}\mathbf{G}'}(0) = \frac{1}{V_q} \int \mathrm{d}\hat{\Omega}_{\mathbf{p}} \int \mathrm{d}p \lambda_\Gamma(p, \hat{\Omega}_{\mathbf{p}}) \frac{\sqrt{4\pi^2}\epsilon^{-1}_{\mathbf{G}\mathbf{G}'}(\hat{\Omega}_{\mathbf{p}})\sqrt{4\pi^2}}{|p\hat{\Omega}_{\mathbf{p}} + \mathbf{G}||p\hat{\Omega}_{\mathbf{p}} + \mathbf{G}'|}. \tag{8.42}$$

Moreover, only those expressions $1/|p\hat{\Omega}_{\mathbf{p}} + \mathbf{G}|$ are kept under the integration sign where $\mathbf{G} = 0$. Otherwise they are replaced by $1/|\mathbf{G}|$. We are now ready to summarize the averaged screened Coulomb interaction. The head of W' is given by

$$W'_{00}(0) = \frac{1}{V_q} \int \mathrm{d}\hat{\Omega}_{\mathbf{p}} \epsilon^{-1}_{00}(\hat{\Omega}_{\mathbf{p}}) \int \mathrm{d}p \lambda_\Gamma(p, \hat{\Omega}_{\mathbf{p}}) \frac{4\pi^2}{p^2}, \tag{8.43}$$

whereas for the wings we obtain

$$W'_{\mathbf{G}0}(0) = \frac{1}{V_q} \frac{\sqrt{4\pi^2}}{|\mathbf{G}|} \int \mathrm{d}\hat{\Omega}_{\mathbf{p}} \epsilon^{-1}_{\mathbf{G}0}(\hat{\Omega}_{\mathbf{p}}) \int \mathrm{d}p \lambda_\Gamma(p, \hat{\Omega}_{\mathbf{p}}) \frac{\sqrt{4\pi^2}}{p}. \tag{8.44}$$

Finally, the body of W' reduces to

$$W'_{\mathbf{G}\mathbf{G}'}(0) = \frac{1}{V_q} \frac{4\pi^2}{|\mathbf{G}||\mathbf{G}'|} \int \mathrm{d}\hat{\Omega}_{\mathbf{p}} \epsilon^{-1}_{\mathbf{G}\mathbf{G}'}(\hat{\Omega}_{\mathbf{p}}) \int \mathrm{d}p \lambda_\Gamma(p, \hat{\Omega}_{\mathbf{p}}). \tag{8.45}$$

The angular dependent inverse dielectric matrix and characteristic function of the domain of integration are expanded in spherical harmonics and a cutoff is used to control the effects of the anisotropy explicitly. The details of the evaluation of $W'_{00}(0)$ and related expressions are quite lengthy. For further information we refer the reader to Ref. (Freysoldt et al. 2007).

Finally, we denote a simple spherical averaging method neglecting the variation of the interpolated function inside the sub-cell completely. The results for averaging the divergent factors $\sqrt{4\pi^2}/q$ and $4\pi^2/q^2$ are given by

$$\frac{1}{V_q}\int \mathrm{d}^3p\,\frac{4\pi^2}{q^2} = \frac{2}{\pi}Vq_s \tag{8.46}$$

$$\frac{1}{V_q}\int \mathrm{d}^3p\,\frac{\sqrt{4\pi^2}}{q} = \frac{1}{\pi}Vq_s^2 \tag{8.47}$$

$$q_s = \left(\frac{6\pi^2}{V}\right)^{\frac{1}{3}}. \tag{8.48}$$

The sub-cell radius q_s appearing above is defined as the radius of the sphere with the same volume as the sub-cell. This strategy has been employed (Hybertson & Louie 1986, Puschnig 2002) for the framework of quasi-particle energies and the Bethe-Salpeter equation, respectively. The choice of the inverse dielectric matrix at the Γ-point is, however, not uniquely defined within this simple approach.

8.4.2 The Direct Interaction

So far we have provided all the quantities necessary for setting up the Hamiltonian matrix of the Bethe-Salpeter equation. We start with the evaluation of the direct interaction kernel, worked out already in Eq. (6.46) and we provide the expression now in more detail, specializing to the Tamm-Dancoff approximation described in Sec. 6.4.1

$$H^{\mathrm{dir}}_{vc\mathbf{k},v'c'\mathbf{k}'} = -\int \mathrm{d}^3r\mathrm{d}^3r'\psi_{v\mathbf{k}}(\mathbf{r})\psi^*_{c\mathbf{k}}(\mathbf{r}')W(\mathbf{r},\mathbf{r}')\psi^*_{v'\mathbf{k}'}(\mathbf{r})\psi_{c'\mathbf{k}'}(\mathbf{r}'). \tag{8.49}$$

We evaluate this term with the help of a Fourier expansion of the screened Coulomb potential according to Eq. (E.20) with coefficients $W_{\mathbf{GG}'}(\mathbf{q})$ which we replace by their averaged counterparts $W'_{\mathbf{GG}'}(\mathbf{q})$. In doing so, we get rid of the divergence at the Γ-point at one hand and solve the problem of the angular dependence on the other hand. The final expression for $H^{\mathrm{dir}}_{vc\mathbf{k},v'c'\mathbf{k}}$ has been worked out already (Puschnig 2002), and only the result is displayed here

$$H^{\mathrm{dir}}_{vc\mathbf{k},v'c'\mathbf{k}'} = -\frac{1}{V}\sum_{\mathbf{GG}'} M^*_{vv'\mathbf{k}}(\mathbf{q}+\mathbf{G})W'_{\mathbf{GG}'}(\mathbf{q})M_{cc'\mathbf{k}}(\mathbf{q}+\mathbf{G}'). \tag{8.50}$$

In Eq. (8.50) $\mathbf{q} = \mathbf{k}' - \mathbf{k}$ but mapped to the first Brillouin zone.

8.4.3 The Exchange Interaction

The evaluation of the matrix elements of the exchange interaction kernel is obtained in a similar, even simpler way as those of the direct interaction. According to Eq. (6.45) they are given by

$$H^{\mathrm{x}}_{vc\mathbf{k},v'c'\mathbf{k}'} = \int \mathrm{d}^3r\mathrm{d}^3r' \psi_{v\mathbf{k}}(\mathbf{r})\psi^*_{c\mathbf{k}}(\mathbf{r})\bar{v}(\mathbf{r},\mathbf{r}')\psi^*_{v'\mathbf{k}'}(\mathbf{r}')\psi_{c'\mathbf{k}'}(\mathbf{r}'). \tag{8.51}$$

The bare Coulomb potential is now Fourier expanded according to Eq. (E.15) and the final result contains, in contrast to Eq. (8.50) a summation with respect to only one $\mathbf{G}$ vector

$$H^{\mathrm{x}}_{vc\mathbf{k},v'c'\mathbf{k}'} = \frac{1}{V}\sum_{\mathbf{G}} M^*_{vc\mathbf{k}}(\mathbf{G})\bar{v}_{\mathbf{G}}(0)M_{v'c'\mathbf{k}'}(\mathbf{G}). \tag{8.52}$$

The derivation of this expression for H^{x} can, again, be found in Ref. (Puschnig 2002). We note that due to the presence of the modified Coulomb potential, the term $\mathbf{G} = 0$ is excluded from the summation.

For the sake of completeness we also provide the diagonal term of the BSE Hamiltonian which reads

$$H^{\mathrm{diag}}_{vc\mathbf{k},v'c'\mathbf{k}'} = (E_{c\mathbf{k}} - E_{v\mathbf{k}})\delta_{vv'}\delta_{cc'}\delta_{\mathbf{k}\mathbf{k}'}. \tag{8.53}$$

8.4.4 The BSE Eigenvalue Problem

We review the BSE eigenvalue problem of Eq. (6.31) in more detail

$$\sum_{v'c'\mathbf{k}'} H_{vc\mathbf{k},v'c'\mathbf{k}'}A^{\lambda}_{v'c'\mathbf{k}'} = \mathcal{E}^{\lambda}A^{\lambda}_{vc\mathbf{k}}, \tag{8.54}$$

where the parts of the BSE Hamiltonian have already been discussed in the previous sections. Now, the various approximations resulting from switching on or off certain terms in this Hamiltonian shall be investigated more carefully. We start to write the effective Hamiltonian as

$$H^{\mathrm{eff}} = H^{\mathrm{diag}} + 2\gamma_{\mathrm{x}}H^{\mathrm{x}} + \gamma_{\mathrm{dir}}H^{\mathrm{dir}}. \tag{8.55}$$

The factors γ_{x} and γ_{dir} allow us to choose several levels of approximation and to distinguish between the spin-singlet and spin-triplet channels (Rohlfing & Louie 2000). For the purpose of describing non-interacting independent

particle transitions with the BSE both are set to zero. By only neglecting the correlation or direct part, H^{dir}, in the effective Hamiltonian we arrive at the RPA including local field effects (LFE). There are two spin-channels, namely the *singlets* described by the full Hamiltonian ($\gamma_{\mathrm{x}} = 1$, $\gamma_{\mathrm{dir}} = 1$) and the *triplets* with the exchange-part H^{x} being absent ($\gamma_{\mathrm{x}} = 0$, $\gamma_{\mathrm{dir}} = 1$).

The expression for the diagonal components of the macroscopic dielectric tensor is finally given in the context of the Tamm-Dancoff approximation in a simpler form[2] (cf. Eq. (6.36))

$$\epsilon_{\mathrm{M}}^{\alpha\alpha}(\omega) = 1 - \frac{8\pi}{V} \sum_{\lambda} |t_{\lambda}^{\alpha}|^2 \left[\frac{1}{\omega - \mathcal{E}_{\lambda} + i\delta} + \frac{1}{-\omega - \mathcal{E}_{\lambda} - i\delta} \right] \tag{8.56}$$

with

$$t_{\lambda}^{\alpha} = \sum_{vc\mathbf{k}} A_{vc\mathbf{k}}^{\lambda} \frac{\langle v\mathbf{k}|\hat{p}_{\alpha}|c\mathbf{k}\rangle}{\varepsilon_{c\mathbf{k}} - \varepsilon_{v\mathbf{k}}}, \tag{8.57}$$

where the index α labels the polarization and V denotes the crystal volume.

8.5 TDDFT within Linear Response

In this section we shall go into more detail as far as the linear response formalism of TDDFT is concerned. We point out different strategies of solving Dyson's equation for the response function and finally discuss the implementation of the xc kernel derived from MBPT, which has already been discussed in a more general framework in Sec. 5.3.

8.5.1 Dyson's Equation

For the practical solution of Dyson's equation for χ, Eq. (6.52), we apply a similar transform to it as already done for the Kohn-Sham response function

$$\begin{aligned} \tilde{\chi}_{\mathbf{G}\mathbf{G}'}(\mathbf{q},\omega) &= \tilde{\chi}^{\mathrm{KS}}_{\mathbf{G}\mathbf{G}'}(\mathbf{q},\omega) \\ &\quad + \sum_{\mathbf{G}_1\mathbf{G}_2} \tilde{\chi}^{\mathrm{KS}}_{\mathbf{G}\mathbf{G}_1}(\mathbf{q},\omega)[\tilde{v}_{\mathbf{G}_1}(\mathbf{q})\delta_{\mathbf{G}_1\mathbf{G}_2} + \tilde{f}^{\mathrm{xc}}_{\mathbf{G}_1\mathbf{G}_2}(\mathbf{q},\omega)]\tilde{\chi}_{\mathbf{G}_2\mathbf{G}'}(\mathbf{q},\omega). \end{aligned} \tag{8.58}$$

[2]Note that in this expression for the macroscopic dielectric function the spin has already been summed over.

Here, the quantities bearing a tilde on top are given by

$$\tilde{\chi}_{\mathbf{G}\mathbf{G}'}(\mathbf{q},\omega) = v^{\frac{1}{2}}_{\mathbf{G}}(\mathbf{q})\chi_{\mathbf{G}\mathbf{G}'}(\mathbf{q},\omega)v^{\frac{1}{2}}_{\mathbf{G}'}(\mathbf{q}) \tag{8.59}$$

$$\tilde{\chi}^{\mathrm{KS}}_{\mathbf{G}\mathbf{G}'}(\mathbf{q},\omega) = v^{\frac{1}{2}}_{\mathbf{G}}(\mathbf{q})\chi^{\mathrm{KS}}_{\mathbf{G}\mathbf{G}'}(\mathbf{q},\omega)v^{\frac{1}{2}}_{\mathbf{G}'}(\mathbf{q}) \tag{8.60}$$

$$\tilde{v}_{\mathbf{G}}(\mathbf{q}) = v^{-\frac{1}{2}}_{\mathbf{G}}(\mathbf{q})v_{\mathbf{G}}(\mathbf{q})v^{-\frac{1}{2}}_{\mathbf{G}}(\mathbf{q}) = 1 \tag{8.61}$$

$$\tilde{f}^{\mathrm{xc}}_{\mathbf{G}}(\mathbf{q}) = v^{-\frac{1}{2}}_{\mathbf{G}}(\mathbf{q})f^{\mathrm{xc}}_{\mathbf{G}\mathbf{G}'}(\mathbf{q})v^{-\frac{1}{2}}_{\mathbf{G}'}(\mathbf{q}). \tag{8.62}$$

This way we ensure that the equations are analytic for all $\mathbf{G}\mathbf{G}'$ vectors and $\mathbf{q}$ points.

In view of the *xc* kernel from MBPT which is given more naturally in terms of $T_{\mathrm{xc}} = \chi^0 f_{\mathrm{xc}} \chi^0$ it is more convenient to work with a symmetric form of the Dyson equation (Sottile et al. 2003)

$$\chi_{\mathbf{G}\mathbf{G}'}(\omega) = \sum_{\mathbf{G}_1\mathbf{G}_2} \chi^0_{\mathbf{G}\mathbf{G}_1}(\omega)\big[\chi^0_{\mathbf{G}_1\mathbf{G}_2}(\omega) - \sum_{\mathbf{G}_3} \chi^0_{\mathbf{G}_1\mathbf{G}_3} v_{\mathbf{G}_3}\chi^0_{\mathbf{G}_3\mathbf{G}_2} - T^{\mathrm{xc}}_{\mathbf{G}_1\mathbf{G}_2}\big]^{-1} \times \chi^0_{\mathbf{G}_2\mathbf{G}'}. \tag{8.63}$$

In both cases, the conventional and the symmetrized Dyson equation, it is sometimes the case that the matrix which has to (at least formally) be inverted is badly conditioned, *i.e.,* , has eigenvalues close to zero. This can be the case if the Kohn-Sham response function has non-trivial vanishing eigenvalues (in its spectral decomposition) for certain frequencies (Mearns & Kohn 1987). Additionally, if the number of $\mathbf{G}$ vectors is larger than the number of transitions ($vc\mathbf{k}$) it can be shown that the Kohn-Sham response function is not invertible for all frequencies (Sottile 2003). In any case, it is safe to use a *singular value decomposition* as an intermediate step in the inversion of a matrix and discard the subspace associated to vanishing or very small singular values. However, such a way of inverting a matrix involves the solution of an eigenvalue problem and is therefore much more time-consuming to perform. Finally, we note that if we are only interested in the head of χ it is sufficient to solve a linear system of equations which is less time consuming and more stable than a direct inversion of a matrix (Sottile 2003).

8.5.2 The *xc* Kernel from MBPT

Here the first order expression for the *xc* kernel derived from many-body perturbation theory appearing in Sec. 5.3 is reviewed in view of its practi-

cal implementation. We mainly follow the work of SOTTILE (Sottile et al. 2003, Sottile 2003), ADRAGNA (Adragna et al. 2003) and MARINI (Marini et al. 2003). We start with the first order T_{xc} from Eq. (5.11), apply the expansion convention in transition space, Eq. (6.23), use Eq. (6.26) and finally apply a Fourier transform according to Eq. (E.19), which yields for vanishing momentum transfer $\mathbf{q} \to 0$

$$T^{\mathrm{xc}}_{\mathbf{G}\mathbf{G}'}(\omega) = \sum_{vc\mathbf{k}} \sum_{v'c'\mathbf{k}'} \frac{M_{vc\mathbf{k}}(\mathbf{G}) W_{vc\mathbf{k},v'c'\mathbf{k}'} M^*_{v'c'\mathbf{k}'}(\mathbf{G}')}{(\varepsilon_{v\mathbf{k}} - \varepsilon_{c\mathbf{k}} + \omega + i\delta)(\varepsilon_{v'\mathbf{k}'} - \varepsilon_{c'\mathbf{k}'} + \omega + i\delta)}, \tag{8.64}$$

where M is the $\mathbf{q}$-dependent matrix element (see Section 8.2) and we have used $W_{vc\mathbf{k},v'c'\mathbf{k}'}$ for the direct term of the BSE Hamiltonian $H^{\mathrm{dir}}_{vc\mathbf{k},v'c'\mathbf{k}'}$. The above expression for T_{xc} is quite demanding to calculate due to the structure of the denominator. By using a partial fraction decomposition of Eq. (8.64), however, we can rewrite it as (Marini et al. 2003)

$$T^{\mathrm{xc}}_{\mathbf{G}\mathbf{G}'}(\omega) = \sum_{vc\mathbf{k}} \Big[\frac{R^{\mathbf{G}\mathbf{G}'}_{vc\mathbf{k}} + h.c.}{\omega - E_{vc\mathbf{k}} + \Delta + i\delta} + \frac{Q^{\mathbf{G}\mathbf{G}'}_{vc\mathbf{k}}}{(\omega - E_{vc\mathbf{k}} + \Delta + i\delta)^2} \Big] \tag{8.65}$$

where the residuals R and Q are given by

$$R^{\mathbf{G}\mathbf{G}'}_{vc\mathbf{k}} = \sum_{v'c'\mathbf{k}'}^{E_{vc\mathbf{k}} \neq E_{v'c'\mathbf{k}'}} \frac{M_{vc\mathbf{k}}(\mathbf{G}) W'_{vc\mathbf{k},v'c'\mathbf{k}'} M_{v'c'\mathbf{k}'}(\mathbf{G}')^*}{E_{vc\mathbf{k}} - E_{v'c'\mathbf{k}'}} \tag{8.66}$$

and

$$Q^{\mathbf{G}\mathbf{G}'}_{vc\mathbf{k}} = \sum_{v'c'\mathbf{k}'}^{E_{vc\mathbf{k}} = E_{v'c'\mathbf{k}'}} M_{vc\mathbf{k}}(\mathbf{G}) W'_{vc\mathbf{k},v'c'\mathbf{k}'} M_{v'c'\mathbf{k}'}(\mathbf{G}')^*, \tag{8.67}$$

and $E_{vc\mathbf{k}}$ denotes the quasi-particle energy difference $\varepsilon_{c\mathbf{k}} - \varepsilon_{v\mathbf{k}}$. The diagonal elements of the Bethe-Salpeter kernel are approximated by a constant

$$\Delta = W_{vc\mathbf{k},vc\mathbf{k}}, \tag{8.68}$$

what is justified since all the diagonal elements have almost the same value. This fact has been observed in literature (Marini et al. 2003) and is confirmed by our results. In Eqs. (8.66) and (8.67), W' is a modified Coulombic part of the Bethe-Salpeter kernel, where the diagonal is set to zero since it merely results in a rigid shift of the spectrum (Marini et al. 2003). This shift is taken into account in the independent quasi-particle polarizability χ_0. As already discussed previously, it is more convenient to work with the transformed kernel from Eq. (8.62).

8.5.3 The ALDA xc Kernel

Finally we provide some remarks on the implementation of the ALDA xc kernel. Since we treat the Dyson equation in reciprocal space a Fourier transform has to be applied to the real space expression of the kernel in Eq. (4.33). Because of its locality in real space this transform is rather easy to perform and we obtain with the help of Eqs. (E.19) and (E.14)

$$\begin{aligned} f_{\mathbf{G}\mathbf{G}'}^{\mathrm{xc,ALDA}}(\mathbf{q}) &= \frac{1}{V}\int \mathrm{d}^3 r\, e^{-i(\mathbf{G}-\mathbf{G}')\mathbf{r}}\, \left.\frac{\mathrm{d}v_{\mathrm{xc}}^{\mathrm{LDA}}(n)}{\mathrm{d}n}\right|_{n=n_0(\mathbf{r})} \\ &= \frac{1}{V}\int \mathrm{d}^3 r\, e^{-i(\mathbf{G}-\mathbf{G}')\mathbf{r}} f^{\mathrm{LDA}}(\mathbf{r}) \\ &= \tilde{f}_{\mathbf{G}-\mathbf{G}'}^{\mathrm{LDA}}. \end{aligned} \tag{8.69}$$

Here we have introduced the variation of the LDA xc-potential with respect to the density

$$f^{\mathrm{LDA}}(\mathbf{r}) = \left.\frac{\mathrm{d}v_{\mathrm{xc}}^{\mathrm{LDA}}(n)}{\mathrm{d}n}\right|_{n=n_0(\mathbf{r})}. \tag{8.70}$$

We observe that the ALDA kernel in reciprocal space is most simply given as the Fourier transform of the xc-potential variation f^{LDA} evaluated at the difference of the $\mathbf{G}\mathbf{G}'$ components. It is important to note that the ALDA kernel is *independent* of the $\mathbf{q}$ vector, but nevertheless it gives remarkably good results on the $\mathbf{q}$ dependent dielectric function describing electron energy loss spectroscopy (Weissker et al. 2006).

The actual expression for f^{LDA} is obtained analytically in this work, stemming from the Perdew-Wang parametrization of the LDA potential (Perdew & Wang 1992). It is straight forward to derive but the expressions are lengthy and of no immediate importance for the scope of this thesis. Since in the LAPW formalism the LDA potential (as any other potential) is expressed differently in the interstitial region as well as in the muffin-tin, we point out that we have performed the Fourier transform of this mixed representation analytically. The expressions are very similar to the case of the $\mathbf{q}$-dependent matrix elements from Sec. 8.2 and shall not be repeated. They involve spherical Bessel functions of first kind and the Fourier transform of the step function. Due to the presence of only two spherical harmonics in the integrations for the muffin-tin part, the Gaunt coefficients are not needed, rendering the formalism simpler in this case. For the sake of completeness, we have tested

our analytical implementation against a numerical differentiation for f^{LDA} and the Fourier transform and found perfect agreement.

Chapter 9

Results

This chapter provides the application of theory and implementation described in the previous chapters. The results presented here also include convergence tests with respect to selected input parameters of the formalism. We treat two semiconductors, GaAs and Si, as representative examples for inorganic semiconductors. The case of an insulator showing strong excitonic effects is discussed for the example of LiF. Such quite simple test systems enable us to thoroughly compare the reliability of both formalisms, the Bethe-Salpeter equation as wells as the time-dependent DFT on the results for the macroscopic dielectric function. Finally we target our study to more advanced materials, being the organic semiconductors trans-polyacetylene and polyphenylene vinylene. These two polymers allow for a study of the electron-hole interactions in low-dimensional anisotropic systems. Whereas the former is interesting rather from the theoretical point of view, the latter has a technological application in organic light emitting diodes.

Here, for the first time results from the Bethe-Salpeter equation and from time-dependent DFT are shown, which are based upon the same all-electron code. This is the main goal of this thesis. Both two state-of-the-art methods to describe excitonic effects in solids shall be compared using the same ground state quantities. Therefore the larger part of this thesis has been dedicated to the implementation of both formalisms in favor of a comprehensive study of many different materials.

9.1 The Dielectric Function of GaAs

As a starting point for this chapter GaAs is chosen as an example to test the BSE implementation as well as various kernels. The xc kernel, derived from MBPT, has been employed already in different groups to study simple systems (Reining et al. 2002, Sottile et al. 2003, Sottile 2003, Marini et al. 2003, Adragna et al. 2003) including GaAs (Adragna et al. 2003). Moreover, examples for the application of the model kernels motivated by MBPT – Eqs. (5.30) and (5.32) – are given in Refs. (Botti et al. 2004, Botti et al. 2005).

Starting from the ground state calculation, carried out within the local density approximation (LDA), the Kohn-Sham band structure and wave functions are the only two ingredients needed in the TDDFT linear-response formalism. For the BSE, the quasi-particle energies and wave functions are required in principle. It has, however, been found to be sufficient shifting the conduction band energies rigidly upward (scissors correction) (Godby et al. 1988) and to use the LDA wave functions in place of the quasi-particle ones. Although this might not hold for arbitrary complex systems it can be regarded a reliable approximation in the case of GaAs.

For the TDDFT calculations, the Kohn-Sham response function Eq. (6.53) is evaluated in reciprocal space. The chosen **k**-mesh consists of 512 off-symmetry shifted **k**-points (corresponding to a $8 \times 8 \times 8$ mesh), and an RK_{max} value (product of the smallest muffin-tin radius and the plane wave cutoff) of 6.0 is used. The aforementioned scissors shift is chosen to be 1.04 eV (Gomez-Abal et al. 2008) in order to mimic the quasi-particle band structure and is used for the response function in all cases except the RPA and the TDLDA. Other groups have taken a different scissors shift of 0.8 eV (Botti et al. 2004, Adragna et al. 2003), or have performed a GW calculation (Rohlfing & Louie 1998). For the response function, the Coulomb potential, as well as the xc kernel in Eq. (6.52), the cutoff parameter for the reciprocal lattice vectors is taken to be 3.0 Bohr^{-1}, corresponding to 137 **G** vectors. The simple model kernels are set up with parameters $\alpha = 0.2$ for the static long-range kernel (static LRC, Eq. (5.30)) (Botti et al. 2004), while $\alpha = 0.15$ and $\beta = 7.43$ are used for the dynamical long-range model (dynamical LRC, Eq. (5.32)) (Botti et al. 2005). For the TDLDA the full self-consistent xc-potential is used. In case of the BSE derived kernel, the matrix elements of the screened Coulomb interaction Eq. (8.50) are required as well. As a next step, the Dyson equation (6.52) is solved for the interacting response function, and hence the macroscopic dielectric function, Eq. (6.10), is obtained.

For the BSE, the inverse dielectric matrix and the screened Coulomb interaction, Eq. (8.38), is calculated on the **k**-mesh mentioned above, where conduction band states up to 4.0 Hartree are included. The terms H^x and H^c of the BSE Hamiltonian are set up according to Eqs. (8.51) and (8.50), the eigenvalue problem is solved, and the macroscopic dielectric function obtained as given by Eq. (8.56). In all spectra, a Lorentzian broadening of 0.15 eV is introduced in order to smear out effects of finite **k**-point sampling.

In the upper panel of Figure 9.1 the imaginary part of the dielectric function is displayed for the RPA and BSE, where the latter agrees quite well with experiment (Lautenschlager, Garriga, Logothetidis & Cardona 1987) and almost coincides with the BSE calculation from Ref. (Rohlfing & Louie 1998).

Using the BSE result as a benchmark the various TDDFT approaches displayed in the lower panel can now be evaluated. The TDLDA results merely into a slight shift towards lower energies and higher oscillator strengths, compared to the RPA spectrum. The TDLDA calculation in Ref. (Botti et al. 2004) shows the second peak with a larger intensity, which might be due to a different **k** point sampling. The static as well as the dynamical LRCs are very similar and come quite close to the BSE result, although they slightly overestimate the first peak and underestimate the second one. In Ref. (Botti et al. 2004) the oscillator strengths in the case of the static LRC are (as mentioned already for the TDLDA) a bit higher.

Finally, the spectrum obtained by the BSE derived kernel can not be distinguished from the one of the full BSE calculation. The spectrum given in Ref. (Adragna et al. 2003) appears somewhat larger in magnitude than in this work while the ratio of the two peak heights is almost the same. Also, the overall line-shapes of the spectra are in very good agreement with data of this work, for both, the BSE and the BSE derived xc kernel.

For the sake of a better comparison to pseudo-potential results, we mimic one of the approximations therein, which is the frozen core. To this end the core density of the atomic calculation is kept fixed throughout the self-consistency cycle. A downward shift of the Ga $3d$ states by 20 meV is observed, while there is no visible effect in the region of the valence- and conduction bands. As a consequence, the macroscopic dielectric function of this particular system is not affected by the frozen-core approximation. For the sake of completeness, a convergence test with respect to the **k** mesh is provided in Fig. 9.2. It has to be mentioned here that both the BSE as well as the TDDFT calculation are not entirely converged with respect to the **k**

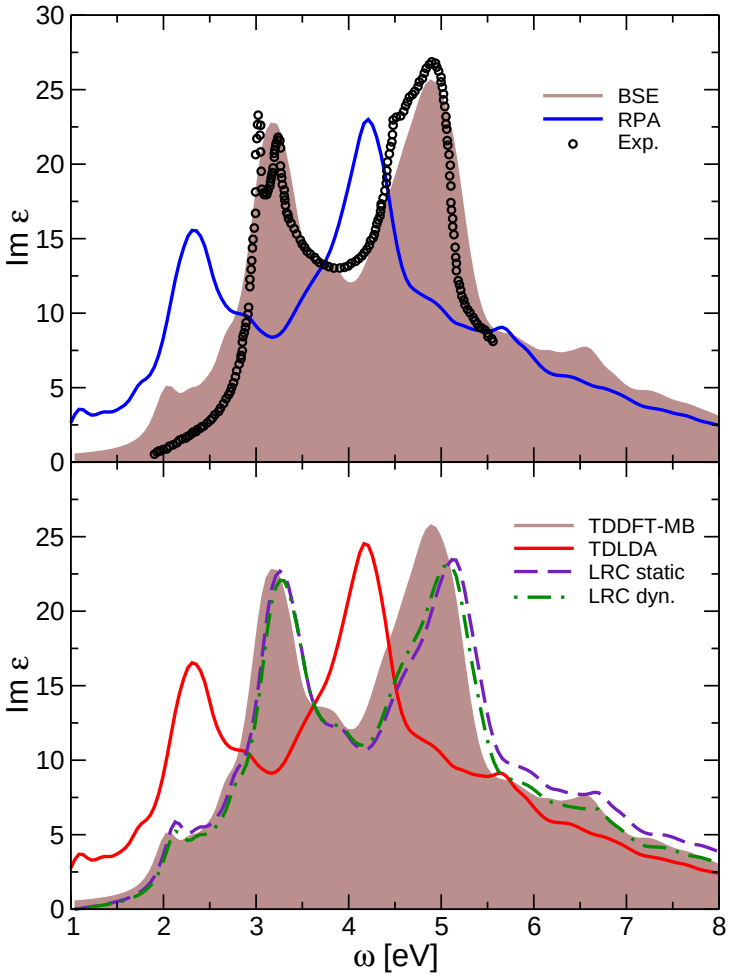

Figure 9.1: In the upper panel, the macroscopic dielectric functions obtained from the BSE (shaded area), the RPA (solid line) and experiment (circles, Ref. (Lautenschlager, Garriga, Logothetidis & Cardona 1987)) are depicted. The lower panel shows the results for the BSE derived kernel (TDDFT-MB, shaded area), the TDLDA (solid line), the static LRC (gray dashed line) as well as the dynamical LRC (dot-dashed line).

mesh. Nevertheless, both methods are indistinguishable in line-shape for the individual **k** mesh which supports the applicability of the BSE derived kernel. Parts of the results of this section have been published in Ref. (Sagmeister & Ambrosch-Draxl 2009).

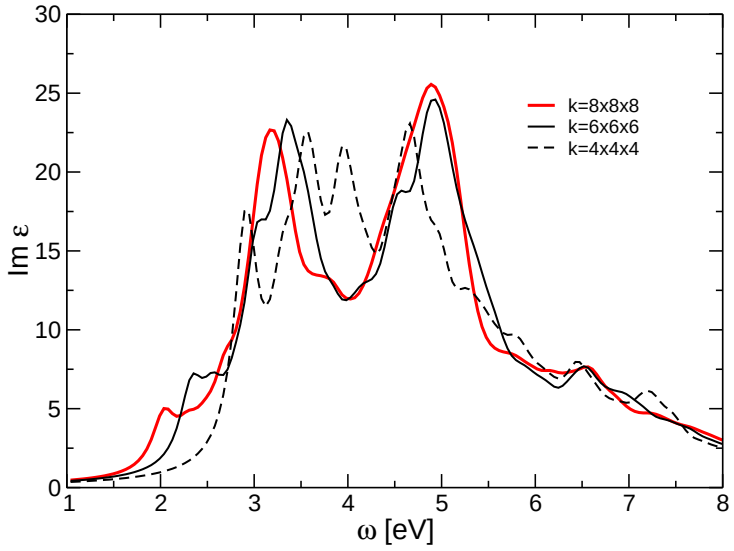

Figure 9.2: The macroscopic dielectric functions of GaAs from the BSE for three different **k** point samplings, which are meshes of $8 \times 8 \times 8$ (red line), $6 \times 6 \times 6$ (black line) and $4 \times 4 \times 4$ (black dashed line). The corresponding results for the BSE derived xc kernel coincide with the BSE ones and hence are not displayed.

9.2 The Dielectric Function of Si

Another even more prominent example to investigate the excitonic effects in semiconductors is bulk silicon. It has been studied widely in the context of optical properties including electron-hole correlations. BSE calculations in combination with the semi-empirical LCAO method are given in Refs. (Hanke & Sham 1979, Hanke & Sham 1980). Ab-initio calculations on the optical properties derived from the BSE have been reported in Refs. (Benedict et al. 1998*b*, Rohlfing & Louie 2000, Albrecht et al. 1998, Arnaud & Alouani 2001, Arnaud 2000) as well as (Puschnig 2002, Puschnig & Ambrosch-Draxl 2002*a*). Results from a TDDFT description of

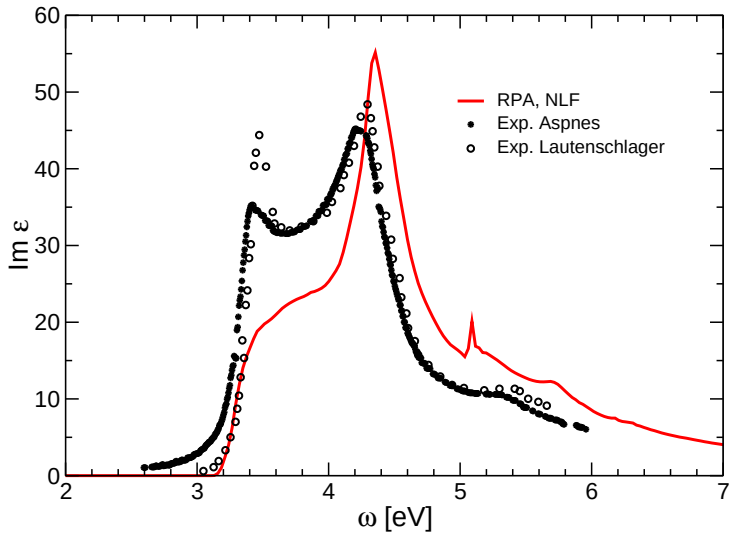

Figure 9.3: The dielectric function of Si obtained from the independent quasiparticle approximation using a highly precise **k** point sampling (solid line). For comparison, experimental data from Ref. (Aspnes & Studna 1983) (stars) and Ref. (Lautenschlager, Garriga, Viña & Cardona 1987) (circles) are depicted.

the macroscopic dielectric function for $\mathbf{q} = 0$ can be found in Refs. (Reining et al. 2002, Sottile et al. 2003, Adragna et al. 2003, Botti et al. 2004, Botti et al. 2005). Finite momentum transfer properties like the loss function or the dynamical structure factor have been reported in Refs. (Ehrnsperger & Bross 1997, Weissker et al. 2006).

We start our discussion in reporting the experimental findings on the macroscopic dielectric function. In Refs. (Aspnes & Studna 1983, Lautenschlager, Garriga, Viña & Cardona 1987) the optical spectrum has two pronounced peaks, the first one (E_1) at ~ 3.5 eV, the second one (E_2) at ~ 4.25 eV.

Next, the result for the RPA dielectric function without taking into account local field effects is provided where Eq. (6.16) has been evaluated. A dense $20 \times 20 \times 20$ **k** mesh is used which is off-symmetry shifted by a submesh shift of $(0.1, 0.3, 0.5)$ in order to obtain crystallographically different **k** points. Such a procedure turned out to improve the convergence with respect to the **k** point sampling considerably. Moreover, the linear tetrahedron method has been employed to further improve the accuracy of the result.

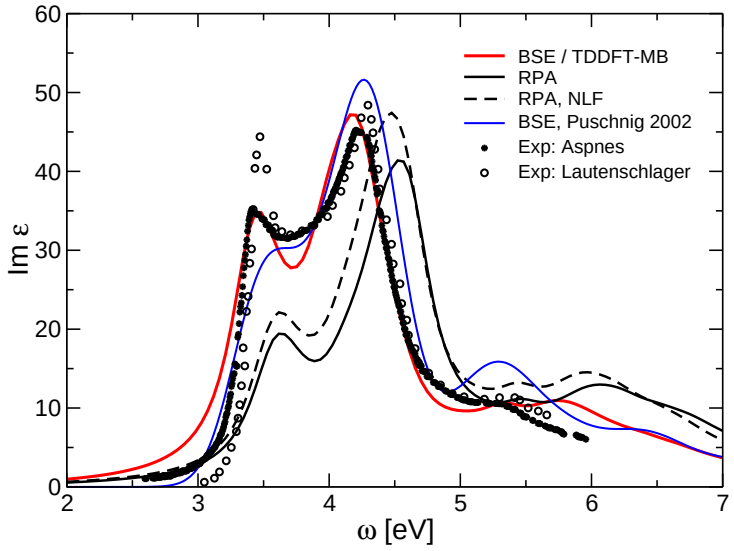

Figure 9.4: The dielectric function of Si obtained from the BSE and the BSE derived kernel (TDDFT-MB) (red solid line). The RPA result is given including local field effects (black solid line) and without local field effects (dashed line). For comparison, the results from a BSE calculation (Puschnig & Ambrosch-Draxl 2002*a*) as well as experimental data from Ref. (Aspnes & Studna 1983) (points) and Ref. (Lautenschlager, Garriga, Viña & Cardona 1987) (circles) are depicted.

For the dielectric function 10 unoccupied bands have been proven sufficient in the energy range under consideration. A simple scissor shift of 0.6 eV is used to match the onset of the absorption to experiment. *GW* calculations, on the other hand, report a scissor shift of 0.51 eV (Gomez-Abal et al. 2008) which, for consistency, should be adopted. However, to compare our results to literature, the shift is chosen in the afore mentioned way. In Fig. 9.3 the corresponding data is depicted. It shows no major peak at the E_1 position and additionally, the E_2 peak is overestimated and located at the wrong position. So far the simplest approximation to the macroscopic dielectric function, namely neglecting local field effects and the electron-hole correlation has been considered, corresponding to a vanishing *xc* kernel. As a next step, those two effects will be switched on, however, at the price of a smaller $\mathbf{k}$ mesh.

The dielectric matrix is calculated on an $8 \times 8 \times 8$ $\mathbf{k}$ mesh for 29 crys-

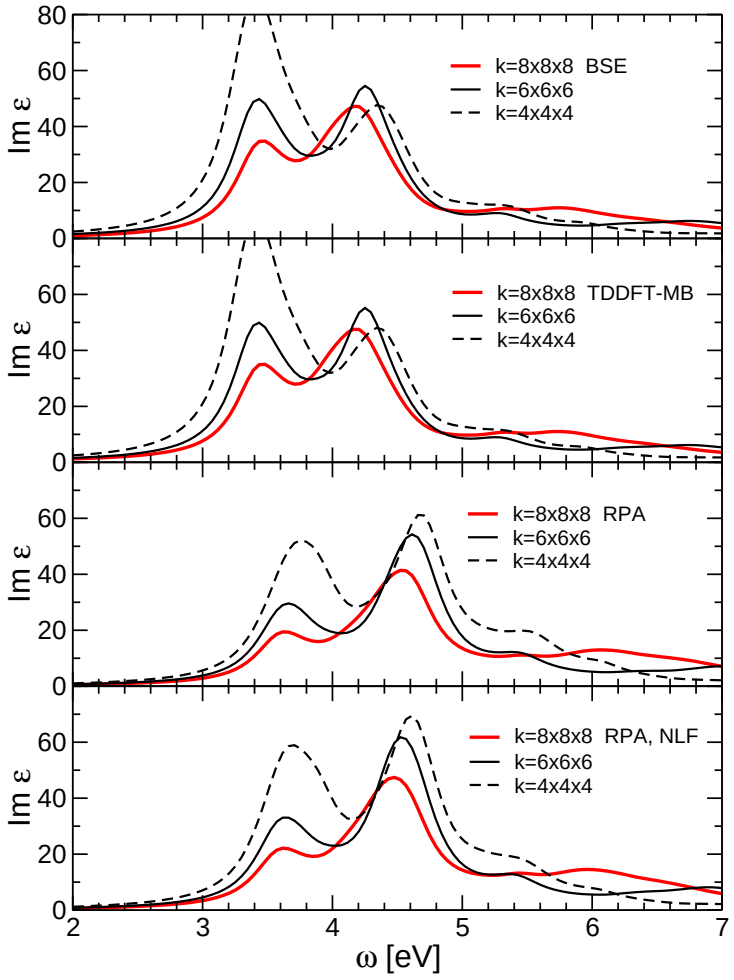

Figure 9.5: The macroscopic dielectric function of Si from the BSE, the BSE derived xc kernel, the RPA, and the RPA without local field effects (from top to bottom). The results are displayed for three different **k** point samplings.

tallographically inequivalent $\mathbf{q}$ points and the full screened interaction W has been taken into account. The $RK_{\max}$ is chosen to be 6.0 and we use an energy cutoff of 5 Hartree for the unoccupied states. For the matrix elements of the effective Bethe-Salpeter Hamiltonian the same $\mathbf{k}$ mesh as for the dielectric matrix has been used, and four valence and conduction bands have been included. The BSE derived xc kernel is set up with the same numbers of valence and conduction bands as for the BSE Hamiltonian. For the screening, the BSE Hamiltonian and the Kohn-Sham response function a reciprocal space cutoff of 3.0 Bohr^{-1} is used. The result is depicted in Fig. 9.4 where a Lorentzian broadening of 0.005 Hartree is chosen. It is now observed that the inclusion of local field effects into the RPA does even worsen the agreement with experiment expressed into a decrease of oscillator strengths as well as a slight blue shift. Only in the BSE result (singlet) the peak positions of the E_1 and E_2 peaks are strongly improved. Additionally, the oscillator strengths of the two peaks perfectly match the experiment of Ref. (Aspnes & Studna 1983). The result of the BSE derived kernel is indistinguishable from the BSE result itself and therefore not displayed.

At this point it is important to note that the BSE result for the dielectric function obtained so far on a $8 \times 8 \times 8$ $\mathbf{k}$ mesh is not expected to be fully converged with respect to the $\mathbf{k}$ point sampling. In Fig. 9.5 this statement is illustrated by a series of calculations with increasing number of $\mathbf{k}$ points. When going from a $6 \times 6 \times 6$ to a $8 \times 8 \times 8$ mesh there are still differences concerning the position of the peaks as well as the distribution of the oscillator strengths. It would be important to perform a BSE calculation on the $20 \times 20 \times 20$ $\mathbf{k}$ mesh for which the independent particle approximation is converged. However, such calculations are computationally extremely demanding and have, to the best of our knowledge, also not been performed by other groups.

Finally we abandon the optical ($\mathbf{q} = 0$) regime and take a look at the dielectric function related to finite momentum transfer as measured in experiments such as EELS. The calculations for the dielectric function are performed within the TDDFT linear response formalism using the TDLDA for momentum transfers vectors parallel to the [111] direction with a magnitude of 0.80, 1.32 and 1.59 Bohr^{-1}. These vectors are $(0.754, 0.754, 0, 754)$, $(1.244, 1.244, 1.244)$ and $(1.499, 1.499, 1.499)$, respectively, given in terms of reciprocal lattice vectors. For all these cases a shifted $13 \times 13 \times 13$ $\mathbf{k}$ mesh is applied, and conduction band states up to 70 eV are included. An $RK_{\max}$ value of 7.0 is proven sufficient. The dielectric function for the afore men-

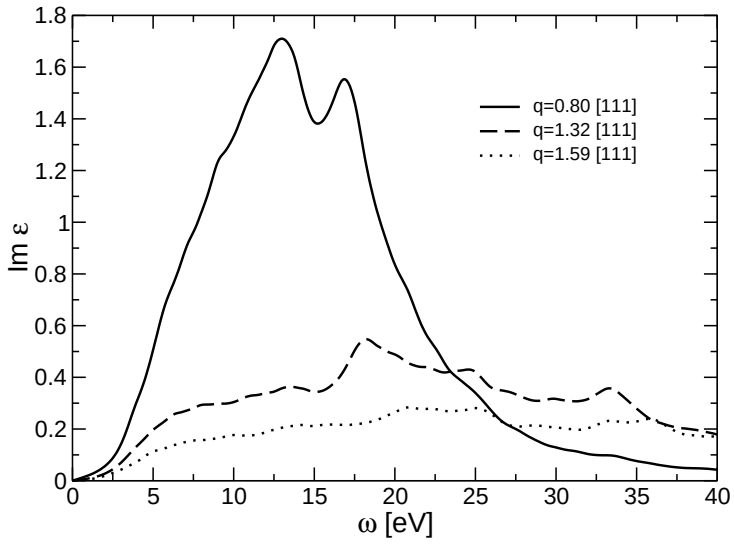

Figure 9.6: The dielectric function of Si obtained from the ALDA for various momentum transfer vectors **q** in [111] direction. A very similar result can be found in Ref. (Weissker et al. 2006).

tioned momentum transfer vectors are given in Fig. 9.6. Very good agreement with the results obtained in Ref. (Weissker et al. 2006) is found, where additionally life time broadening in the Kohn-Sham response function has been used. Moreover, our implementation is consistent with the loss function of Si from earlier work (Ehrnsperger & Bross 1997) (not shown here).

9.3 The Dielectric Function of LiF

We continue our study of excitonic effects for the example of LiF. It is characterized by a large fundamental band gap which is obtained from GW calculations as 14.4 eV (Rohlfing & Louie 1998), 14.3 eV (Benedict et al. 1998*a*), and 13.2 (Gomez-Abal et al. 2008). The static dielectric constant of 1.9 is very small (Rohlfing & Louie 1998) resulting into a large (attractive) screened Coulomb interaction. Such a situation gives rise to strong excitonic effects. Looking at the optical spectrum from experiment (Roessler & Walker 1967) in Fig. 9.7 we observe a strong excitonic peak at approximately 12.7 eV and a rather shallow line-shape in the remaining region of frequencies up to 25

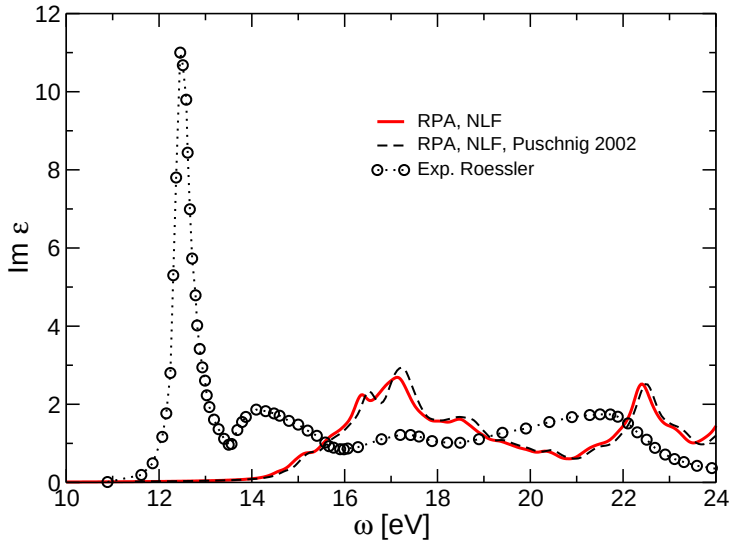

Figure 9.7: The dielectric function of LiF obtained from the independent quasi-particle approximation, *i.e.,* the RPA neglecting local field effects (solid line). The result is compared to the RPA spectrum of Ref. (Puschnig & Ambrosch-Draxl 2002*a*) (dashed line) and to experimental data taken from Ref. (Roessler & Walker 1967) (circles).

eV. The peak is far below the quasi-particle gap and therefore describing a strongly bound exciton.

We calculate the RPA dielectric function, as for the previously studied materials, within both the TDDFT linear response and the BSE formalism. A $8\times8\times8$ **k** is used for either the dielectric matrix, the Kohn-Sham response function, as well as the effective Hamiltonian matrix of the BSE. Furthermore, the $RK_{\max}$ is chosen as 7.0, and local field effects are taken into account up to a cutoff of 3.0 Bohr^{-1}. For the dielectric matrix conduction band states up to 7.5 Hartree are used, and for the BSE Hamiltonian matrix 4 valence and 4 conduction band states are taken into account. As a broadening for the Kohn-Sham response function as well as the BSE derived xc kernel and the spectrum obtained from the BSE a value of 0.2 eV is used.

In our calculations the Kohn-Sham gap is corrected by a rigid shift of 5.7 eV for the BSE as well as the TDDFT calculations. As mentioned in the case of Si recent *GW* calculations based on a full-potential method give rise to a lower quasi-particle gap of 13.2 eV (Gomez-Abal et al. 2008). However, as

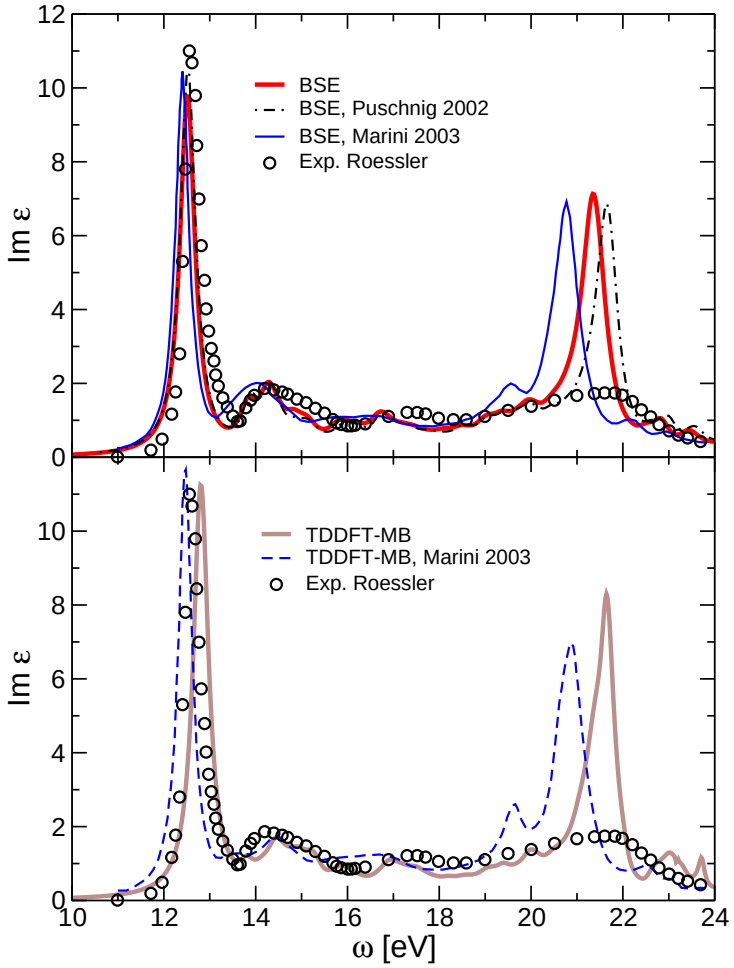

Figure 9.8: In the upper panel, the macroscopic dielectric function obtained from the BSE (thick solid line) is displayed. It is compared to the BSE calculations of Refs. (Puschnig & Ambrosch-Draxl 2002*a*) (dot-dashed line) and (Marini et al. 2003) (solid line). The lower panel shows the result for the BSE derived kernel (TDDFT-MB, solid line), which is compared to the one of Ref. (Marini et al. 2003). Experimental data from Ref. (Roessler & Walker 1967) are displayed in both panels.

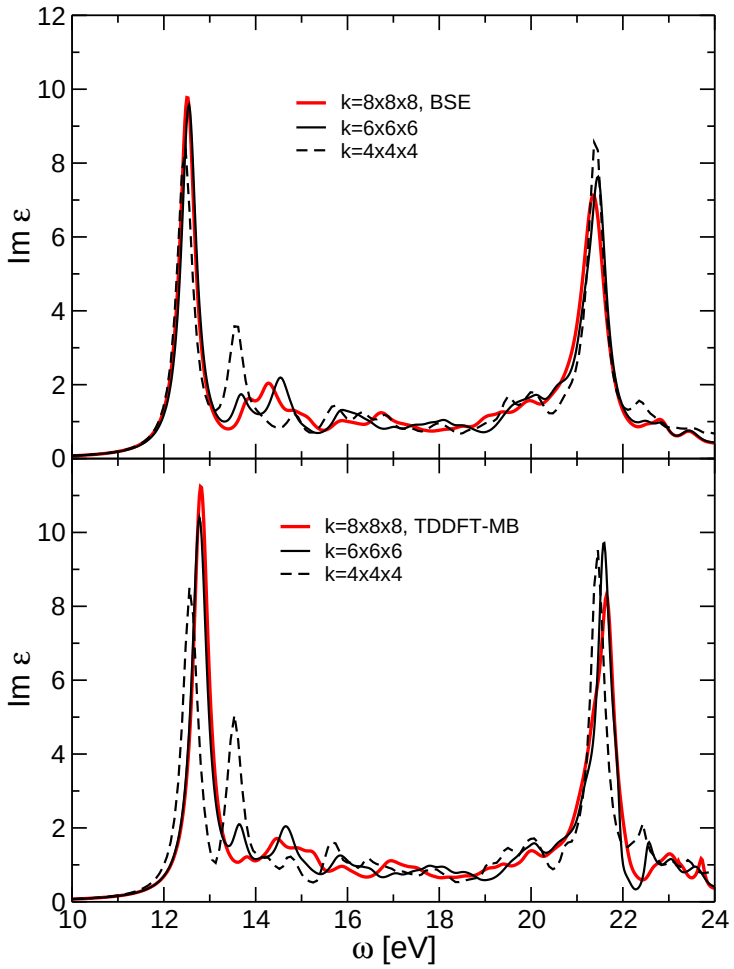

Figure 9.9: The dependence of the macroscopic dielectric function of LiF from the BSE (upper panel) and the BSE derived xc kernel (lower panel) on the **k** mesh. Three different **k** point samplings are displayed.

it is widely observed in literature we do not directly use this *GW* correction as it should be the case, but the final BSE result is matched to experiment.

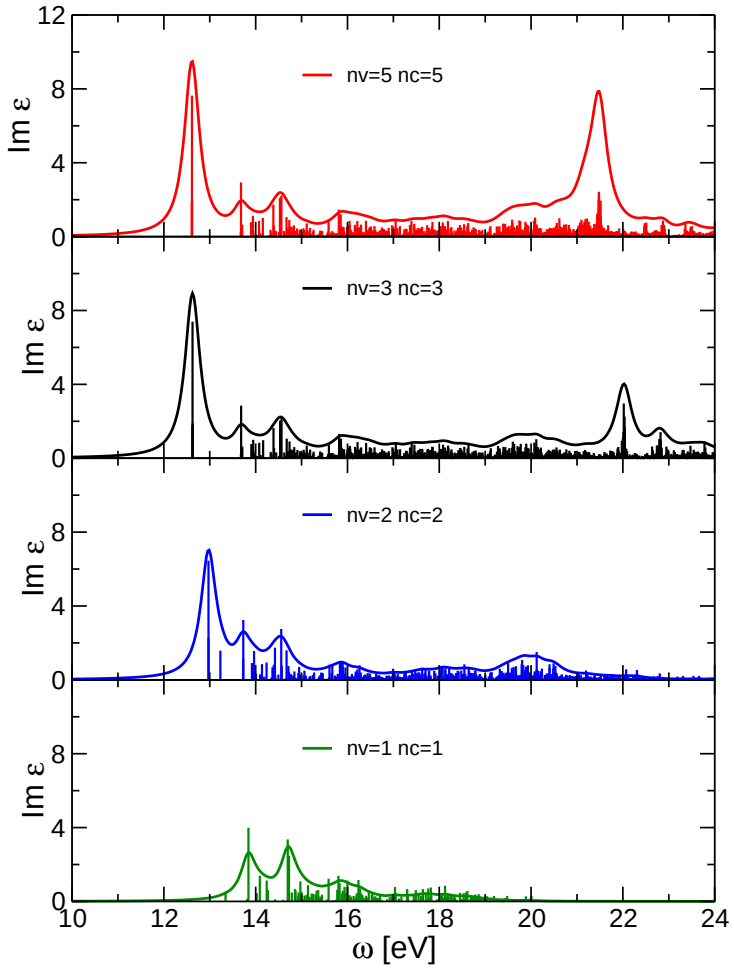

Figure 9.10: The dependence of the macroscopic dielectric function of LiF on the number of valence and conduction bands in the effective BSE Hamiltonian. In the topmost panel, the converged result is displayed. The oscillator strengths (bars) are plotted for comparison to the full spectrum (solid lines). The panels below show the dielectric function for 3, 2 and 1 valence and conduction bands, respectively.

In Fig. 9.7, the RPA result is compared to a calculation from Ref. (Puschnig & Ambrosch-Draxl 2002*a*) and to experimental data from Ref. (Roessler &

Walker 1967). We find good overall agreement of the RPA result to the one of Ref. (Puschnig & Ambrosch-Draxl 2002*a*), whereas the excitonic peak below the quasi-particle gap is completely missing, as has been already discussed extensively in literature.

When switching on the correlations between the electrons and the holes the shape of the spectrum changes drastically. In Fig. 9.8 (upper panel) we observe a perfect agreement of our BSE result to experiment (Roessler & Walker 1967) and to one of the BSE calculations (Puschnig & Ambrosch-Draxl 2002*a*) for the position as well as strength of the first largest excitonic peak. The second peak in the region between 20 and 22 eV is, however, shifted to lower energies by 0.3 eV. This peak, does not show up in the experimental spectrum and might be an artefact related to the finite **k** point sampling or other numerical issues. The main peak in the data by MARINI (Marini et al. 2003) appears at an energy lower by 0.1 eV. At this point it should be noted that even at the level of the RPA all the results reported in literature (see Ref. (Puschnig 2002)) exhibit pronounced differences. Hence one cannot clearly distinguish to which extent discrepancies in the BSE spectra are due to differences in the ground state or excited state calculations.

The situation for the BSE derived *xc* kernel (lower panel in Fig. 9.8) is slightly different. The spectrum calculated that way is shifted to higher energies by approximately 0.30 eV compared to the BSE calculation. In Ref. (Marini et al. 2003), however, the discrepancy of 0.05 eV between the full BSE calculation and the BSE derived *xc* kernel is not as large. A possible explanation for this is attributed to the fact that we are only using the resonant terms (transitions from valence to conduction bands) for the Kohn-Sham response function as well as the BSE derived *xc* kernel. Another reason could be a different **k** point sampling used in Ref. (Marini et al. 2003). In the context of the exact position of the excitonic peak it is important to discuss the effect of the **k** point sampling on the resulting spectrum.

In Fig. 9.9 we see that for the excitonic peak obtained from the BSE already a sampling of $6 \times 6 \times 6$ **k** points gives a converged peak position, whereas the $4 \times 4 \times 4$ mesh also provides a good result differing by 0.05 eV from the converged one. For the BSE derived *xc* kernel we find the situation to be different. If we go from a $4 \times 4 \times 4$ mesh to a $6 \times 6 \times 6$ mesh in the peak position already shifts by 0.25 eV to higher energies. Going then to the $8 \times 8 \times 8$ mesh affects the peak position only negligibly. Comparing the peak positions of BSE and the TDDFT result obtained on a $4 \times 4 \times 4$ mesh the difference is only 0.08 eV. However, by increasing the **k** mesh this difference

grows. Although both, techniques are assumed to be converged for the first excitonic peak, they approach different values. The reason why our result for the BSE derived kernel is not identical to the one of Ref. (Marini et al. 2003) cannot be fully clarified, since in this reference not enough information about the parameters of the calculations are provided.

Now, the dependence of the macroscopic dielectric function on the number of valence and conduction bands used for the electron-hole correlations is discussed shortly. In Fig. 9.10 it can be seen that the position of the first strong peak is already converged if three bands are taken into account. In using up to five bands for both valence and conduction bands, convergence for the second peak is achieved.

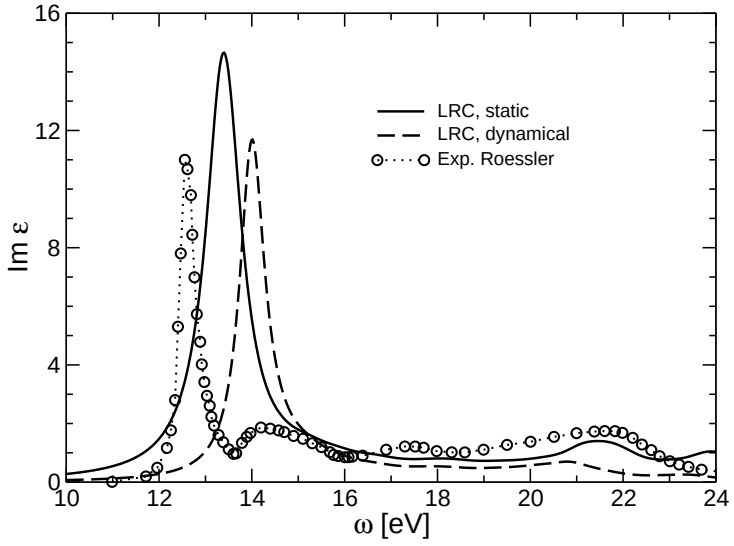

Figure 9.11: The dielectric function of LiF obtained from the LRC *xc* kernels. The result for the static approximation ($\alpha = 9.7$) is displayed (solid line) in contrast to the dynamical approximation ($\alpha' = 1.5$, $\beta' = 25$, dashed line). The experimental result of Ref. (Roessler & Walker 1967) is shown for comparison.

Finally, the LRC model kernels are applied to LiF. It has been found by other groups that these kernels are able to reproduce the excitonic peak to some extent, although at the price of a parameter dependence of the kernel. We have evaluated the LRC kernel for the static case, Eq. (5.30), with a parameter $\alpha = 9.7$ and for the dynamical case, Eq. (5.32) with parameters

$\alpha' = 1.5$ and $\beta' = 25$, as reported in Ref. (Botti et al. 2005). We find the position of the excitonic peak at 13.4 eV for the static case and at 14 eV for the dynamical case. Although, from the physics point of view it is remarkable that a strong excitonic peak can be generated by simply rescaling the Coulomb potential in the Dyson equation for the TDDFT linear response, the results are mostly qualitative and the choice of the average absorption gap is ambiguous, especially in the case of strongly bound excitons. We conclude that these model kernels are, by virtue of their semi-empirical laws, Eqs. (5.31) and (5.33), suitable to take a first, coarse look at the optical spectrum. However, since they are not fully ab-initio one has to take great care to use them for predicting or explaining materials properties. In the case of low-symmetry systems like polymers we will see in the next section that further complications arise in combination with this type of kernels.

9.4 The Dielectric Function of Poly-acetylene

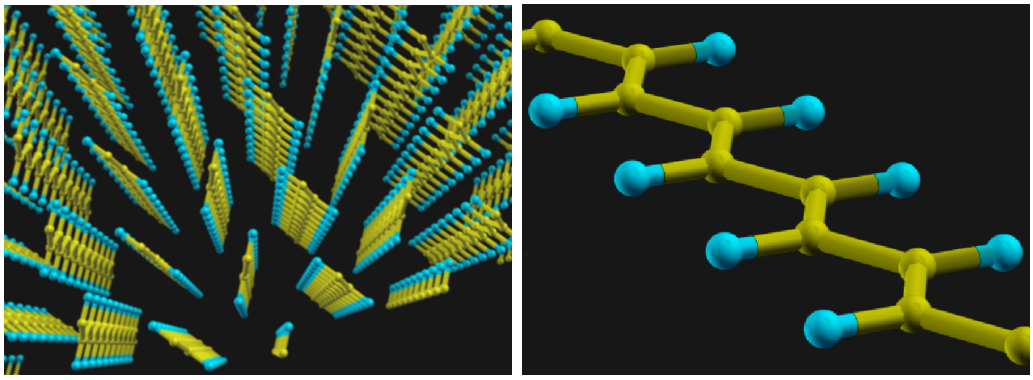

Figure 9.12: The herring-bone structure of PA being typical to polymers (left) and one polymer chain (right). The yellow balls indicate carbon atoms whereas the blue balls denote hydrogen atoms.

As final part of this thesis, we concentrate on organic semiconducting polymers, starting with the most prominent example, namely bulk trans-polyacetylene (PA). Similar to other conjugated polymers, it crystallizes in the herring-bone arrangement (Fig. 9.12) containing two polymer chains in the unit cell. Each of these chains consists of carbon and hydrogen atoms

depicted in Fig. 9.12. There are two possible space groups for bulk polyacetylene, namely $P2_1/a$ and $P2_1/n$, differing by the shift of the polymer chains. We have restricted our study to the $P2_1/a$ space group. The LDA band structure is depicted in Fig. 9.13. It shows a large dispersion along the k_z direction (paths from Y to D and Z to Γ) whereas for the k_x and k_y direction the dispersion is less pronounced. We find a Kohn-Sham band gap of 0.27 eV in accordance with other all-electron calculations (Puschnig & Ambrosch-Draxl 2002*b*). In order to mimic the quasi-particle band structure a scissor shift of 0.74 eV (Vogl & Campbell 1990) is introduced. The macroscopic dielectric function parallel to the direction of the polymer chain is now calculated within the RPA, from a solution of the BSE and from TDDFT linear response including various xc kernels. For the LRC model kernels we apply Eq. (5.29) for the static case as well as Eq. (5.32) for the dynamical case. The parameter α is obtained form the semi-empirical law, Eq. (5.31), whereas the parameters α' and β' are determined according to Eq. (5.33).

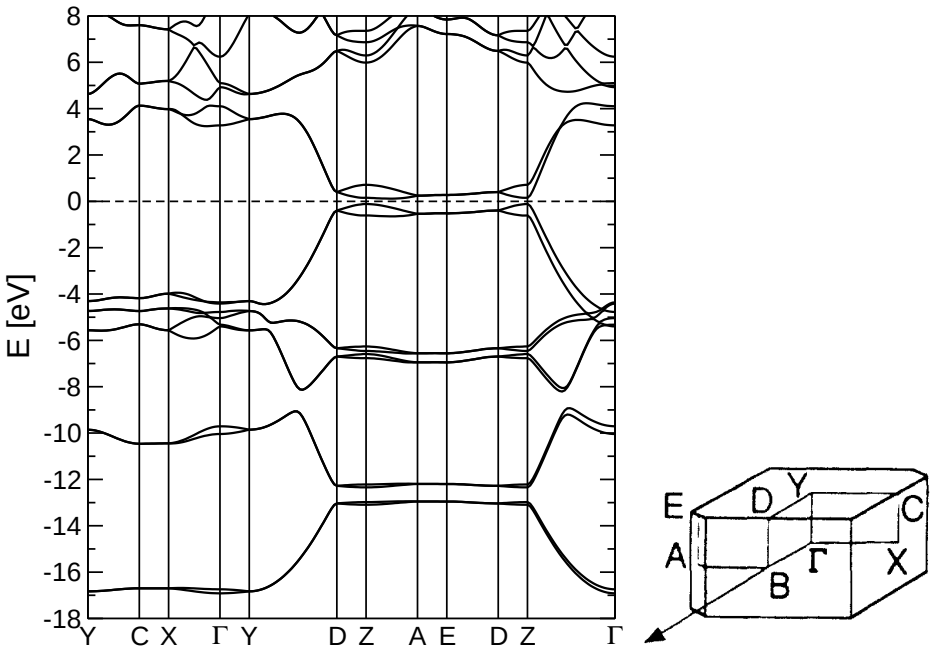

Figure 9.13: The electronic band structure of PA along a path of high symmetry points in the Brillouin zone.

As a first step, the loss function is evaluated within the RPA in order

to obtain the plasmon frequencies which, in turn, serve as input for the dynamical LRC kernel. The static dielectric constant which appears in the static and dynamical LRC kernel is calculated within the RPA as well.

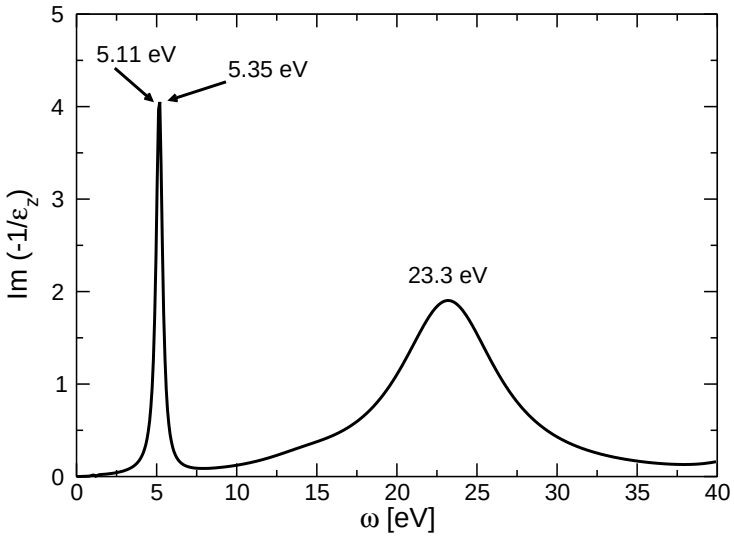

Figure 9.14: The loss function of PA as obtained from the RPA. The frequency values denote the peaks of the spectrum.

To this end, the Kohn-Sham response function is calculated on a $4\times4\times48$ **k** mesh to account for the large band-dispersion in the k_z direction. Since the features of the loss function usually appear at higher energies compared to the optical spectra we include conduction bands up to 1.7 Hartree. As cutoff for the LAPW basis set an $RK_{\max}$ value of 3.5 is chosen and for the loss function a broadening of 0.1 eV is applied.

In the loss function in Fig. 9.14 we observe 3 main features corresponding to the peak positions of 5.11, 5.35, and 23.3 eV, respectively. At this point it becomes obvious that the existence of more than one plasmon frequency renders the concept of the dynamical LRC kernel ambiguous, since it was derived considering a single Lorentz oscillator. For this reason the influence of the choice of the plasmon frequency will be discussed in the following. For the dynamical LRC kernel, the average absorption gap in Eq. (5.33) is chosen to be 1.7 eV corresponding to the middle of the absorption region in the RPA dielectric function.

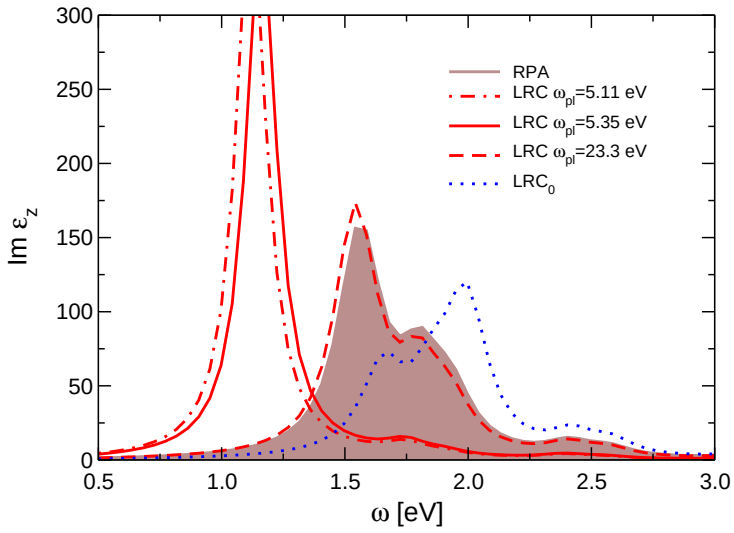

Figure 9.15: The dielectric function of PA as obtained from the LRC kernels compared to the RPA (shaded area). The results are given for the static LRC kernel (blue dotted line) as well as the dynamical LRC kernel corresponding to different plasmon frequencies (red lines).

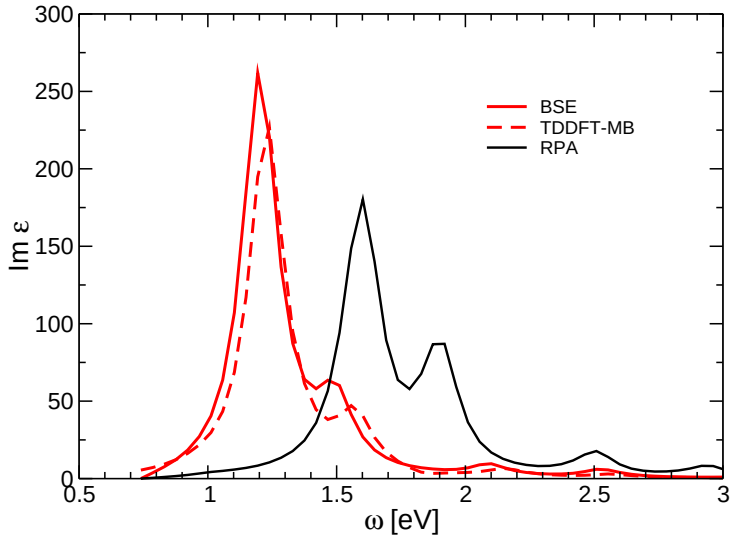

Figure 9.16: The dielectric function of PA as obtained from the BSE (red solid line), the BSE derived xc kernel (red dashed line), and the RPA (black line).

Having all relevant parameters for the evaluation of the xc kernels at hand, the TDDFT linear response equation is solved and the macroscopic dielectric function is obtained within the optical range. In the RPA spectrum in Fig. 9.15 the first peak occurs at about 1.55 eV. Turning to the result obtained from the static LRC kernel the situation is different compared to the materials studied so far. Here, the first absorption peak is shifted to *higher* energies instead of lower ones. Consequently the static model kernel leads to negative exciton binding energies and has therefore to be discarded for this system. The dielectric function stemming from the dynamical model kernel is also displayed in Fig. 9.15 for different plasmon frequencies as input to the kernel. We observe a significant dependence of the resulting optical spectra on the plasmon energy. While for the plasmon at 23.3 eV the corresponding optical spectrum is not much different from the RPA result, the spectra associated to the plasmons as 5.11 and 5.35 eV, respectively, show a strong red shift in energy by as much as 0.4 and 0.45 eV, respectively. Hence, the spectra related to different plasmon frequencies for the dynamical xc kernel show a shift of the main absorption peak ranging from several eV to almost zero. Therefore, an assignment of the optical spectrum to a specific plasmon peak in the loss function as input for the LRC model is not possible. The results obtained so far show that the simple LRC models are not able to describe the absorption spectrum in complex systems including excitonic effects.

As final investigation on PA, the electron-hole correlations are included in the optical spectrum through the solution of the Bethe-Salpeter equation and through the BSE derived xc kernel in TDDFT. The calculation of the dielectric matrix as well as the BSE Hamiltonian is carried out on an $4\times4\times32$ $\mathbf{k}$ mesh. The dielectric matrix has been evaluated for 198 crystallographically different $\mathbf{q}$ points with conduction band states up to 4.5 Hartree. For the BSE matrix four valence and conduction band are chosen and the cutoff in reciprocal space for the Coulomb and screened Coulomb interaction is set to 2.5. In Fig. 9.16 both results for the BSE and the BSE derived kernel, as well as the RPA result are displayed. The main excitonic peak of the BSE result is found at 1.2 eV whereas the peak subject to the BSE derived kernel lies at 1.25 eV. From a comparison with the RPA, the binding energy of the exciton is 0.35 eV for the BSE result and 0.30 for the result stemming from the TDDFT spectrum. These findings also confirm that the BSE derived xc kernel is able to reproduce the full BSE spectrum semi-quantitatively. Nevertheless, a deviation of 0.05 eV corresponding to an error of 15% can be

problematic for the interpretation of exciton binding energies.

9.5 The Dielectric Function of PPV

As last example crystalline poly(phenylene vinylene) (PPV) is investigated. It is of recent technological interest, as it can be used for light-emitting diodes based on polymers (Burroughes et al. 1990). Being built up by two phenyl rings (see Fig. 9.17) the structure of PPV is more complex than the one of PA, consisting of 28 atoms (16 carbon and 12 hydrogen atoms) in the unit cell. It shall be noted already here, that the results are not fully converged with respect to the **k** mesh and such converged results are also not found in literature. As mentioned for the simpler materials studied in the previous sections, such convergence studies on the **k** point sampling are already very time-consuming. However, for PPV they are beyond the limit of state-of-the-art computer ressorces.

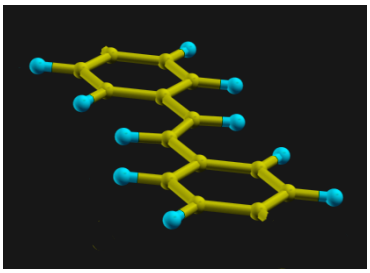

Figure 9.17: The building block of PPV consisting of carbon (yellow) and hydrogen (blue) atoms.

The electronic band structure of PPV is displayed in Fig. 9.18 and has also been studied several years ago (Costa et al. 1993). It shows a strong dispersion along the axis of the polymer chain whereas in the perpendicular direction it appears rather flat. In order to mimic the quasi-particle band gap a scissor shift of 1.75 eV (Voss et al. 1991) has been applied. As in the case of PA, the **k** mesh is chosen to be dense in the chain direction ($4 \times 4 \times 40$) to account for the large band-dispersion. In addition, the **k** points are shifted off-symmetry in order to achieve an improved sampling.

When looking at the loss function in Fig. 9.19 the structure is even more complicated as for PA. There are now four major peaks, namely at 2.52, 3.4,

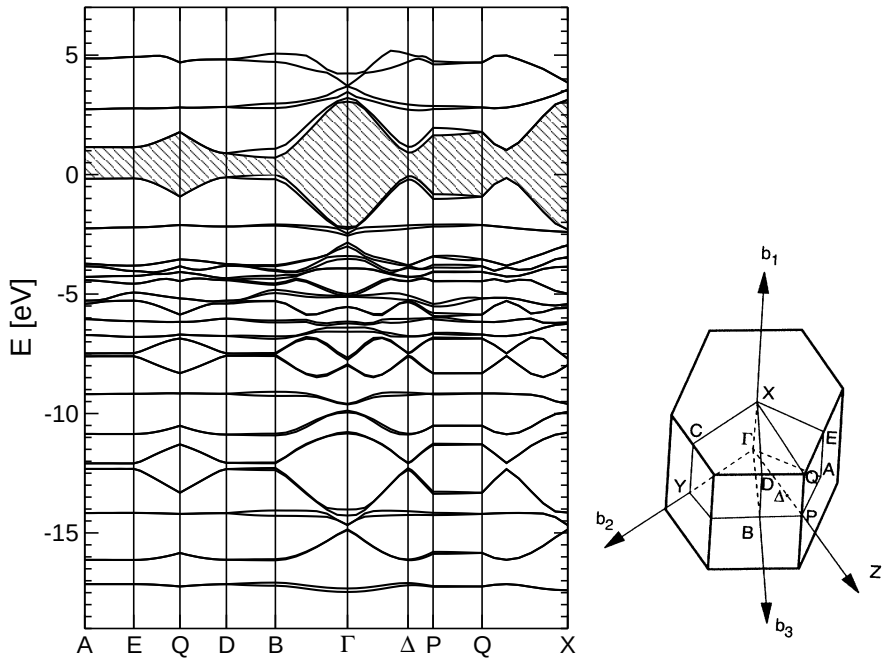

Figure 9.18: The electronic band structure of PPV along a path including high symmetry points in the Brillouin zone.

6.0 and 22.8 eV. The procedure to set up the LRC kernels is the same as for the case of PA and shall not be repeated here. In Fig. 9.20 the results for the LRC kernels as well as for the RPA are depicted. Furthermore, a calculation from Ref. (Ruini et al. 2002) has been added for comparison. Similar to what is observed for PA, the resulting optical spectra sensitively depend on the plasmon energy. One of these energies, located at 2.52 eV, generates a completely collapsed optical spectrum (not even visible in Fig. 9.20), whereas the one at 3.4 eV lies 1.7 eV below the quasi-particle gap. The remaining plasmon energies are either in between the RPA and the BSE result (plasmon at 6.0 eV) or do not improve over the RPA spectrum (plasmon at 22.8 eV). For the static LRC even a small blue shift of the spectrum is observed.

Finally, the plasmon energy entering the dynamical LRC model is chosen in a way that the resulting optical spectrum matches the BSE result of Ref. (Ruini et al. 2002), which has been adapted to the quasi-particle shift chosen here. Only a value of 8.5 eV for the plasmon energy is able to re-

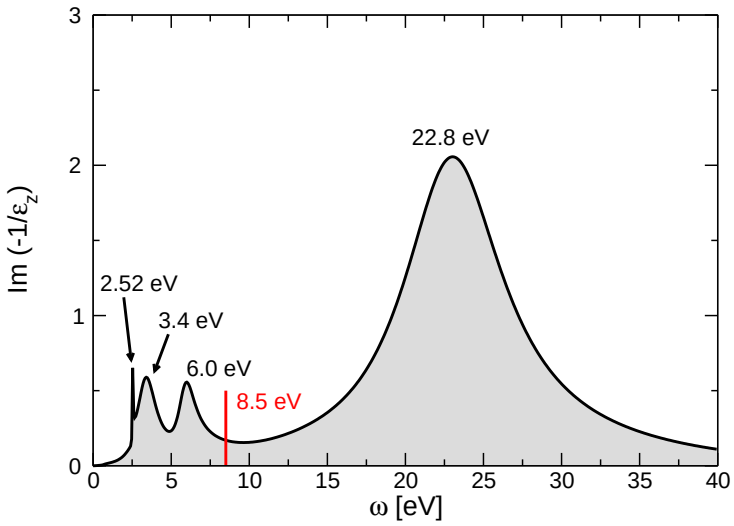

Figure 9.19: The loss function of PPV in the RPA. The values indicate the peak positions of the spectrum whereas 8.5 eV is the frequency for which the peak position of the dielectric function obtained from the LRC model corresponds to the BSE peak position.

produce the peak position of the BSE calculation, however, resulting in an oscillator strength which is too large. From Fig. 9.19 it is evident that the fitted value of 8.5 eV does not correspond to any particular feature of the loss function.

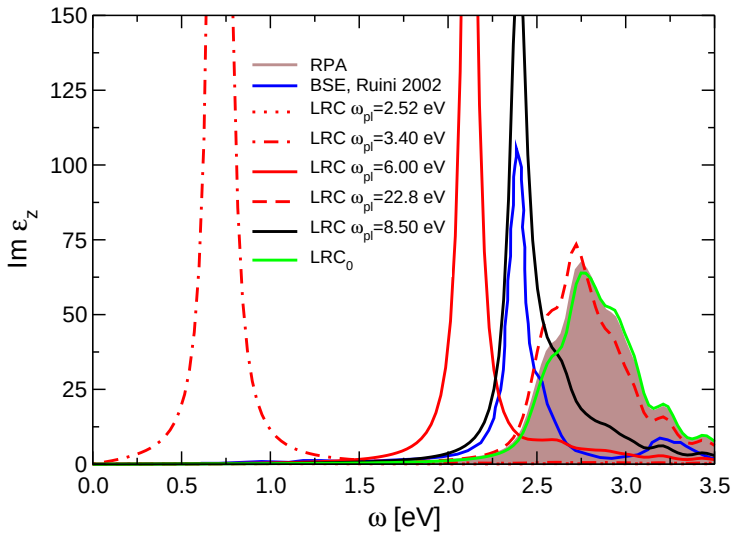

Figure 9.20: The macroscopic dielectric function of PPV for different LRC kernels and the RPA. The results are given for the static LRC kernel as well as the dynamical LRC kernel corresponding to different plasmon frequencies. For comparison, we display a BSE calculation taken from Ref. (Ruini et al. 2002).

9.6 Conclusions

In general, we conclude from the findings in this chapter, that on the one hand the simple model kernels are – although semi-empirical – suitable to describe the excitonic effects in the semiconductors GaAs and Si. More importantly, the *xc* kernel derived from the BSE performs excellently and can easily be used in place of a full BSE calculation.

Turning to LiF, the situation changes significantly. The presence of a large band gap together with weak screening causes strong excitonic effects. Here, the simple model kernels are not capable to capture the bound exciton within the desired accuracy, although a qualitative agreement is achieved by tuning the parameters of the model kernel. The situation for the BSE derived kernel is much better, although still a discrepancy in the excitonic peak position is observed, but the overall agreement with the BSE result is quite good.

Finally, turning to the organic materials, it shall be noted that neither of the LRC model kernels is able to properly account for the excitonic effects in the low-dimensional complex systems PA and PPV. It is rather the full BSE calculation that still constitutes the state of the art method for an accurate determination of excitonic effects due to electron-hole correlations. As it is seen in the case of PA also the BSE derived *xc* kernel comes quite close to the full BSE calculation. However, further theoretical improvements on the BSE derived *xc* kernel are needed in order to establish it with the same reliability as the solution of the BSE. In this context it would also be desirable to calculate the BSE derived kernel up to second order in the screened interaction.

Since, besides the computation time for the matrix elements of the BSE Hamiltonian themselves, the BSE eigenvalue problem constitutes a bottleneck of the numerical performance, it is much more favorable to solve Dyson's equation in reciprocal space, despite the fact that one has to solve it separately for each frequency. We therefore conclude that the combination of TDDFT and the BSE derived *xc* kernel could be the better choice for the investigation of large systems, such as polymers and related materials, since in this way the very time-consuming eigenvalue problem of the Bethe-Salpeter equation is circumvented. However, at present the results are not satisfactory enough as evidenced in the examples shown. Nevertheless, further applications of the BSE derived kernel to various types of gap systems are needed in

order to evaluate its final role in the calculation and prediction of excitonic effects.

Appendix A

Second Quantization

Before discussing the second quantization we briefly review the Schrödinger equation of a many particle system. We use atomic units throughout this thesis. This means that $\hbar = 1$, the electron charge $e = 1$, the electron mass $m_e = m = 1$ and the Bohr radius $a_0 = 1$. Note that $e^2/(4\pi\varepsilon_0) = 1$ as well.

The Hamiltonian $\hat{h}$ of a single particle in an external potential is given by

$$\hat{h}(\mathbf{r}) = \hat{t}(\mathbf{r}) + \hat{v}_{\text{ext}}(\mathbf{r}) = -\frac{1}{2}\nabla^2_{\mathbf{r}} + \hat{v}_{\text{ext}}(\mathbf{r}) \tag{A.1}$$

where $\hat{t}$ is the kinetic energy operator and $\hat{v}_{\text{ext}}$ the multiplicative operator of the external potential. Let us now consider a system of n particles which interact with each other via a potential v and on which an external potential is acting:

$$\hat{H} = \sum_{i=1}^{n} \hat{h}(\mathbf{r}_i) + \frac{1}{2}\sum_{i\neq j}^{n} v(\mathbf{r}_i, \mathbf{r}_j). \tag{A.2}$$

We can rewrite this equation in order to highlight the similarity to Eq.(A.1)

$$\hat{H} = \hat{T} + \hat{V_{\text{ext}}} + \hat{U} \tag{A.3}$$

where

$$\hat{T} = \sum_{i=1}^{n} \hat{t}(\mathbf{r}_i) \tag{A.4}$$

is the kinetic energy operator,

$$\hat{V}_{\text{ext}} = \sum_{i=1}^{n} \hat{v}_{\text{ext}}(\mathbf{r}_i) \tag{A.5}$$

represents the external potential for the many-particle system and

$$\hat{U} = \frac{1}{2}\sum_{i\neq j}^{n} v(\mathbf{r}_i, \mathbf{r}_j) \tag{A.6}$$

is the Coulomb interaction between the particles, where

$$v(\mathbf{r}, \mathbf{r}') = v(\mathbf{r} - \mathbf{r}') = \frac{1}{|\mathbf{r} - \mathbf{r}'|} \tag{A.7}$$

If the external potential $\hat{v}_{\text{ext}}(\mathbf{r})$ is subject to point charges (e.g. atomic nuclei in a solid) at positions $\mathbf{R}_l$, $l = 1, ..., N$, (each of them is carrying a charge of $-Z_l e$)

$$\hat{v}_{\text{ext}}(\mathbf{r}) = \sum_{l=1}^{N} Z_l v(\mathbf{r}, \mathbf{R}_l), \tag{A.8}$$

the Hamiltonian of the interacting system is given by

$$\hat{H} = -\sum_{i=1}^{n} \frac{1}{2}\nabla_{\mathbf{r}_i}^2 + \sum_{i=1}^{n}\sum_{l=1}^{N} Z_l v(\mathbf{r}_i, \mathbf{R}_l) + \frac{1}{2}\sum_{i\neq j}^{n} v(\mathbf{r}_i, \mathbf{r}_j). \tag{A.9}$$

An interaction between the nuclei has not been taken into account in our considerations and will not be subject to further studies in this work. For the sake of simplicity, we now omit the hat indicating an operator in the following. The Hamiltonian given in the equations above is explicitly dependent on the number of particles under consideration which does not prove to be advantageous for the framework of many-body physics. It is the so called second quantization (Fetter & Walecka 1971, Schöne 2001, Evertz 2004) that naturally leads to the development of many-body perturbation theory; a formulation that does not depend on the number of particles because the operators are defined on a larger Hilbert space that indeed contains all possible many-body Hilbert spaces $\mathcal{H}_i = \otimes_{j=1}^{i}\mathcal{H}^{(j)}$ corresponding to a finite number of particles. This large Hilbert space is called the Fock-space $\mathcal{F}$

$$\mathcal{F} = \oplus_{i=0}^{\infty}\mathcal{H}_i. \tag{A.10}$$

Let us consider a complete set of basis vectors $\{|i\rangle\}_i$ for the one particle space. The corresponding many-particle basis for $\mathcal{H}_N$ would be

$$|i_1, \ldots, i_N\rangle = |i_1\rangle \otimes \cdots \otimes |i_N\rangle. \tag{A.11}$$

We can now expand the many-particle state $|\Psi\rangle$ in terms of the basis defined above

$$|\Psi\rangle = \sum_{i_1,\ldots,i_N} c_{i_1,\ldots,i_N} |i_1,\ldots,i_N\rangle. \tag{A.12}$$

Since we are dealing with a system of identical particles (*i.e.* particles that cannot be distinguished from one another by any kind of measurement under the same conditions) the exchange (permutation) of any pair of particles cannot have any effect on a measurement, implying that the wave function can only change its phase on applying a permutation operator $\mathcal{P}$ to it.

$$\mathcal{P}|\Psi\rangle = e^{i\lambda}|\Psi\rangle. \tag{A.13}$$

In fact this phase can only be ± 1 because the permutation operator is idempotent[1]. Experiments show that the phases are $+1$ for bosons and -1 for fermions and from the spin-statistics theorem (Duck & Sudarshan 1998) we know that particles with integer spin are bosons and particles with half-integer spin are fermions. From now on we will concentrate on Fermions only, since we want to study an electronic system. The fact that the wave function changes its sign upon permuting two particles allows only for occupation numbers 0 and 1 (Pauli principle) and makes it necessary to symmetrize the many-particle state accordingly. The symmetrization operator is given by

$$\hat{S} = \sum_{\mathcal{P}} \mathrm{sign}(\mathcal{P})\mathcal{P} \tag{A.14}$$

which is just the building of the Slater-determinant, and we obtain for the symmetrized basis

$$|i_1,\ldots,i_N\rangle_{\mathrm{Ferm}} = \hat{S}|i_1,\ldots,i_N\rangle. \tag{A.15}$$

For the following we will assume the proper symmetrization of the basis. Now, if n_i are the occupation numbers of the single-particle states i, the N-particle basis is already determined by the occupation numbers

$$|n_1, n_2, \ldots; N\rangle = |i_1,\ldots,i_N\rangle, \tag{A.16}$$

where $\sum_j n_j = N$.

[1]Note that in two dimensions the topological properties of the plane do not restrict the phases, since exchanging two particles can be done in topologically different ways.

A complete and orthonormal basis $|n_1, n_2, \ldots\rangle$ for the Fock space is found if we release the constraint that the occupation numbers have to sum up to the fixed number N. The Fock space also includes the space of the vacuum state $\mathcal{H}_0$ with the basis vector $|\text{vac}\rangle$.

Now, we introduce creation and annihilation operators $\hat{a}_j^\dagger$ and $\hat{a}_j$ (the hat is usually omitted) to transform between different numbers of particles. Utilizing these operators will enable us to build a basis vector from the vacuum state and will be necessary when we study Green's functions. The creation operator $\hat{a}_j^\dagger$ is defined via its application to an N-particle state

$$\hat{a}_j^\dagger |i_1, \ldots, i_N\rangle = \delta_{n_j,0} |j, i_1, \ldots, i_N\rangle. \tag{A.17}$$

A particle in the state j is created only if this state was previously unoccupied. If it were already occupied in the first place the result of the application of the creation operator is zero. The purpose of the creation operator $\hat{a}_j^\dagger$ is to create a particle in a specific one-particle state $|j\rangle$. We can also write the above definition in occupation number representation

$$\hat{a}_j^\dagger |\ldots, n_j, \ldots\rangle = \delta_{n_j,0} (-1)^{\tilde{n}_j} |\ldots, n_j + 1, \ldots\rangle \tag{A.18}$$

where $\tilde{n}_j = \sum_{l<j} n_l$ is the number of commutations of the creation operator in order to be placed properly within the initial sequence of Fermion states. Repeated application of the creation operator to the vacuum state gives us just the basis vectors in the occupation number representation

$$|n_1, n_2, \ldots\rangle = (\hat{a}_1^\dagger)^{n_1} (\hat{a}_2^\dagger)^{n_2} \cdots |\text{vac}\rangle. \tag{A.19}$$

The annihilation operator's action is defined via adjungation and is found to be

$$\hat{a}_j |\ldots, n_j, \ldots\rangle = \delta_{n_j,1} (-1)^{\tilde{n}_j} |\ldots, n_j - 1, \ldots\rangle. \tag{A.20}$$

The properties of the creation and annihilation operators lead to two important relations between them, namely the commutation relations

$$\begin{aligned} \{\hat{a}_j^\dagger, \hat{a}_{j'}^\dagger\} &= \{\hat{a}_j, \hat{a}_{j'}\} = 0 \\ \{\hat{a}_j, \hat{a}_{j'}^\dagger\} &= \delta_{j,j'} \end{aligned} \tag{A.21}$$

expressed with the help of the anti-commutator $\{a, b\} = ab + ba$.

Let us now consider a one-particle operator $\hat{t}$ which is given within a one-particle basis $\{|i\rangle\}_i$ as

$$\hat{t} = \sum_{i,j} t_{ij} |i\rangle\langle j| \tag{A.22}$$

where $t_{ij} = \langle i|\hat{t}|j\rangle$ are the matrix elements of the operator. A many-particle operator which is a sum of single-particle operators $\hat{t}_{(\alpha)}$ for each particle α

$$\hat{T} = \sum_{\alpha} \hat{t}_{(\alpha)} \tag{A.23}$$

now reads in second quantization

$$\hat{T} = \sum_{i,j} t_{ij} \hat{a}_i^\dagger \hat{a}_j \tag{A.24}$$

and, in fact, if we use an eigenbasis of $\hat{t}$ the expression simplifies to

$$\hat{T} = \sum_{i} t_{ii} \hat{n}_i, \tag{A.25}$$

where we have introduced the particle number operator

$$\hat{n}_i = \hat{a}_i^\dagger \hat{a}_i. \tag{A.26}$$

Note that the operator in the second quantization is expressed using the matrix elements from the corresponding one-particle operator. In a similar manner an expression for a many-particle operator $\hat{F}$ that is written as a sum over two-particle operators $\hat{f}$ can be derived. Let

$$\hat{F} = \frac{1}{2} \sum_{\alpha \neq \beta} \hat{f}_{\alpha\beta} \tag{A.27}$$

where

$$\hat{f} = \sum_{i,j,k,l} f_{ijkl} |i\rangle \otimes |j\rangle\langle k| \otimes \langle l| \tag{A.28}$$

and

$$f_{ijkl} = \langle i, j|\hat{f}|k, l\rangle. \tag{A.29}$$

The many-particle operator $\hat{F}$ then takes the form

$$\hat{F} = \frac{1}{2} \sum_{ijkl} f_{ijkl} \hat{a}_i^\dagger \hat{a}_j^\dagger \hat{a}_l \hat{a}_k. \tag{A.30}$$

In a basis where $\hat{f}$ is diagonal

$$\langle i,j|\hat{f}|k,l\rangle = \delta_{i,k}\delta_{j,m}\langle i,j|\hat{f}|i,j\rangle = f_{ij}, \tag{A.31}$$

the expression for $\hat{F}$ simplifies to

$$\hat{F} = \frac{1}{2} \sum_{i \neq j} f_{ij} \hat{n}_i \hat{n}_j \tag{A.32}$$

for a fermionic system. A change in the one-particle basis from $\{|i\rangle\}_i$ to $\{|\lambda\rangle\}_\lambda$, given by

$$\{|\lambda\rangle\}_\lambda = \sum_i |i\rangle\langle i|\lambda\rangle \tag{A.33}$$

leads to the transformation of the creation and annihilation operators

$$\begin{aligned} \hat{a}_\lambda^\dagger &= \sum_i \langle\lambda|i\rangle^* \hat{a}_i^\dagger \\ \hat{a}_\lambda &= \sum_i \langle\lambda|i\rangle \hat{a}_i. \end{aligned} \tag{A.34}$$

If we use the position basis $|\mathbf{r}\rangle$ for the transformation and the fact that the wave function is defined as $\psi_i(\mathbf{r}) = \langle\mathbf{r}|i\rangle$ we arrive at the so-called field operators $\hat{\psi}^\dagger(\mathbf{r})$ and $\hat{\psi}(\mathbf{r})$

$$\begin{aligned} \hat{\psi}^\dagger(\mathbf{r}) &= \sum_i \psi_i^*(\mathbf{r}) \hat{a}_i^\dagger \\ \hat{\psi}(\mathbf{r}) &= \sum_i \psi_i(\mathbf{r}) \hat{a}_i. \end{aligned} \tag{A.35}$$

They fulfill the same type of commutation relations as the creation and annihilation operators $\hat{a}_i^\dagger$ and $\hat{a}_i$

$$\begin{aligned} \{\hat{\psi}^\dagger(\mathbf{r}), \hat{\psi}^\dagger(\mathbf{r}')\} &= \{\hat{\psi}(\mathbf{r}), \hat{\psi}(\mathbf{r}')\} = 0 \\ \{\hat{\psi}(\mathbf{r}), \hat{\psi}^\dagger(\mathbf{r}')\} &= \delta(\mathbf{r} - \mathbf{r}'). \end{aligned} \tag{A.36}$$

Finally, we have the tools at hand to express our Hamiltonian Eq. (A.2) in the language of second quantization with the help of the field operators $\hat{\psi}^\dagger(\mathbf{r})$ and $\hat{\psi}(\mathbf{r})$

$$H = \int \mathrm{d}^3 r\, \hat{\psi}^\dagger(\mathbf{r}) \hat{h}(\mathbf{r}) \hat{\psi}(\mathbf{r}) + \frac{1}{2} \int \mathrm{d}^3 r \int \mathrm{d}^3 r'\, \hat{\psi}^\dagger(\mathbf{r}) \hat{\psi}^\dagger(\mathbf{r}') v(\mathbf{r}, \mathbf{r}') \hat{\psi}(\mathbf{r}') \hat{\psi}(\mathbf{r}), \tag{A.37}$$

with $\hat{h}(\mathbf{r})$ from (A.1) and $v(\mathbf{r}, \mathbf{r}')$ being the Coulomb potential. The first part of Eq. (A.37) expresses the kinetic energy and the influence of the external potential on the individual particles, whereas the second part contains the interaction between the particles due to the Coulomb potential. Recalling the field operators in the Heisenberg picture

$$\hat{\psi}(\mathbf{r}, t) = e^{iHt} \hat{\psi}(\mathbf{r}) e^{-iHt}, \tag{A.38}$$

an equation of motion for the field operators is found by utilizing the commutation relations (A.36) in the Heisenberg picture

$$\begin{aligned} i \frac{\partial}{\partial t} \hat{\psi}(\mathbf{r}, t) &= \left[\hat{\psi}(\mathbf{r}, t), H \right] \\ &= \left[\hat{h}(\mathbf{r}) + \int \mathrm{d}^3 r'\, v(\mathbf{r}, \mathbf{r}') \hat{\psi}^\dagger(\mathbf{r}', t) \hat{\psi}(\mathbf{r}', t) \right] \hat{\psi}(\mathbf{r}, t). \end{aligned} \tag{A.39}$$

In the Eq. (A.39) the time-evolution of the field operators is governed by the single-particle Hamiltonian $\hat{h}(\mathbf{r})$ and a term containing the interaction between the particles. This term causes the relation to be a non-linear integro-differential equation being extremely difficult to solve. A perturbative approach has to be applied to that interaction term, which we will develop in the next sections.

Appendix B

Functional Derivative Identities

At this place we shall review very briefly some identities related to the functional calculus. A useful compilation of the latter can be found in Ref. (Strinati 1988). Let $F[g]$ be a functional, depending on a function $g(x)$, so that we can write in a more complete but sloppy way $F[g(x)]$ which nevertheless should not be confused with $F(g(x))$ being the concatenation of two functions. Let us apply a small change $\delta g(x)$ to the argument function $g(x)$ and investigate the difference in the value of the functional

$$\delta F[g(x)] = F[g(x) + \delta g(x)] - F[g(x)], \tag{B.1}$$

which we can approximate for a fixed $g(x)$ to first order as

$$F[g(x) + \delta g(x)] - F[g(x)] = \int \mathrm{d}y\, \phi(y)\delta g(y), \tag{B.2}$$

where $\phi(x)$ is the *functional derivative* $\delta F[g]/\delta g(x)$ at the fixed function $g(x)$. Summarizing, the functional derivative of a functional $F[g(x)]$ is defined in the following equation

$$F[g(x) + \delta g(x)] - F[g(x)] = \int \mathrm{d}y\, \frac{\delta F[g]}{\delta g(y)}\delta g(y), \tag{B.3}$$

which is required to hold up to first order in $\delta g(x)$. As in the case of ordinary calculus, the same identities are valid for differentiating a product and for the chain rule. Special care has to be taken with the case

$$\frac{\delta g(x)}{\delta g(y)} = \delta(x, y). \tag{B.4}$$

We briefly annotate a relation between the derivative of the inverse of a functional and the functional itself. Let $F[g(x)]$ be a functional and $F^{-1}[g(y)]$ be its inverse, defined with the help of the following equation

$$\int \mathrm{d}z\, F[g;x,z]F^{-1}[g;z,y] = \delta(x,y). \tag{B.5}$$

If this equation is varied with respect to g, multiplied with $F[g;z,v]$ and integrated over z the following identity is obtained

$$\frac{\delta F[g;x,y]}{\delta g(z)} = -\int \mathrm{d}u \int \mathrm{d}v\, F[g;x,u]\frac{\delta F^{-1}[g;u,v]}{\delta g(z)}F[g;v,y]. \tag{B.6}$$

An equivalent expression is found when F and F^{-1} are swapped. Further manipulation of Eq. (B.6) leads to the relation

$$\int \mathrm{d}v\, \frac{\delta F[g;x,v]}{\delta g(z)}F^{-1}[g;v,y] = -\int \mathrm{d}v\, F[g;x,v]\frac{\delta F^{-1}[g;v,y]}{\delta g(z)}. \tag{B.7}$$

Appendix C

Density Matrices

We define the one- and two particle density matrices, denoted as $n_1(\mathbf{r}, \mathbf{r}')$ and $n_2(\mathbf{r}_1, \mathbf{r}_1'; \mathbf{r}_2, \mathbf{r}_2')$, and the corresponding diagonals, $n_1(\mathbf{r})$ and $n_2(\mathbf{r}, \mathbf{r}')$ in the following way[1] (von Barth 2004, Tokatly 2005)

$$n_1(\mathbf{r}, \mathbf{r}') = \langle \Psi | \hat{n}_1(\mathbf{r}, \mathbf{r}') | \Psi \rangle \tag{C.1}$$

$$n_2(\mathbf{r}_1, \mathbf{r}_1'; \mathbf{r}_2, \mathbf{r}_2') = \langle \Psi | \hat{n}_2(\mathbf{r}_1, \mathbf{r}_1'; \mathbf{r}_2, \mathbf{r}_2') | \Psi \rangle \tag{C.2}$$

$$n_1(\mathbf{r}) = n_1(\mathbf{r}, \mathbf{r}) \tag{C.3}$$

$$n_2(\mathbf{r}, \mathbf{r}') = n_2(\mathbf{r}, \mathbf{r}'; \mathbf{r}, \mathbf{r}'). \tag{C.4}$$

Here, the corresponding density operators are given by

$$\hat{n}_1(\mathbf{r}, \mathbf{r}') = \hat{\psi}^\dagger(\mathbf{r}) \hat{\psi}(\mathbf{r}') \tag{C.5}$$

$$\hat{n}_2(\mathbf{r}_1, \mathbf{r}_1'; \mathbf{r}_2, \mathbf{r}_2') = \hat{\psi}^\dagger(\mathbf{r}_1) \hat{\psi}^\dagger(\mathbf{r}_1') \hat{\psi}(\mathbf{r}_2') \hat{\psi}(\mathbf{r}_2). \tag{C.6}$$

We note that the density matrices (and their diagonals) are positive definite and Hermitian as well as that the diagonal of the one particle density matrix is trivially just the particle density

$$n(\mathbf{r}) = n_1(\mathbf{r}). \tag{C.7}$$

The *pair-correlation function* $g(\mathbf{r}, \mathbf{r}')$ is defined with the help of the two-particle density matrix and the density itself by

$$n_2(\mathbf{r}, \mathbf{r}') = n(\mathbf{r}) n(\mathbf{r}') g(\mathbf{r}, \mathbf{r}'). \tag{C.8}$$

[1] Note that in these definitions the spin has already been summed over. Otherwise each argument of the density matrix would be augmented by a spin variable.

If the electrons were completely independent, the two-particle density would simply be the product of the two one-electron densities with a pair-correlation function equal to unity.

We assume now that the many-body wave function is just a single Slater determinant, defined with the help of the symmetrization operator[2], Eq. (A.14)

$$\Psi(\mathbf{r}_1, \ldots, \mathbf{r}_N) = (N!)^{-\frac{1}{2}} \hat{S}[\phi_1(\mathbf{r}_1) \cdots \phi_N(\mathbf{r}_N)]. \tag{C.9}$$

As a consequence, the expression for the one-particle density matrix reduces to

$$n_1(\mathbf{r}, \mathbf{r}') = \sum_{i=1}^{N} \phi_i^*(\mathbf{r}) \phi_i(\mathbf{r}') \tag{C.10}$$

whereas the density itself is given by

$$n(\mathbf{r}) = \sum_{i=1}^{N} |\phi_i(\mathbf{r})|^2. \tag{C.11}$$

[2]Here, the permutations, present in the symmetrization operator, act on the indices of the one-particle wave functions.

Appendix D

Details on the Runge-Gross Theorem

D.1 The Time Evolution of the Current Density

In this appendix we shall work out the expectation value of the commutator of the current and the difference in the Hamiltonian

$$\langle\Phi_0|[\mathbf{j}(\mathbf{r}), \hat{H}(t_0) - \hat{H}'(t_0)]|\Phi_0\rangle = \langle\Phi_0|[\mathbf{j}(\mathbf{r}), \hat{V}(t_0) - \hat{V}'(t_0)]|\Phi_0\rangle. \tag{D.1}$$

This expression appears in the proof of the Runge-Gross theorem and equals the difference in the time-evolution of the current densities subject to the two different external potentials. Let us investigate the commutator in the above equation in more detail by means of Eq. (2.15)

$$\begin{aligned}&[\mathbf{j}(\mathbf{r}), \hat{V}(t) - \hat{V}'(t)] \\ &\quad = \frac{1}{2i} \lim_{\mathbf{r}'\to\mathbf{r}} \int \mathrm{d}^3 z \, \left[(\nabla_{\mathbf{r}'} - \nabla_{\mathbf{r}})[\hat{\psi}^\dagger(\mathbf{r}')\hat{\psi}(\mathbf{r})], \hat{\psi}^\dagger(\mathbf{z})\hat{\psi}(\mathbf{z})\right] [v(\mathbf{r}, t) - v'(\mathbf{r}, t)].\end{aligned} \tag{D.2}$$

Further evaluation of the commutator on the right hand side of the Eq. (D.2) leads to

$$\begin{aligned}&\left[(\nabla_{\mathbf{r}'} - \nabla_{\mathbf{r}})[\hat{\psi}^\dagger(\mathbf{r}')\hat{\psi}(\mathbf{r})], \hat{\psi}^\dagger(\mathbf{z})\hat{\psi}(\mathbf{z})\right] \\ &\quad = (\nabla_{\mathbf{r}'} - \nabla_{\mathbf{r}}) \left[\hat{\psi}^\dagger(\mathbf{r}')\hat{\psi}(\mathbf{z})\delta(\mathbf{r} - \mathbf{z}) - \hat{\psi}^\dagger(\mathbf{z})\hat{\psi}(\mathbf{r})\delta(\mathbf{r}' - \mathbf{z})\right].\end{aligned} \tag{D.3}$$

Carrying out the integration in Eq. (2.15), applying the gradients and taking the limit $\mathbf{r} \to \mathbf{r}'$ finally leads to a connection to the density operator and the gradient of the difference in the external potential

$$[\mathbf{j}(\mathbf{r}), \hat{V}(t) - \hat{V}'(t)] = i\hat{n}(\mathbf{r})\nabla[v(\mathbf{r},t) - v'(\mathbf{r},t)], \tag{D.4}$$

and we obtain the following expression for the expectation value of the commutator

$$\langle\Phi_0|[\mathbf{j}(\mathbf{r}), \hat{H}(t_0) - \hat{H}'(t_0)]|\Phi_0\rangle = in(\mathbf{r},t_0)\nabla[v(\mathbf{r},t) - v'(\mathbf{r},t)]. \tag{D.5}$$

D.2 The Iterated Equation of Motion for the Current Density

In Eq. (4.6) in section 4.2 we have investigated the equation of motion for the current density and drawn a connection to the external potential. Here we shall prove that if we apply the equation of motion k-times the expression of Eq. (4.7) is obtained. From the considerations in Sect. D.1 we note that

$$i\frac{\partial}{\partial t}\mathbf{j}(\mathbf{r},t) = [\hat{j}(\mathbf{r}), \hat{H}(t)] = \langle i\hat{n}(\mathbf{r})\nabla w(\mathbf{r},t) + \hat{K}(\mathbf{r})\rangle_t, \tag{D.6}$$

where $\hat{K}(\mathbf{r}) = [\hat{j}(\mathbf{r}), \hat{T} + \hat{U}]$ is the part of the commutator corresponding to the kinetic energy and the electron-electron interaction. By using the equation of motion, Eq. (4.5) in combination with the previous equation we obtain

$$\begin{aligned}
&\left(i\frac{\partial}{\partial t}\right)^2 \mathbf{j}(\mathbf{r},t) \qquad\qquad (D.7)\\
&= \left\langle i\frac{\partial}{\partial t}[\hat{j}(\mathbf{r}), \hat{H}(t)] + [[\hat{j}(\mathbf{r}), \hat{H}(t)], \hat{H}(t)] \right\rangle \\
&= \left\langle \left[i\nabla\left(i\frac{\partial}{\partial t}\right)v(\mathbf{r},t)\right]\hat{n}(\mathbf{r}) + [[\hat{j}(\mathbf{r}), \hat{H}(t)], \hat{H}(t)] \right\rangle .
\end{aligned}$$

If the equation of motion is applied another $k-1$ times to Eq. (D.7) it is given schematically by

$$\left(i\frac{\partial}{\partial t}\right)^{k+1} \mathbf{j}(\mathbf{r},t) = \left\langle u_k(\mathbf{r},t)\hat{n}(\mathbf{r}) + \hat{K}_{k-1}(\mathbf{r},t) \right\rangle , \tag{D.8}$$

where

$$u_k(\mathbf{r},t) = i\nabla \left(i\frac{\partial}{\partial t}\right)^k v(\mathbf{r},t), \tag{D.9}$$

and the part $\hat{K}_{k-1}(\mathbf{r},t)$ consists of time-derivatives up to $k-1$st order of multiple commutators of $\hat{n}(\mathbf{r})$ and $\hat{\mathbf{j}}(\mathbf{r})$ with $\hat{H}(t)$ and the functions $u_l(\mathbf{r},t)$. Now we combine the time evolution of both systems at $t = t_0$

$$\left(i\frac{\partial}{\partial t}\right)^{k+1} [\mathbf{j}(\mathbf{r},t) - \mathbf{j}'(\mathbf{r},t)]\big|_{t_0} = \langle [u_k(\mathbf{r},t) - u'(\mathbf{r},t)]\hat{n}(\mathbf{r})\rangle_{t_0} + \langle \hat{K}_{k-1}(\mathbf{r},t) - \hat{K}'_{k-1}(\mathbf{r},t)\rangle_{t_0}. \tag{D.10}$$

The terms in $\hat{K}'_{k-1}(\mathbf{r},t)$ are equal to those in $\hat{K}_{k-1}(\mathbf{r},t)$, except that $H'(t)$ and $u'(\mathbf{r},t)$ enter in place of $H(t)$ and $u(\mathbf{r},t)$. In the following we want to show that the contributions of $\hat{K}_{k-1}$ and $\hat{K}'_{k-1}$ are the same for $t = t_0$. To this end we note that the commutators in $\hat{K}'_{k-1}$ are of the form

$$[\ldots[\ldots[\hat{A},\hat{H}'(t)],\ldots(\partial^l/\partial t^l)\hat{H}'(t)],\ldots\hat{H}'(t)]u'_j(\mathbf{r},t), \tag{D.11}$$

where $\hat{A} \in \{\hat{n}(\mathbf{r}),\hat{\mathbf{j}}(\mathbf{r})\}$ and $j,l \leq k-1$. Since from Eq. (4.10) we know that for $l < k$

$$w_l(\mathbf{r}) = w_l = \text{const.} \tag{D.12}$$

we can write for the l-th time-derivative of $\hat{H}'(t)$

$$\begin{aligned}\frac{\partial^l}{\partial t^l}\,\hat{H}'(t)\Big|_{t_0} &= \frac{\partial^l}{\partial t^l}\,\hat{H}(t)\Big|_{t_0} - \frac{\partial^l}{\partial t^l}\,[\hat{H}(t) - \hat{H}'(t)]\Big|_{t_0} \\ &= \frac{\partial^l}{\partial t^l}\,\hat{H}(t)\Big|_{t_0} - \int \mathrm{d}^3r\,\hat{n}(\mathbf{r})\frac{\partial^l}{\partial t^l}\,w(\mathbf{r},t)|_{t_0} \\ &= \frac{\partial^l}{\partial t^l}\,\hat{H}(t)\Big|_{t_0} - w_l N\hat{1}.\end{aligned} \tag{D.13}$$

The second term in Eq. (D.13) does not contribute inside a commutator and hence, the commutators in Eq. (D.11) can be factored out for the systems subject to $\hat{H}(t)$ and $\hat{H}'(t)$. The only thing which remains to prove is that the u_j and u'_j are the same, but this is trivial since by assumption

$$[u_j(\mathbf{r},t) - u'_j(\mathbf{r},t)]\big|_{t_0} = i\nabla w_j = 0. \tag{D.14}$$

Therefore, Eq. (D.10) reduces to Eq. (4.7).

D.3 The Surface Integral in the Proof of the Runge-Gross Theorem

Let us note the first Green's formula (the functions f and g depend on $\mathbf{r}$)

$$\int_V \mathrm{d}^3r\,(f\nabla^2 g + (\nabla f)(\nabla g)) = \oint_{\partial V} \mathrm{d}\mathbf{S}\, f\nabla g, \tag{D.15}$$

which is written for $f = n_0 w_k$ and $g = w_k$ (see Eq. (4.11)) as

$$\begin{aligned}\oint \mathrm{d}\mathbf{S}\, n_0 w_k \nabla w_k &= \int \mathrm{d}^3r\,[n_0 w_k \nabla^2 w_k + w_k(\nabla n_0)(\nabla w_k) + n_0(\nabla w_k)^2] \\ &= \int \mathrm{d}^3r\,[w_k \nabla[n_0 \nabla w_k] + n_0(\nabla w_k)^2].\end{aligned} \tag{D.16}$$

This is exactly the relation between Eq. (4.11) and Eq. (4.12).

Appendix E

Fourier Transforms in Periodic Systems

A Fourier transform pair can be defined with two arbitrary constants a and b as

$$F(y) = \sqrt{\frac{|b|}{(2\pi)^{1-a}}} \int_{-\infty}^{\infty} \mathrm{d}x\, f(x) e^{ibyx} \tag{E.1}$$

$$f(x) = \sqrt{\frac{|b|}{(2\pi)^{1+a}}} \int_{-\infty}^{\infty} \mathrm{d}y\, F(y) e^{-ibyx} \tag{E.2}$$

In physics one usually uses $(a, b) = (1, 1)$ for transforming from time to frequency, *i.e.*:

$$F(\omega) = \int_{-\infty}^{\infty} \mathrm{d}t\, f(t) e^{i\omega t} \tag{E.3}$$

$$f(t) = \frac{1}{2\pi} \int_{-\infty}^{\infty} \mathrm{d}\omega\, F(\omega) e^{-i\omega t} \tag{E.4}$$

whereas for transforming from real (coordinate) space to reciprocal space a product of three Fourier transforms with parameters $(a, b) = (-1, 1)$ leads to

$$F(\mathbf{k}) = \int_{\mathbb{R}^3} \mathrm{d}^3 r\, f(\mathbf{r}) e^{-i\mathbf{kr}} \tag{E.5}$$

$$f(\mathbf{r}) = \frac{1}{(2\pi)^3} \int_{\mathbb{R}^3} \mathrm{d}^3 k\, F(\mathbf{k}) e^{i\mathbf{kr}} \tag{E.6}$$

For functions that obey the Born-von-Karman boundary conditions, *i.e.*: $f(\mathbf{r} + N_j\mathbf{a}_j) = f(\mathbf{r})$ for $j \in \{1, 2, 3\}$ and $N_j \in \mathbb{Z}$, it is possible to define a Fourier transform with parameters a and b in such a way that

$$F(\mathbf{k}) = \frac{1}{V}\int_V \mathrm{d}^3r\, f(\mathbf{r})e^{-i\mathbf{kr}} \tag{E.7}$$

$$f(\mathbf{r}) = \sum_{\mathbf{k}} F(\mathbf{k})e^{i\mathbf{kr}} \tag{E.8}$$

where $\Omega = (\mathbf{a}_1, \mathbf{a}_2, \mathbf{a}_3)$ is the volume of the parallelepiped spanned by the basis vectors, $V = N_1N_2N_3\Omega$, the periodicity-volume and the vectors $\mathbf{k}$ are restricted by the conditions for their coefficients

$$k_j = \frac{n_j}{N_j}, n_j \in \mathbb{Z} \tag{E.9}$$

For the basis $\{\mathbf{a}_j\}$ we define a reciprocal basis $\{\mathbf{b}_j\}$ that we call reciprocal by the conditions

$$\mathbf{a}_i\mathbf{b}_j = 2\pi\delta_{ij}. \tag{E.10}$$

The factor of 2π comes for convenience with the Fourier transform. Now we decompose a vector $\mathbf{k}$ into a part belonging to the parallelepiped Ω (the unit cell) and a part specifying the position of the parallelepiped inside the volume V. In other words, one decomposes the components of $\mathbf{k}$, namely k_j in the frame of the reciprocal lattice vectors into a fractional part q_j and an integer part G_j with the properties

$$\begin{aligned} &\mathbf{k} = \mathbf{q} + \mathbf{G} \\ &|q_j| < 1 \\ &G_j \in \mathbb{Z}. \end{aligned} \tag{E.11}$$

Now, we can rewrite the Eqs. (E.7)

$$F(\mathbf{q}, \mathbf{G}) = \frac{1}{V}\int_V \mathrm{d}^3r\, f(\mathbf{r})e^{-i(\mathbf{q}+\mathbf{G})\mathbf{r}} \tag{E.12}$$

$$f(\mathbf{r}) = \sum_{\mathbf{q},\mathbf{G}} F(\mathbf{q}, \mathbf{G})e^{i(\mathbf{q}+\mathbf{G})\mathbf{r}}. \tag{E.13}$$

As we see from Eq. (E.9) there are as many $\mathbf{q}$-vectors for each j-coordinate direction as numbers N_j that define the periodicity-volume. The larger the

volume, the more $\mathbf{q}$ vectors we have in the unit cell. In case of a function with the periodicity of the unit cell, the above expression simplifies to

$$F(\mathbf{G}) = \frac{1}{\Omega}\int_{\Omega} \mathrm{d}^3 r\, f(\mathbf{r}) e^{-i\mathbf{G}\mathbf{r}} \tag{E.14}$$

$$f(\mathbf{r}) = \sum_{\mathbf{G}} F(\mathbf{G}) e^{i\mathbf{G}\mathbf{r}}.. \tag{E.15}$$

For a function $h(\mathbf{r}, \mathbf{r}')$ depending on two real-space arguments we can write (by using two different Fourier transform pairs)

$$H(\mathbf{q}, \mathbf{G}; \mathbf{q}', \mathbf{G}') = \frac{1}{V}\int_V \mathrm{d}^3 r \int_V \mathrm{d}^3 r'\, e^{-i(\mathbf{q}+\mathbf{G})\mathbf{r}} h(\mathbf{r}, \mathbf{r}') e^{i(\mathbf{q}'+\mathbf{G}')\mathbf{r}'} \tag{E.16}$$

$$h(\mathbf{r}, \mathbf{r}') = \frac{1}{V}\sum_{\mathbf{q},\mathbf{G}}\sum_{\mathbf{q}',\mathbf{G}'} e^{i(\mathbf{q}+\mathbf{G})\mathbf{r}} H(\mathbf{q}, \mathbf{G}; \mathbf{q}', \mathbf{G}') e^{-i(\mathbf{q}'+\mathbf{G}')\mathbf{r}'} \tag{E.17}$$

If the function h is periodic with respect to a shift of both variables by the same primitive lattice vector $\mathbf{R}$

$$h(\mathbf{r} + \mathbf{R}, \mathbf{r}' + \mathbf{R}) = h(\mathbf{r}, \mathbf{r}') \tag{E.18}$$

one can show that Eq. (E.16) depends only on one $\mathbf{q}$ vector:

$$H(\mathbf{q}; \mathbf{G}, \mathbf{G}') = \frac{1}{V}\int_V \mathrm{d}^3 r \int_V \mathrm{d}^3 r'\, e^{-i(\mathbf{q}+\mathbf{G})\mathbf{r}} h(\mathbf{r}, \mathbf{r}') e^{i(\mathbf{q}+\mathbf{G}')\mathbf{r}'} \tag{E.19}$$

$$h(\mathbf{r}, \mathbf{r}') = \frac{1}{V}\sum_{\mathbf{q}}\sum_{\mathbf{G},\mathbf{G}'} e^{i(\mathbf{q}+\mathbf{G})\mathbf{r}} H(\mathbf{q}; \mathbf{G}, \mathbf{G}') e^{-i(\mathbf{q}+\mathbf{G}')\mathbf{r}'} \tag{E.20}$$

Appendix F

Spectral Representation of a Non-Hermitian Operator

In order to express the macroscopic dielectric function – obtained from the solution of the BSE – as a summation over excitons one has to employ a spectral representation of a function of an effective Hamiltonian operator H, which, in general, might not be Hermitian. Suppose that the operator is non-singular (if not so we can always reduce it to a subspace where it is) and that we have already solved the eigenvalue problem

$$H|\lambda\rangle = E_\lambda|\lambda\rangle \tag{F.1}$$

with eigenvalues E_λ corresponding to eigenvectors $|\lambda\rangle$. Note that the eigenvectors are not necessarily orthogonal or normalized but we require them to build a basis for the subspace where the operator is defined (which is not a restriction as one can prove). We want to evaluate the operator

$$H^{-1}(\omega) \equiv (H - \omega I)^{-1} \tag{F.2}$$

in a certain basis $\{|a\rangle\}$, namely the $\{|nm\mathbf{k}\rangle\}$ basis, which is orthonormal. The action of $H(\omega)$ upon an eigenvector $|\lambda\rangle$ of H is given by

$$H(\omega)|\lambda\rangle = (H - \omega I)|\lambda\rangle = (E_\lambda - \omega)|\lambda\rangle \tag{F.3}$$

which follows immediately from the eigenvalue equation for H. Now we want to identify the matrix elements of $H^{-1}(\omega)$ within the eigenbasis $\{|\lambda\rangle\}$. Recalling that the identity operator for a general non-orthogonal basis can

be expressed as

$$I = \sum_{\nu,\nu'} |\nu\rangle M^{-1}_{\nu,\nu'} \langle\nu'| \tag{F.4}$$

with M being the overlap matrix

$$M_{\nu,\nu'} = \langle\nu|\nu'\rangle \tag{F.5}$$

we are able to write

$$\begin{aligned} I &= IH(\omega)IH^{-1}(\omega)I \\ &= \sum_{\lambda,\lambda'}\sum_{\mu,\mu'}\sum_{\nu,\nu'} |\lambda\rangle M^{-1}_{\lambda,\mu}\langle\mu|H - I\omega|\mu'\rangle M^{-1}_{\mu',\nu}\langle\nu|H^{-1}(\omega)|\nu'\rangle M^{-1}_{\nu',\lambda'}\langle\lambda'|. \end{aligned} \tag{F.6}$$

From the above equation, additionally, one can derive the spectral representation of an operator within a non-orthogonal basis, namely

$$H = \sum_{\mu,\mu'} E_\mu M^{-1}_{\mu\mu'} |\mu\rangle\langle\mu'|. \tag{F.7}$$

In contrast, a simpler spectral representation of a Hermitian operator within an orthonormal basis of eigenvectors is given with the help of the projection operators $|\mu\rangle\langle\mu|$,

$$H_{\text{herm}} = \sum_{\mu} E_\mu |\mu\rangle\langle\mu|. \tag{F.8}$$

A representation of our operator H in terms of projection operators is also possible if one defines the bra vectors

$$\langle\bar{\lambda}| = \sum_{\lambda'} M^{-1}_{\lambda,\lambda'}\langle\lambda'|. \tag{F.9}$$

Now, utilizing Eq. (F.7) and the previous equation, we express the operator H as

$$H = \sum_{\mu} E_\mu |\mu\rangle\langle\bar{\mu}| \tag{F.10}$$

which is a spectral representation in terms of projection operators $|\mu\rangle\langle\bar{\mu}|$ and eigenvalues E_λ. But turning back to Eq.(F.6) and comparing it to Eq. (F.4) we conclude that

$$\delta_{\mu,\lambda'} = \sum_{\mu'}\sum_{\nu,\nu'} M_{\mu,\mu'}(E_{\mu'} - \omega) M^{-1}_{\mu',\nu} H^{-1}_{\nu,\nu'}(\omega) M^{-1}_{\nu',\lambda'} \tag{F.11}$$

where we have used

$$H^{-1}_{\nu,\nu'}(\omega) = \langle\nu|H^{-1}(\omega)|\nu'\rangle. \tag{F.12}$$

With the help of $D_{\mu,\mu'}(\omega) = \delta_{\mu,\mu'}(E_{\mu'} - \omega)$ and by employing a shorthand matrix notation suppressing indices we find for the matrix elements of $(H^{-1}_{\mu,\mu'}(\omega)) = \mathcal{M}$ in the eigenbasis

$$\begin{aligned} \mathcal{I} &= \mathcal{M}\mathcal{D}\mathcal{M}^{-1}\mathcal{H}^{-1}\mathcal{M}^{-1} = \mathcal{D}\mathcal{M}^{-1}\mathcal{H}^{-1} \\ \mathcal{H}^{-1} &= \mathcal{M}\mathcal{D}^{-1}. \end{aligned} \tag{F.13}$$

which reads more explicitly

$$H^{-1}_{\mu,\mu'}(\omega) = \sum_{\nu} M_{\mu,\nu} D^{-1}_{\nu,\mu'}(\omega). \tag{F.14}$$

For the transformation to the $|a\rangle$ basis we make use of Eq. (F.4) twice

$$\begin{aligned} H^{-1}_{a,a'}(\omega) &= \langle a|H^{-1}(\omega)|a'\rangle \\ &= \sum_{\lambda,\lambda'}\sum_{\mu,\mu'}\langle a|\lambda\rangle M^{-1}_{\lambda,\mu} H^{-1}_{\mu,\mu'}(\omega) M^{-1}_{\mu',\lambda'}\langle\lambda'|a'\rangle \\ &= \sum_{\lambda,\lambda'}\sum_{\mu,\mu',\nu}\langle a|\lambda\rangle M^{-1}_{\lambda,\mu} M_{\mu,\nu} D^{-1}_{\nu,\mu'}(\omega) M^{-1}_{\mu',\lambda'}\langle\lambda'|a'\rangle \\ &= \sum_{\lambda,\lambda'}\sum_{\mu',\nu}\langle a|\lambda\rangle \delta_{\lambda,\nu} D^{-1}_{\nu,\mu'}(\omega) M^{-1}_{\mu',\lambda'}\langle\lambda'|a'\rangle \\ &= \sum_{\lambda,\lambda'}\sum_{\mu'}\langle a|\lambda\rangle D^{-1}_{\lambda,\mu'}(\omega) M^{-1}_{\mu',\lambda'}\langle\lambda'|a'\rangle \\ &= \sum_{\lambda,\lambda'}\sum_{\mu'}\langle a|\lambda\rangle \delta_{\lambda,\mu'}(E_\lambda - \omega)^{-1} M^{-1}_{\mu',\lambda'}\langle\lambda'|a'\rangle \\ &= \sum_{\lambda,\lambda'}\langle a|\lambda\rangle (E_\lambda - \omega)^{-1} M^{-1}_{\lambda,\lambda'}\langle\lambda'|a'\rangle. \end{aligned} \tag{F.15}$$

Since the $|a\rangle$-basis is orthonormal we can write

$$|\lambda\rangle = \sum_a |a\rangle\langle a|\lambda\rangle, \tag{F.16}$$

and we clearly identify $\langle a|\lambda\rangle$ as the expansion coefficient A^λ_a of the eigenstate $|\lambda\rangle$ in the $|a\rangle$-basis. Finally, the desired matrix elements read

$$H^{-1}_{a,a'}(\omega) = \sum_{\lambda,\lambda'} \frac{A^\lambda_a M^{-1}_{\lambda,\lambda'} [A^{\lambda'}_{a'}]^*}{E_\lambda - \omega}. \tag{F.17}$$

It remains to show that the coefficients A_a^λ are in fact eigenvectors of the matrix $H_{a,a'}$, *i.e.*:

$$\sum_{a'} H_{a,a'} A_{a'}^\lambda = E_\lambda A_a^\lambda \tag{F.18}$$

but this is trivial if we multiply Eq. (F.1) with the identity $\sum_a |a\rangle\langle a|$ from the left side and expand the eigenstates $|\lambda\rangle$ in the $|a\rangle$-basis. Note that we did not use the concept of a function of an operator in our derivations.

Acknowledgments

I want to thank Claudia Ambrosch-Draxl for supervising my thesis and her steady support throughout this time. The nice atmosphere in her group made it very enjoyable to work. She was never tired of explaining things and discussing various aspects of my work. I want to thank her for giving me the freedom to let me finish this thesis in my own way.

I am grateful to Martin Oehzelt and Georg Heimel for providing the initial contact to Claudia, or – as some might say – selling me to her.

Many thanks from my side go to Kerstin Hummer for giving me initial support on the WIEN code and Peter's BSE code. I am grateful to Peter Puschnig for his support on the details of my implementation. His thesis as well as his BSE code served as a very important starting point for my work.

I want to thank Jürgen Spitaler for the very enjoyable time that we shared at the Institute. I mention the *a cappella* sessions in the Dissertantenzimmer and, not to forget, the many breakfasts in combinations with aspects of group theory in solid state physics, called the *Gruppenfrühstück*.

I am thankful to Kay Dewhurst for helping me to understand the mysteries of the Exciting code and to Sangeeta Sharma for her initial support with the local basis from exact exchange.

I want to thank Asier Eiguren in many ways. He supported me scientifically and was never short of time for discussions and looking at my derivations. Not only did he support me scientifically, he steadily encouraged me during this time. I keep in mind the many times that we had been sitting drinking a beer and discussing various things.

Also I am thankful to Markus Wenin, the physicist and philosopher. I mention the coffee breaks at the Institute in Graz as well as the various

beers in combination with discussions about Franz Kafka.

I want to thank the people from the Chair of Atomistic Modelling and Design of Materials at the University of Leoben. The multi-cultural environment made is very enjoyable to work. I mention the many celebrations with a large variety of delicious food. Thanks to Andrei, Lorenz and Monodeep for the perfect company in the room that we share and also many thanks to all former group members.

I am very thankful to Christian Meisenbichler for helping me with various aspects concerning computers and software.

Several collaborators and visiting scientist have contributed to the success of this work through fruitful discussions.

Many thanks go to Ulrich Hohenester for being the reviewer of this thesis and to Clas Persson for various discussions and, most notably, for carefully reading this manuscript.

The steady support from my family and friends shall be especially highlighted.

Finally, thank you Lisa, for your support during all the years.

Stephan Sagmeister
Graz, August 2009

List of Figures

Bibliography

Abt R 1997 Berechnung optischer Eigenschaften von Hochtemperatursupraleitern in der LAPW – Methode Ph. D. Thesis Karl–Franzens–Universität Graz/Austria.

Adler S L 1962 *Phys. Rev.* **126**, 413.

Adragna G, Del Sole R & Marini A 2003 *Phys. Rev. B* **68**, 165108.

Albrecht S, Reining L, Del Sole R & Onida G 1998 *Phys. Rev. Lett.* **80**, 4510.

Ambegaokar V & Kohn W 1960 *Phys. Rev.* **117**, 423.

Ambrosch-Draxl C 2004 *Phys. Scr.* **T109**, 48–53.
*http://stacks.iop.org/1402-4896/T109/48

Ambrosch-Draxl C, Sagmeister S, Meisenbichler C & Spitaler J 2009 'Exciting code' to be published.
*http://exciting-code.org

Ambrosch-Draxl C & Sofo J 2006 *Comput. Phys. Commun.* **175**, 1.

Andersen O K 1975 *Phys. Rev. B* **12**, 3060.

Arfken G B & Weber H J 2005 *Mathematical Methods For Physicists* Academic Press.

Arnaud B 2000 Effets des correlations sur les proprietes electroniques et optiques des semiconducteurs et isolant Ph. D. Thesis Universite Louis Pasteur Strasbourg/France.

Arnaud B & Alouani M 2001 *Phys. Rev. B* **63**, 085208–1.

Aspnes D E & Studna A A 1983 *Phys. Rev. B* **27**, 985.

Baym G 1962 *Phys. Rev.* **127**, 1391.

Baym G & Kadanoff L P 1961 *Phys. Rev.* **124**, 287.

Bechstedt F, Tenelsen K, Adolph B & Del Sole R 1997 *Phys. Rev. Lett.* **78**, 1528.

Benedict L X, Shirley E L & Bohn R B 1998*a* *Phys. Rev. Lett.* **80**, 4514.

Benedict L X, Shirley E L & Bohn R B 1998*b* *Phys. Rev. B* **57**, R9385.

Blöchl P E, Jepsen O & Andersen O K 1994 *Phys. Rev. B* **49**, 16223.

Botti S, Fourreau A, Nguyen F, Renault Y, Sottile F & Reining L 2005 *Phys. Rev. B* **72**, 125203.

Botti S, Sottile F, Vast N, Olevano V, Reining L, Weissker H C, Rubio A, Onida G, del Sole R & Godby R W 2004 *Phys. Rev. B* **69**, 155112.

Bruneval F 2005 Exchange and Correlation in the Electronic Structure of Solids, from Silicon to Cuprous Oxide: GW Approximation and beyond PhD thesis Ecole Polytechnique.

Bruneval F, Sottile F, Olevano V, Sole R D & Reining L 2005 *Phys. Rev. Lett.* **94**, 186402.

Burke K & Gross E K U 1998 Springer, Berlin chapter A Guided Tour of Time-Dependent Density Functional Theory, pp. 116–146.

Burroughes J H, Bradley D D C, Brown A R, Marks R N, Mackay K, Friend R H, Burn P L, Kraft A & Holmes A B 1990 *Nature* **347**, 539.

Capelle K 2006 *Braz. J. Phys.* **36**(4a), 1318.

Ceperly D M 1978 *Phys. Rev. B* **18**, 3126.

Ceperly D M & Alder B J 1980 *Phys. Rev. Lett.* **45**, 566.

Costa P G D, Dandrea R G & Conwell E M 1993 *Phys. Rev. B* **47**, 1800.

Del Sole R, Adragna G, Olevano V & Reining L 2003 *Phys. Rev. B* **67**, 045207.

Del Sole R & Fiorino E 1984 *Phys. Rev. B* **29**, 4631.

Del Sole R & Girlanda R 1993 *Phys. Rev. B* **48**, 11789.

Dewhurst J K, Sharma S & Ambrosch-Draxl C 2005 'EXCITING Code development under the RT network EXCITING funded by the EU, HPRN-CT-2002-00317'.

Dreizler R M & Gross E K U 1990 *Density Functional Theory* Springer Verlag, Berlin.

Duck I & Sudarshan E C G 1998 *Am. J. Phys.* **66**, 284.

Economou E N 2006 *Green's Functions in Quantum Physics* 3 edn Springer.

Ehrenreich H & Cohen M H 1959 *Phys. Rev.* **115**, 786.

Ehrnsperger M & Bross H 1997 *J. Phys.: Condens. Matter* **9**(6), 1225–1240. *http://stacks.iop.org/0953-8984/9/1225

Eschrig H 1996 *The Fundamentals of Density Functional Theory* Teubner, Stuttgart - Leipzig.

Evertz H G 2004 *Fortgeschrittene Quantenmechanik* Skriptum TU Graz.

Fetter A L & Walecka H D 1971 *Quantum Theory of Many-Particle Systems* McGraw-Hill.

Feynman R P 1949*a* *Phys. Rev.* **76**(6), 769–789.

Feynman R P 1949*b* *Phys. Rev.* **76**(6), 749–759.

Fiolhais C, Nogueira F & Marques M A L, eds 2003 *A Primer in Density Functional Theory* Springer, Berlin.

Freysoldt C, Eggert P, Rinke P, Schindlmayr A, Godby R W & Scheffler M 2007 *Comput. Phys. Commun.* **176**, 1.

Gaunt J A 1929 *Phil. Trans. Roy. Soc. (London) A* **228**, 151.

Gell-Mann M & Low F 1951 *Phys. Rev.* **84**(2), 350–354.

Godby R W, Schlüter M & Sham L J 1986 *Phys. Rev. Lett.* **56**, 2415.

Godby R W, Schlüter M & Sham L J 1988 *Phys. Rev. B* **37**, 10159.

Gomez-Abal R, Li X, Ambrosch-Draxl C & Scheffler M 2009 Tetrahedron integration library. to be published.

Gomez-Abal R, Li X, Scheffler M & Ambrosch-Draxl C 2008 *Phys. Rev. Lett.* **101**, 106404.

Greiner W 2000 *Relativistic Quantum Mechanics* Springer, Berlin.

Gross E K U, Dobson F J & Petersilka M 1996 Springer, New York chapter Density Functional Theory of time-dependent phenomena, p. 81.

Gross E K U & Kohn W 1985 *Phys. Rev. Lett.* **55**, 2850.

Gross E K U, Ullrich C A & Gossmann U J 1994 Plenum, New York chapter Density functional theory of time-dependent systems, pp. 149–171.

Gross E & Kohn W 1990 *Adv. Quant. Chem.* **21**, 255–291.

Gunnarsson O & Lundqvist B I 1976 *Phys. Rev. B* **13**, 4274.

Hanke W & Sham L J 1979 *Phys. Rev. Lett.* **43**, 387.

Hanke W & Sham L J 1980 *Phys. Rev. B* **21**, 4656.

Harris J & Jones R O 1974 *J. of Physics F* **4**, 1170.

Hedin L 1965 *Phys. Rev.* **139**, A796.

Hedin L & Lundquist S 1969 *Solid State Physics* Vol. 23 Academic, New York.

Hohenberg P & Kohn W 1964 *Phys. Rev.* **136**, B864.

Hubbard J 1957 *Proc. Roy. Soc.* **A240**, 539.

Hybertson M S & Louie S G 1986 *Phys. Rev. B* **34**, 5390.

Itzykson C & Zuber J B 1980 *Quantum Field Theory* McGraw-Hill, New York.

Jackson J D 1998 *Classical Electrodynamics* Wiley New York.

Janak J F 1978 *Phys. Rev. B* **18**, 7165.

Jones R O & Gunnarsson O 1989 *Rev. Mod. Phys.* **61**, 689.

Koelling D D & Harmon B N 1977 *J. Phys. C: Solid State Phys.* **10**, 3107.

Kohn W 1958 *Phys. Rev.* **110**, 857.

Kohn W 1985 *Reprint from Highlights of Condensed- Matter Theory, Soc. Italiana di Fisica* **Course LXXXIX**, 4.

Kohn W 1999 *Rev. Mod. Phys.* **71**, 1253.

Kohn W & Sham L J 1965 *Phys. Rev.* **140**, A1133.

Ku W & Eguiluz A G 1999 *Phys. Rev. Lett.* **82**(11), 2350–2353.

Langreth D C & Perdew J P 1975 *Sol. Stat. Comm.* **17**, 1425.

Lautenschlager P, Garriga M, Logothetidis S & Cardona M 1987 *Phys. Rev. B* **35**(17), 9174–9189.

Lautenschlager P, Garriga M, Viña L & Cardona M 1987 *Phys. Rev. B* **36**, 4821.

Lee K H & Chang K J 1996 *Phys. Rev. B* **54**(12), R8285–R8288.

Lehmann G & Taut M 1972 *Phys. Status Solidi* **54**, 469.

Levine Z H & Allen D C 1989 *Phys. Rev. Lett.* **63**, 1719.

Levine Z H & Allen D C 1991 *Phys. Rev. B* **43**, 4187.

Levy M 1982 *Phys. Rev. A* **26**, 1200.

Maitra N T, Burke K, Appel H, Gross E K U & van Leeuwen R 2002 World Scientific Publishing chapter Ten topical questions in time-dependent density functional theory, p. 1.

Marini A 2003 Bound excitons in TDDFT. unpublished.

Marini A, Hogan C, Grüning M & Varsano D 2009 *Comput. Phys. Commun.* **180**, 1392.

Marini A, Sole R D & Rubio A 2003 *Phys. Rev. Lett.* **91**, 256402.

Marques M & Gross E 2004 *Annu. Rev. Phys. Chem.* **55**, 427–455.

Marques M, Ullrich C, Nogueira F, Rubio A, Burke K & Gross E K U, eds 2006 *Time-dependent density functional theory* Vol. 706 of *Lecture notes in physics* Springer.

Martin P & Schwinger J 1959 *Phys. Rev.* **115**, 1342.

Mattuck R D 1992 *A Guide to Feynman Diagrams in the Many-Body Problem* Dover, New York.

Mattuck R D & Theumann A 1971 *Adv. Phys.* **20**, 721.

Mearns D & Kohn W 1987 *Phys. Rev. A* **35**(11), 4796–4799.

Nozieres P & Pines D 1958*a* *Phys. Rev.* **109**, 762.

Nozieres P & Pines D 1958*b* *Phys. Rev.* **109**, 741.

Nozieres P & Pines D 1958*c* *Phys. Rev.* **109**, 1062.

Onida G, Reining L & Rubio A 2002 *Rev. Mod. Phys.* **74**, 601.

Perdew J P, Burke K & Ernzerhof M 1998 *Phys. Rev. Lett.* **80**, 891.

Perdew J P & Levy M 1983 *Phys. Rev. Lett.* **51**, 1884.

Perdew J P & Wang Y 1992 *Phys. Rev. B* **45**, 13244.

Petersilka M, Gossmann U J & Gross E K U 1996 *Phys. Rev. Lett.* **76**, 1212.

Pick R M, Cohen M H & Martin R M 1970 *Phys. Rev. B* **1**(2), 910–920.

Puschnig P 2002 Excitonic Effects in Organic Semi-Conductors - An Ab-initio Study within the LAPW Method PhD thesis University Graz.

Puschnig P & Ambrosch-Draxl C 2002*a* *Phys. Rev. B* **66**(16), 165105.

Puschnig P & Ambrosch-Draxl C 2002*b* *Phys. Rev. Lett.* **89**(5), 056405.

Rayleigh J W 1870 *Phil. Trans.* **161**, 77.

Reining L, Olevano V, Rubio A & Onida G 2002 *Phys. Rev. Lett.* **88**(6), 066404.

Roessler D M & Walker W C 1967 *J. Opt. Soc. Am.* **57**, 835.

Rohlfing M, Krüger P & Pollmann J 1995 *Phys. Rev. B* **52**, 1905.

Rohlfing M & Louie S G 1998 *Phys. Rev. Lett.* **81**, 2312.

Rohlfing M & Louie S G 2000 *Phys. Rev. B* **62**, 4927.

Ruini A, Caldas M J, Bussi G & Molinari E 2002 *Phys. Rev. Lett.* **88**, 206403.

Runge E & Gross E K U 1984 *Phys. Rev. Lett.* **52**, 997.

Sagmeister S & Ambrosch-Draxl C 2009 *Phys. Chem. Chem. Phys.* **11**, 4451–4457.

Salpeter E E & Bethe H A 1951 *Phys. Rev.* **84**(6), 1232–1242.

Schöne W D 2001 *Theoretische Festkörperphysik* Skriptum Freie Universität Berlin.

Schwinger J 1951 *Proc. Nat. Acad. Sci. U.S.A.* **37**, 452.

Sham L J 1985 *Phys. Rev. B* **32**, 3876.

Sham L J & Rice T M 1966 *Phys. Rev.* **144**, 708.

Sham L J & Schlüter M 1983 *Phys. Rev. Lett.* **51**, 1888.

Sham L J & Schlüter M 1985 *Phys. Rev. B* **32**, 3883.

Singh D 1994 *Planewaves, Pseudopotentials and the LAPW Method* Kluwer Academic Publishers Boston/Dordrecht/London. ISBN 0–7923–9412–7.

Singh D & Krakauer H 1991 *Phys. Rev. B* **43**(2), 1441–1445.

Sjöstedt E, Nordström L & Singh D J 2000 *Sol. Stat. Comm.* **114**, 15.

Slater J C 1937 *Phys. Rev.* **51**, 846.

Sottile F 2003 Response functions of semiconductors and insulators: from the Bethe-Salpeter equation to time-dependent density functional theory PhD thesis Ecole Polytechnique.

Sottile F, Olevano V & Reining L 2003 *Phys. Rev. Lett.* **91**, 056402.

Strinati G 1982 *Phys. Rev. Lett.* **49**, 1519.

Strinati G 1984 *Phys. Rev. B* **29**, 5718.

Strinati G 1988 *Riv. Nuovo Cimento* **11**, 1.

Stubner R 2005 Diagrammatic techniques for time-dependent density-functional theory PhD thesis Friedrich-Alexander-Universität Erlangen-Nürnberg.

Stubner R, Tokatly I V & Pankratov O 2004 *Phys. Rev. B* **70**(24), 245119.

Tokatly I V 2005 *Phys. Rev. B* **71**(16), 165104.

van Leeuwen R 1998 *Phys. Rev. Lett.* **80**(6), 1280–1283.

van Leeuwen R 2006 Springer chapter Beyond the Runge-Gross Theorem, pp. 17–31.
*http://www.springerlink.com/content/56w0227050164v63

Vidberg H & Serene J 1977 *J. Low Temp. Phys.* **29**, 179–192.

Vogl P & Campbell D K 1990 *Phys. Rev. B* **41**, 12797.

von Barth U 2004 *Physica Scripta* **T109**, 9–39.
*http://stacks.iop.org/1402-4896/T109/9

Voss K F, Foster C M, Smilowitz L, D. Mihailovi D, Askari S, Srdanov G, Ni Z, Shi S, Heeger A J & Wudl F 1991 *Phys. Rev. B* **43**(6), 5109–5118.

Weissker H C, Serrano J, Huotari S, Bruneval F, Sottile F, Monaco G, Krisch M, Olevano V & Reining L 2006 *Phys. Rev. Lett.* **97**(23), 237602.
*http://link.aps.org/abstract/PRL/v97/e237602

Wiser N 1963 *Phys. Rev.* **129**, 62.

Zagoskin A M 1998 *Quantum theory of many body systems* Springer.

List of Publications

Here, a list of publications is given including contributions which have not been displayed in this thesis. They are all related to the optical properties and excitonic effects in semiconductors and have been written during the course of this thesis.

[P–1] S. Sagmeister, K. Hummer, P. Puschnig, C. Ambrosch-Draxl, Excitonic effects of biphenyl under pressure (2004). Proceedings of the The International Conference on the Science and Technology of Synthetic Metals (ICSM) 2004.

[P–2] C. Ambrosch-Draxl, K. Hummer, S. Sagmeister, P. Puschnig, On the nature of the lowest optical absorption in organic semiconductors (2004). Proceedings of the The International Conference on the Science and Technology of Synthetic Metals (ICSM) 2004.

[P–3] C. Ambrosch-Draxl, K. Hummer, S. Sagmeister, P. Puschnig, *Chem. Phys.* **325**, 3 (2006).

[P–4] K. Hummer, P. Puschnig, S. Sagmeister, C. Ambrosch-Draxl, *Mod. Phys. Lett. B* **20**, 261 (2006).

[P–5] S. Sagmeister, C. Ambrosch-Draxl, *Phys. Chem. Chem. Phys.* **11**, 4451 (2009).